NAVAL POSTGRADUATE SCHOOL
Monterey, California

THESIS

CHANGES IN THE OCEAN MIXED LAYER
FOLLOWING EXTRAORDINARY ATMOSPHERIC FORCING

by

Theodore R. Mettlach

December 1985

THESIS ADVISOR: R. L. Haney

UNCLASSIFIED
CURITY CLASSIFICATION OF THIS PAGE

REPORT DOCUMENTATION PAGE

. REPORT SECURITY CLASSIFICATION	1b. RESTRICTIVE MARKINGS
. SECURITY CLASSIFICATION AUTHORITY	3 DISTRIBUTION/AVAILABILITY OF REPORT Approved for public release;
. DECLASSIFICATION/DOWNGRADING SCHEDULE	distribution is unlimited.
PERFORMING ORGANIZATION REPORT NUMBER(S)	5. MONITORING ORGANIZATION REPORT NUMBER(S)
. NAME OF PERFORMING ORGANIZATION: Naval Postgraduate School	6b. OFFICE SYMBOL (If applicable): 63
	7a. NAME OF MONITORING ORGANIZATION: Naval Postgraduate School
ADDRESS (City, State, and ZIP Code): Monterey, California 93943-5100	7b. ADDRESS (City, State, and ZIP Code): Monterey, California 93943-5100
. NAME OF FUNDING/SPONSORING ORGANIZATION	8b. OFFICE SYMBOL (If applicable)
	9. PROCUREMENT INSTRUMENT IDENTIFICATION NUMBER
ADDRESS (City, State, and ZIP Code)	10. SOURCE OF FUNDING NUMBERS

PROGRAM ELEMENT NO.	PROJECT NO.	TASK NO	WORK UNIT ACCESSION NO

TITLE (Include Security Classification)
CHANGES IN THE OCEAN MIXED LAYER FOLLOWING EXTRAORDINARY ATMOSPHERIC FORCING

PERSONAL AUTHOR(S)
Mettlach, Theodore R.

a. TYPE OF REPORT	13b. TIME COVERED	14 DATE OF REPORT (Year, Month, Day)	15 PAGE COUNT
Master's Thesis	FROM _____ TO _____	1985 December	95

SUPPLEMENTARY NOTATION

COSATI CODES		
FIELD	GROUP	SUB-GROUP

18. SUBJECT TERMS (Continue on reverse if necessary and identify by block number)
nuclear effects; ocean mixed layer (model); nuclear war; climate model; nuclear winter

ABSTRACT (Continue on reverse if necessary and identify by block number)

A 1D ocean planetary boundary layer model is used to predict the evolution of the thermal structure of the ocean mixed layer at six locations in the ocean following the hypothetical effects on the atmosphere of a major nuclear war. The inputs to the ocean model are the heat and momentum fluxes computed from a 3D climate model designed to simulate "nuclear winter" effects in the atmosphere. The experiment gives evidence that the summertime mixed layer can cool 5°C within 30 days and that the effect of increased wind along coastal regions due to sudden ocean-land temperature differences will deepen the mixed layer 20 to 0 meters.

The scientific literature on the subject of "nuclear winter" is reviewed and interpreted to trace the evolution of the "nuclear winter" hypothesis and to assess the quality of the results of the mixed layer experiment.

DISTRIBUTION/AVAILABILITY OF ABSTRACT ☒ UNCLASSIFIED/UNLIMITED ☐ SAME AS RPT. ☐ DTIC USERS	21. ABSTRACT SECURITY CLASSIFICATION Unclassified
a NAME OF RESPONSIBLE INDIVIDUAL Prof. R. L. Haney	22b TELEPHONE (Include Area Code) 408-646-2308 / 22c. OFFICE SYMBOL 63Hy

D FORM 1473, 84 MAR 83 APR edition may be used until exhausted
All other editions are obsolete

SECURITY CLASSIFICATION OF THIS PAGE
UNCLASSIFIED

Approved for public release; distribution is unlimited.

Changes in the Ocean Mixed Layer Following Extraordinary Atmospheric Forcing

by

Theodore R. Mettlach
Lieutenant, United States Navy
B.S., The Florida State University, 1979

Submitted in partial fulfillment of the
requirements for the degree of

MASTER OF SCIENCE IN METEOROLOGY AND OCEANOGRAPHY

from the

NAVAL POSTGRADUATE SCHOOL
December 1985

ABSTRACT

A 1D ocean planetary boundary layer model is used to predict the evolution of the thermal structure of the ocean mixed layer at six locations in the ocean following the hypothetical effects on the atmosphere of a major nuclear war. The inputs to the ocean model are the heat and momentum fluxes computed from a 3D climate model designed to simulate "nuclear winter" effects in the atmosphere. The experiment gives evidence that the summertime mixed layer can cool 5°C within 30 days and that the effect of increased wind along coastal regions due to sudden ocean-land temperature differences will deepen the mixed layer 20 to 30 meters.

The scientific literature on the subject of "nuclear winter" is reviewed and interpreted to trace the evolution of the "nuclear winter" hypothesis and to assess the quality of the results of the mixed layer experiment.

TABLE OF CONTENTS

I. INTRODUCTION 9

II. NUCLEAR WINTER 12

A. THE NUCLEAR WINTER HYPOTHESIS 12

B. DEVELOPMENT OF THE HYPOTHESIS 13

1. Martian Dust Storms 13

2. Cretaceous-Tertiary Extinction 14

3. Widespread Fires 15

4. One-dimensional Modelling of Nuclear Winter 16

5. Energy Balance Climate Models (EBCMs) . . 18

6. Multidimensional Models of Nuclear Winter 18

C. UNCERTAINTIES IN THE HYPOTHESIS 21

1. Initial Production of Smoke 22

2. Injection,Transport, and Removal of Smoke and Dust 23

3. Consequent Climate Effects 23

III. NUCLEAR WINTER AND THE UPPER OCEAN 25

A. THE MIXED LAYER 25

B. DESCRIPTION OF THE UPPER OCEAN 25

C. SURFACE FLUXES 29

D. NUCLEAR WINTER CONSIDERATIONS 30

IV. THE EXPERIMENT 32

A. THE ATMOSPHERIC DATA 32

B. THE OCEAN PLANETARY BOUNDARY LAYER MODEL (OPBL) 36

C. PROCEDURE 37

D. THE GCM DATA 39

V. RESULTS 62

A. POINT ONE (50°N 150°W) 62

B. POINT TWO (50°N 150°E) 65

C. POINT THREE (50°N 50°W) 67

D. POINT FOUR (30°N 150°W) 69

E. POINT FIVE (10°N 150°W) 70

F. POINT SIX (30°N 125°E) 71

G. SUMMARY 72

H. RECOMMENDATIONS FOR FURTHER RESEARCH 73

LIST OF REFERENCES 89

INITIAL DISTRIBUTION LIST 93

LIST OF TABLES

1. BIAS FACTORS USED 38
2. 30-DAY AVERAGE TOTAL ENERGY FLUX 41
3. 30-DAY AVERAGE WIND STRESS 42
4. SST AND MLD CHANGES:CONTROL 63
5. SST AND MLD CHANGES:SMOKE 63
6. 30-DAY TIME AVERAGED SST (°C) AND MAXIMUMS . . . 65
7. 30-DAY TIME AVERAGED MLD (METERS) 66

LIST OF FIGURES

1.1 Locations of Experiment Points 11
3.1 Idealized Thermal Profile (Warrenfeltz, 1980) . . . 27
4.1 Initial Optical Depth (from Ghan et al., 1985) . . 35
4.2 Energy Fluxes at Point One (50°N 150°W) CONTROL . . 43
4.3 Energy Fluxes at Point One (50°N 150°W) SMOKE . . . 44
4.4 Energy Fluxes at Point Two (50°N 150°E) CONTROL . . 45
4.5 Energy Fluxes at Point Two (50°N 150°E) SMOKE . . . 46
4.6 Energy Fluxes at Point Three (50°N 50°W) CONTROL 47
4.7 Energy Fluxes at Point Three (50°N 50°W) SMOKE . . 48
4.8 Energy Fluxes at Point Four (30°N 150°W) CONTROL 49
4.9 Energy Fluxes at Point Four (30°N 150°W) SMOKE . . 50
4.10 Energy Fluxes at Point Five (10°N 150°W) CONTROL 51
4.11 Energy Fluxes at Point Five (10°N 150°W) SMOKE . . 52
4.12 Energy Fluxes at Point Six (30°N 125°E) CONTROL . . 53
4.13 Energy Fluxes at Point Six (30°N 125°E) SMOKE . . . 54
4.14 Wind Stress at Point One (50°N 150°W) 55
4.15 Wind Stress at Point Two (50°N 150°E) 56
4.16 Wind Stress at Point Three (50°N 50°W) 57
4.17 Wind Stress at Point Four (30°N 150°W) 58
4.18 Wind Stress at Point Five (10°N 150°W) 59
4.19 Wind Stress at Point Six (30°N 125°E) 60
4.20 Salinity Flux at Point Five (10°N 150°W) 61
5.1 Sea Surface Temperature at Point One (50°N 150°W) 75
5.2 Mixed Layer Depth at Point One (50°N 150°W) 76
5.3 Sea Surface Temperature at Point Two (50°N 150°E) 77
5.4 Mixed Layer Depth at Point Two (50°N 150°E) 78

5.5 Sea Surface Temperature at Point Three (50°N 50°W) 79
5.6 Mixed Layer Depth at Point Three (50°N 50°W) . . . 80
5.7 Sea Surface Temperature at Point Four (30°N 150°W) 81
5.8 Mixed Layer Depth at Point Four (30°N 150°W) . . . 82
5.9 Sea Surface Temperature at Point Five (10°N 150°W) 83
5.10 Mixed Layer Depth at Point Five (10°N 150°W) . . . 84
5.11 Sea Surface Temperature at Point Six (30°N 125°E) 85
5.12 Mixed Layer Depth at Point Six (30°N 125°E) 86
5.13 Temperature Structure at Point Two (50°N 150°E) CONTROL 87
5.14 Temperature Structure at Point Two (50°N 150°E) SMOKE 88

I. INTRODUCTION

In the past five years much attention has been given to the long term potential climatic consequences of a major nuclear exchange between the superpowers. The results of this attention has been the formulation of the "nuclear winter" hypothesis: that tremendously large amounts of smoke and dust injected into the atmosphere from the fires from thousands of nuclear detonations during a major nuclear war could block enough sunlight that the interiors of the earth's continents would cool on the order of ten degrees Celsius for periods of the order of a month. The development of this hypothesis has progressed slowly in the light of several physical analogs and recent theoretical considerations. Despite this progress, refinements to the current results will be necessary to satisfy the rigid demands of climate prediction, which itself is an unproven skill. Nevertheless, the stakes are high. The nuclear winter hypothesis has suggested that nations which wage general nuclear war in the future may cause damage to the Earth's ecosystems that is well in excess of the immediate effects of the nuclear explosions themselves.

This study focuses first on a review of the more significant works on the subject of nuclear winter, and secondly on the response of the ocean's mixed layer to the hypothetical atmospheric effects of a major nuclear exchange. The many facets of the nuclear winter hypothesis requires a literature review, while current climate research requires some quantitative estimate of the response of the ocean to this extraordinary atmospheric forcing (National Research Council, 1985).

An examination of the ocean's role in a "nuclear winter" is important because of the possibly large feedback processes that might occur. The sea-surface temperature

(SST) affects the flux of outgoing infrared radiation from the ocean, as well as the fluxes of sensible and latent heat. SST has a direct influence on the formation of fog and low-level clouds and the development of cumulus convection. Clouds and fog have some control over the amount of solar radiation that reaches the ocean. Precipitation causes salinity flux in the ocean mixed layer which in turn influences buoyant overturning within the mixed layer. The interrelationships between SST, energy fluxes, precipitation and cloud formation are complex; and a realistic representation of the effects of a "nuclear winter" requires a fully coupled air-ocean climate model. The present study is a step in that direction.

This experimental numerical study examines the response of a one-dimensional ocean planetary boundary layer (OPBL) model to the atmospheric forcing of a three-dimensional general circulation model (GCM). The OPBL was run at six geographical locations for periods of thirty days. See Fig. 1.1. The results of control ("normal" climate) runs and nuclear winter ("smoke") runs were compared.

The GCM data were provided by the Lawrence Livermore National Laboratory, Livermore, CA. The smoke case represented a 150 teragram (1 teragram [Tg] = 10^{12} grams) injection of smoke into the atmosphere following a hypothetical nuclear exchange in the northern hemisphere in July. The additional effect of dust lofted into the air from nuclear weapons detonations was neglected. An analysis of the GCM data revealed that many of the control run values of surface fluxes were inconsistent with empirically derived average climatological values. Therefore biased control run values of the fluxes were constructed to obtain more realistic estimates of the mixed layer changes during "control" runs. These bias factors were also applied to the corresponding "smoke" runs.

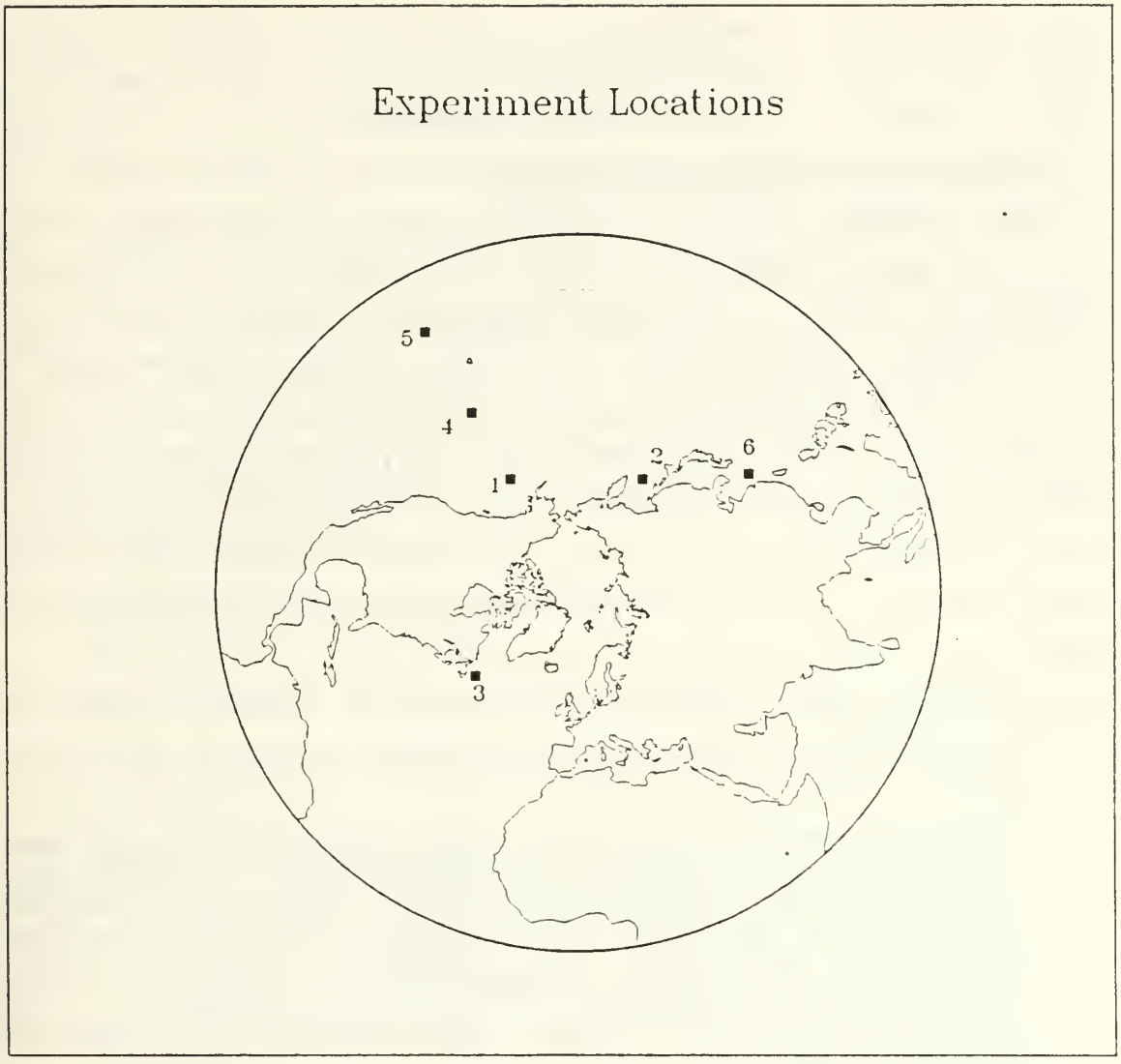

Fig. 1.1 Locations of Experiment Points.

An evaluation of the results has been made to estimate their usefulness for practical applications. The question of nuclear winter is a factor in U.S. defense policy: nuclear weapons policy (including targeting, planning, command and control, procurement and deployment), nuclear arms control policy and civil defense policy. Therefore, an estimate is made of the reliability of the results presented with regard to data quality and the methods used.

II. NUCLEAR WINTER

A. THE NUCLEAR WINTER HYPOTHESIS

The nuclear winter hypothesis can be stated simply. The dust and smoke from fires ignited by the direct and indirect effects of multiple nuclear weapons detonations over cities and forest areas during a general nuclear war could be injected high enough and in large enough quantities into the atmosphere to blot out sufficient sunlight so that temperatures at the earth's surface could be reduced significantly. For nuclear winter to occur, it is important that three requirements be met simultaneously (MacCracken and Walton, 1984):

- that a large amount of smoke be injected into the atmosphere,
- that the smoke be highly absorbent of solar radiation, and
- that the smoke be injected high enough into the upper tropopause, or higher, that precipitation scavenging of smoke particles does not readily occur. Precipitation scavenging is a mechanism by which atmospheric aerosols are removed from the atmosphere. Water droplets tend to collect and carry down atmospheric aerosols. Water droplets also act as aggregation centers for soot particles. Therefore; if a droplet evaporates, it can leave behind a relatively large aerosol with a settling rate which is much greater than the settling rate of a primary particle.

Injection of sooty material into the upper atmosphere has been interpreted two different ways (Cess, 1985). If large amounts of smoke are injected into the *stratosphere*, absorption of solar radiation is assumed to occur, well above the convective troposphere, and cooling of the surface is a result of reduced amounts of solar radiation reaching the troposphere. The second interpretation is that smoke and dust injected into the *troposphere* will actually result in anomalous warming of the troposphere due to the increased absorption by the abundant smoke particles. Cooling of the surface will still occur owing essentially to a decoupling of the convective troposphere and the atmospheric boundary

layer. Static stability will increase to such an extent that small-scale convective processes will virtually cease. Normally, a stop in convection would result in warming when the surface heat budget becomes governed primarily by radiative processes, but the decrease here in solar radiation will result in a net cooling at the surface.

The resultant temperature structure in the troposphere following the initial injection will suppress precipitation over both ocean and land areas. Scavenging of smoke and dust by precipitation in the upper-level smoke areas will be ineffective (MacCracken, 1983), and nuclear winter-producing mechanisms will be prolonged.

B. DEVELOPMENT OF THE HYPOTHESIS

The nuclear winter hypothesis has developed from three unrelated fields. The first was from the meteorological data from satellite exploration of Mars during the Mariner and Viking projects. The second was from the development of the theory that large amounts of dust lofted into the atmosphere by a large asteroidal impact against the earth was responsible for blocking out sunlight and cooling the earth's surface to the point that the food chains supporting the dinosaurs collapsed (Alvarez et al., 1980). Thirdly was an analysis of the possible smoke production following a massive nuclear attack (Crutzen and Birks, 1982). These studies prompted quantitative investigation of the response of the atmosphere to severe smoke and dust loading.

1. Martian Dust Storms

The flights of Mariner 9 in late 1971 and Viking during 1977 revealed dramatic transient global scale dust storms on the planet Mars (Kieffer, 1979). The dust shrouded the Martian atmosphere to such a degree that only the largest topographic features were visible from orbit. The 7-μm channel of the Viking infrared thermal mapper (IRTM) was used to determine the surface temperature of Mars during both clear and dusty periods. Slight cooling was

evident during the dusty periods (Martin et al., 1979). Similarly, the 15-μm carbon dioxide band of the IRTM was used to discern temperature changes at the 0.6 mbar level (25 km) of the Martian atmosphere during both clear and dusty periods. At this altitude dramatic temperature increases (as much as 80K) occured during the global dust storms (Martin and Kieffer, 1979).

The importance of the above was immediately recognized. Martin et al. (1979) explained that the thermal changes act to quell these global disturbances by increasing atmospheric static stability and reducing lower atmosphere radiative-convective activity.

The Martian dust storms have offered a striking physical analog to the nuclear winter hypothesis. However, caution should be taken in applying direct comparisons (National Research Council, 1985). The dust particle size distribution and total amount of dust would be quite different on Earth compared to Mars; precipitation processes do not occur on Mars as on Earth; and smoke is not a factor on Mars while it is presumed to be a significant factor in nuclear winter modelling.

2. Cretaceous-Tertiary Extinction

It is surprising that the experimental results and theoretical interpretation of the cause of the extinction of the dinosaurs has had such an influence on the development of the nuclear winter hypothesis. Alvarez et al. (1980) observed high concentrations of the noble metal iridium at three sites (Italy, Denmark, and New Zealand) in the stratigraphic boundary between the Cretaceous and Tertiary periods of 65 million years ago. It was hypothesized that ablation of a massive incoming asteroid and the ejection of dust from its impact left great amounts of fine dust in the stratosphere for a sufficiently long time (several years), that the lack of sunlight suppressed photosynthesis to such an extent that the food chain of the great dinosaurs was

disrupted. The asteroid impact hypothesis provides a scenario that explains most or all of the biological and physical evidence available (Alvarez et al., 1980). This hypothesis provides a plausible physical analog in support of the fundamental idea of the nuclear winter hypothesis.

Further evidence in support of this general hypothesis has been reported by Wolbach et al. (1985), who have shown that relatively large quantities of graphitic or elemental carbon exist at three Cretaceous boundary sites. These large amounts of soot correspond to a burning of an estimated ten per cent of the present biomass of the earth. They have shown that the mean carbon abundance at the boundary (0.021 g/cm^2) implies a worldwide flux of carbon 10,000 times the present one. The report suggests that the extinction of the great dinosaurs was caused by the cooling of the earth by a nuclear winter-type mechanism generated from wildfires that were started by the thermal radiation of the incoming asteroid.[1]

3. Widespread Fires

Although Broido (1960) discussed the likelihood of widespread fires following a nuclear war, the first quantitative evidence of the possible importance of smoke in blocking sunlight was provided by Crutzen and Birks (1982). They estimated the amount of smoke and soot that would be lofted into the atmosphere following the hypothetical fires of a nuclear war. Fires ignited by thousands of nuclear detonations in forests, urban and industrial areas, agricultural fields, and oil and gas fields were considered. They

[1]The impact-extinction theory does have its critics. In an article in the *New York Times* on 29 October 1985, Malcolme Browne pointed out that, at the annual meeting of the Society of Vertebrate Paleontologists in October, 1985 at Rapid City, South Dakota, of 118 participants in an informal survey, 32 paleontologists asserted that there was no need to speculate about a catastrophic extinction of the dinosaurs at all because the extinction of the dinosaurs probably occurred slowly over a period of perhaps a million years. However, only twelve participants in the poll denied that an asteroid impact had occurred.

estimated that the average sunlight penetration reaching the earth's surface would be reduced by a factor between 2 and 150 at noontime in the summer, using current estimated values of the size and absorptivity of soot, ash, tar and organic particulate matter.

Crutzen and Birks (1982) noted four significant atmospheric changes following smoke loading:

- that large fractions of solar radiation would be screened out,
- that the structure of the tropopause would be altered significantly by the absorption of solar radiation high in the atmosphere,
- that stable conditions in the troposphere would be established which would restrict removal rates of fire-produced pollutants due to suppressed convection and,
- that the cloud droplet size distribution would be narrowed and rain drop formation by coalescence suppressed, thereby decreasing the rain production efficiency of clouds.

This work laid the foundation for the first quantitative estimate of surface temperature changes following nuclear war.

4. One-dimensional Modelling of Nuclear Winter

Turco et al. (1983) used a one-dimensional radiative-convective model (1D RCM) to estimate the first-order climate response of the atmosphere. Their model consisted of three major components:

- a nuclear war scenario model,
- a particle microphysics model, and
- a radiative-convective model.

Many runs were made using a variety of parameters. Their baseline 5000 megaton (mt) exchange scenario, with a total atmospheric injection of 225 Tg of smoke and 960 Tg of dust, was modified to include several combinations of weapon burst height, smoke/dust proportioning, and smoke scavenging parameterizations. For these runs with the surface heat capacity set to a very small value, the average surface temperature, that is, the vertically averaged temperature of the lowest two kilometers of the atmosphere,

characteristically dropped 20 to 30°C within a month's time (Turco et al., 1983; Covey et al., 1984; National Research Council, 1985). Simulations for an ocean surface boundary with a very high heat capacity resulted in the lowest layer cooling 3°C or less.

MacCracken (1983) used a more sophisticated 1D RCM to obtain results similar to Turco et al. (1983). In this case 150 Tg of soot aerosol was injected from cities and immediately dispersed with 57 Tg of soot injected from forest fires for a period of one week following the exchange. Also, 118 Tg of dust was injected initially. For a low heat capacity surface (land), the maximum surface temperature drop varied from 30 to 70°C depending on the scavenging rates used. For damped scavenging, the maximum temperature decrease was greater and occurred later than with normal scavenging. The time of maximum temperature change varied from 10 to 70 days after the nuclear war.

One dimensional models offer a rough estimate of the climatic damage following a war, but have three serious limitations:

- These models are restricted to global averages of an all-land or all-ocean planet. That is, they neglect the ameliorating surface effects of the high thermal inertia of the ocean over coastal or ocean areas for land simulations (National Research Council, 1985).
- One dimensional models do not account for the patchiness or streakiness that may occur with smoke and dust dispersal. The assumption made by Turco et al. (1983) and MacCracken (1983) that smoke aerosols are instantly well-mixed implies that more solar radiation is absorbed and scattered than would be the case if thicker smoke covered smaller areas (MacCracken, 1983).
- Cloud distributions were accounted for by neither Turco et al. (1983) nor MacCracken (1983) [(National Research Council, 1985)]. The importance of doing so was demonstrated by MacCracken (1983) who did make a run with no cloud cover. For this case the surface temperature drop was 20°C more than an identical run with cloud cover.

5. Energy Balance Climate Models (EBCMs)

Energy balance models constitute another class of models that have been used to investigate nuclear winter effects. Such models no not include the advective processes of full primitive equation 3D GCMs and therefore their results must be interpreted judiciously (National Research Council, 1985). They have been used to study the climate feedback effects of changes in ice, snow, and SST. Robock (1984) has shown that snow and ice cover provide important climate feedback mechanisms with an EBCM. Such a model was used to evaluate the importance of snow and ice areas and snow and ice meltwater with respect to planetary albedo and what is termed the ice-thermal inertia feedback. The ice-thermal inertia feedback mechanism accounts for the change in the heat capacity of the surface when sea ice forms or melts. Robock used the baseline nuclear war scenario of Turco et al. (1983) and simulated temperature drops in the northern hemisphere of 21.4°C, 45 to 60 days after the beginning of the war. Maximum surface air temperature drops over ocean areas were as much as 10.7°C, from 90 to 105 days after the smoke injection. (Robock did not report SST changes.) The mixed layer ocean model used in the simulation had a fixed layer depth and did not account for diffusive heat transport.

6. Multidimensional Models of Nuclear Winter

Two- and three-dimensional climate models have been used to refine the first order estimates of the 1D RCMs previously discussed. Such multidimensional models can account for the differences in heat capacity between land and ocean, and the heterogeneity of smoke distributions.

MacCracken (1983) used zonally averaged transport and precipitation data from a 3D GCM, and applied it to a 2D particle transport model which was used to spread smoke north and south, and scavenge it through precipitation processes, from an initial distribution. The smoke and dust

distributions from the transport model were fed into a two-dimensional (latitude and vertical) climate model. Land-ocean distribution was based on a longitudinal average of several surface types. The average temperature drop for a 207 Tg smoke and 57 Tg dust war scenario was a maximum of between 7 and 8°C ten to twenty days after the exchange over land, and a maximum of 2°C ninety days after the exchange over the ocean. The smoke and dust dispersal was not interactive with the precipitation scavenging and cloud formation processes in the model, and this modelling technique probably over estimates removal rates. Vertical wind shear was also neglected in accounting for the smoke movement. This probably causes an underestimation of the dispersal of the injected pollutants.

Aleksandrov and Stenchikov (1984) used a coupled air-ocean 3D GCM to simulate nuclear winter effects. They used a modified obsolete version of the Oregon State two-level GCM (Gates and Schlesinger,1977) with a 12 degree longitude and 15 degree latitude grid and proper topography. Smoke and dust injection amounts were taken from Turco et al. (1983). At the beginning of the simulation all pollutants were injected and instantly dispersed north of 12 degrees north latitude. It was found that the global horizontally- and vertically-averaged atmospheric temperature increased steadily by more than 20°C for the first 180 days, then it began to slowly decrease. The horizontally-averaged land temperature decreased by more than 15°C within 20 days (when it then began to slowly warm), and the horizontally-averaged ocean temperature dropped 1.2°C in ten months. At 40 days, the air temperature over oceans dropped at various locations, with the largest drop of 40°C in the Sea of Okhotsk (Thompson et al., 1984).

The study of Aleksandrov and Stenchikov (1984) is limited by a radiative approximation that greatly overestimates the amount of smoke put into the atmosphere. The

effect of smoke on the transfer of solar radiation is simulated by decreasing the solar constant. This was done by initiating the experiment with an atmosphere that had an optical depth of seven and decreasing it as the experiment proceeded. According to the National Research Council (1985) report the optical depth is defined as follows:

> The optical depth is a dimensionless quantity that determines the light transmission properties of a layer of gas or aerosols. If the layer has an optical depth, δ, $\exp(-\delta)$ is the fraction of a beam of light perpendicularly incident on the layer that suffers no scattering or absorption in passing through the layer.

An optical depth of seven corresponds to smoke and dust far in excess of that used by MacCracken (1983) who used an optical depth of three. By changing the solar constant to artificially and unrealistically "parameterize" the amount of smoke in the atmosphere the model loses energy. This has the effect of creating excessive static stability in the troposphere.

Aleksandrov and Stenchikov (1984) were the first to discuss cross-hemispheric flow of smoke and dust into the southern hemisphere and the melting of high altitude glacial ice from the strong upper-level temperature increase. Despite these advances there has been criticism of this particular work and disappointment with the Soviet contributions to date (Secretary of Defense, 1985; Gouré, 1985).

Covey et al. (1984) have used the higher resolution National Center for Atmospheric Research (NCAR) community climate model (CCM) to simulate the atmospheric response to high smoke loading out to twenty days. The model has a latitude resolution of approximately 4.5 degrees and a longitude resolution of approximately 7.5 degrees. There are nine vertical layers representing the troposphere and stratosphere. Cloud formation is parameterized by relative humidity and convective activity. Absorption of sunlight is

partially dependent on ozone, water vapor, carbon dioxide and molecular oxygen. Unlike the Aleksandrov and Stenchikov study, SST is prescribed. Unlike MacCracken and Turco et al., land surface heat capacity is assumed to be zero. Smoke transport is not time dependent. Smoke appeared instantly and was assumed to be immediately totally dispersed. Smoke distribution remained fixed in place for the entire twenty-day run. The optical depth was held fixed at three for the twenty-day run. This value is more realistic than the extremely high value used by Aleksandrov and Stenchikov.

For the CCM runs, using the National Research Council (1985) baseline nuclear exchange of 6500 mt, with 180 Tg of smoke injected into the atmosphere, land cooling after ten days for the summer case ranged from 15 to 20°C. Cooling over the ocean was very small at day ten, presumably due to the prescribed constant ocean temperatures. Significant cross hemispheric flow occurred in the spring simulation. The normal bi-Hadley circulation was replaced by a large single cell which had upward motion in the smoke region of the northern hemisphere and a low-level return flow across the equator from 30°S to 30°N.

C. UNCERTAINTIES IN THE HYPOTHESIS

The nuclear winter hypothesis can be examined broadly in terms of three component parts (Secretary of Defense, 1985):

- the initial production of smoke and dust.
- the injection, transport and removal of smoke within the atmosphere.
- the consequent climatic effects.

There are serious questions regarding how to model these aspects of the problem. Each is discussed in detail below.

1. Initial Production of Smoke

The main question here concerns how a nuclear war will be fought. Although it is not U.S. policy to target cities *per se* for reasons of retribution or punishment, it is generally recognized that sufficient military targets exist in and around major cities that damage to cities would occur in a large exchange. Translating the number of bursts, their heights, their location, and the thermal effects of each fireball into an amount of fuel ignited and burned for a given duration is extremely difficult at best. The National Research Council (1985) report has used 2.1 to estimate the smoke mass released into the atmosphere.

$$S = Y\ A\ F\ f\ e\ 10^{10} \qquad (2.1)$$

S is the total smoke emission (in grams), Y is the total explosion yield in megatons in air bursts that ignite fires, A is the average area ignited per megaton (km^2/mt), F is the average loading of flammable material (g/cm^2), f is the fraction of F actually burned, and e is the mean smoke emission factor [g(smoke)/g(material)]. The values of many of these variables have been established from past firestorms (Dresden, Hamburg, Tokyo, Hiroshima, and Nagasaki) and nuclear weapons tests (Glasstone and Dolan, 1977).

Modelling a war is perhaps the most uncertain aspect of the nuclear winter hypothesis, but realistic scenarios can be used. Reported values of the world's nuclear arsenals allow speculation from minimal sub-kiloton detonations to massive worst-case scenarios. Turco et al. used scenarios with as much as 10,000 mt and as little as 100 mt. Forest fire burning is another open question, but data are available from many large forest fires that have occurred this century.

2. Injection,Transport, and Removal of Smoke and Dust

Models to date have not been fully interactive with radiative transfer, smoke and dust removal and transport, and cloud and precipitation processes. One of the largest uncertainties has to do with the amount of smoke in the atmosphere one to two days after the fires begin (Thompson et al., 1984). The problem is that initial smoke concentrations and early particle removal by convective-precipitative processes occur on spatial scales unresolvable by GCMs (Covey et al., 1984). Therefore, models of nuclear winter have been initialized by smoke distributions conceivably representative of a condition many hours or days after the fires begin. It is possible that precipitation scavenging from cumulus clouds formed as a result of large fires could cause substantial initial scavenging of smoke. Past firestorms and conflagrations do offer some indication of scavenging processes, but there is no really conclusive evidence. For example, the Hamburg firestorm of WWII had little associated precipitation, but the Hiroshima nuclear fire did (Thompson et al., 1984). The transformation and coagulation of smoke aerosols is a difficult microphysical problem that needs to be parameterized more accurately. Finally, the question of the impact of sedimentation needs to be addressed. Crutzen et al. (1984) and Robock (1984) point out that deposition of aerosols on the Earth's surface may cause additional stress on the environment by complicating the surface radiative heat balance by altering the Earth's albedo. Some estimate of the effect of a quickly changing surface radiative balance may be important for time periods of the order of a season.

3. Consequent Climate Effects

Some mesoscale atmospheric effects of nuclear winter have not been taken into account by current models. Some of the more important of these atmospheric effects include boundary layer processes that control formation of fog and

low clouds which are an important factor with regard to aerosol scavenging. There are further uncertainties about the nature of monsoonal circulations that could be induced, the precipitation processes induced by coastal surface temperature gradients, thunderstorm development following convection from fire plumes, and the effect of chemical transformations in the atmosphere on the radiative heat balance.

Except for Aleksandrov and Stenchikov (1984), ocean temperatures have been prescribed to be either fixed or slowly varying in 3D GCMs. This is a limitation for current GCMs and is the motivation for this study.

III. NUCLEAR WINTER AND THE UPPER OCEAN

A. THE MIXED LAYER

The uppermost layer of the ocean is a dynamic region which responds rapidly to those fluid mechanical and thermodynamical atmospheric processes which can be represented in terms of wind, sunlight, precipitation, air-ocean temperature, momentum and density differences; and atmospheric humidity changes. The structure of the upper ocean is a result of these processes, the chemical and physical properties of seawater, and horizontal and vertical advective processes. Changes in the ocean mixed layer are described within the general principles of conservation of mass, energy and momentum. Because the upper ocean is a turbulent boundary layer, a rigorous mathematical theory for its structure is not possible (Holton, 1979). Military, economic and academic interests have made successful attempts at simulating the structure of the ocean mixed layer by using a variety of parameterizations and approximate mathematical closures. The purpose of this chapter is to provide a background discussion of the observed structure of the mixed layer, and how, using fundamental physical principles; the mixed layer will change following nuclear winter effects.

B. DESCRIPTION OF THE UPPER OCEAN

The upper ocean is observed to be approximately vertically homogeneous in salinity, temperature, and, therefore; density. Mixing occurs as a result of wind stirring, and thermohaline convection within the layer. Climatologically, the open ocean mixed layer depth usually varies seasonally between 20 and 100 meters and rarely exceeds 200 meters depth. Bathen (1972) found that in the North Pacific Ocean the mixed layer depth ranged from 15 meters off Panama to

122 meters in the Bering Sea, with an average depth of 65 meters. The mixed layer undergoes its largest seasonal changes in mid-latitudes and in eastern equatorial regions. An idealized temperature profile of the upper 200 meters of the ocean, from Warrenfeltz (1980), is shown in Fig. 3.1.

The mixed layer extends to the depth h where there is a temperature jump ΔT, across the depth interval Δh. In this study this temperature discontinuity is assumed to occur over one meter. This region of temperature discontinuity is called the entrainment zone and it is where cooler water from the stably stratified layer below is mixed into the upper region when there is enough turbulent kinetic energy in the upper layer to penetrate below and entrain the cooler water. Dissipation and buoyant damping of turbulent kinetic energy in the mixed layer will cause the entrainment zone to retreat upwards (i.e., to re-form at a shallower depth). Below the entrainment zone there is a gradual but steady decrease of temperature called the thermocline.

The salinity structure in the upper ocean affects dynamical processes for cases where salinity is important to the density distribution of the thermocline. Typical salinity profiles in the ocean vary much more in characteristic shape than do temperature traces. Because temperature usually has the largest influence on density structure, $\partial S/\partial z$ can be either positive or negative, but $\partial T/\partial z$ is usually positive (Fig. 3.1). Trade wind latitudes frequently have the highest average mixed layer salinities due to the high evaporation rate at these latitudes. Mixed layer salinity decreases from the trades northward. The tropical oceans often have a salinity maximum within the upper layer near 100 meters depth as a result of the sinking of dense saline water formed from evaporation.

The density profile of the upper ocean is a function of temperature and salinity, and the homogeneity of temperature and salinity forms a density structure in the upper mixed

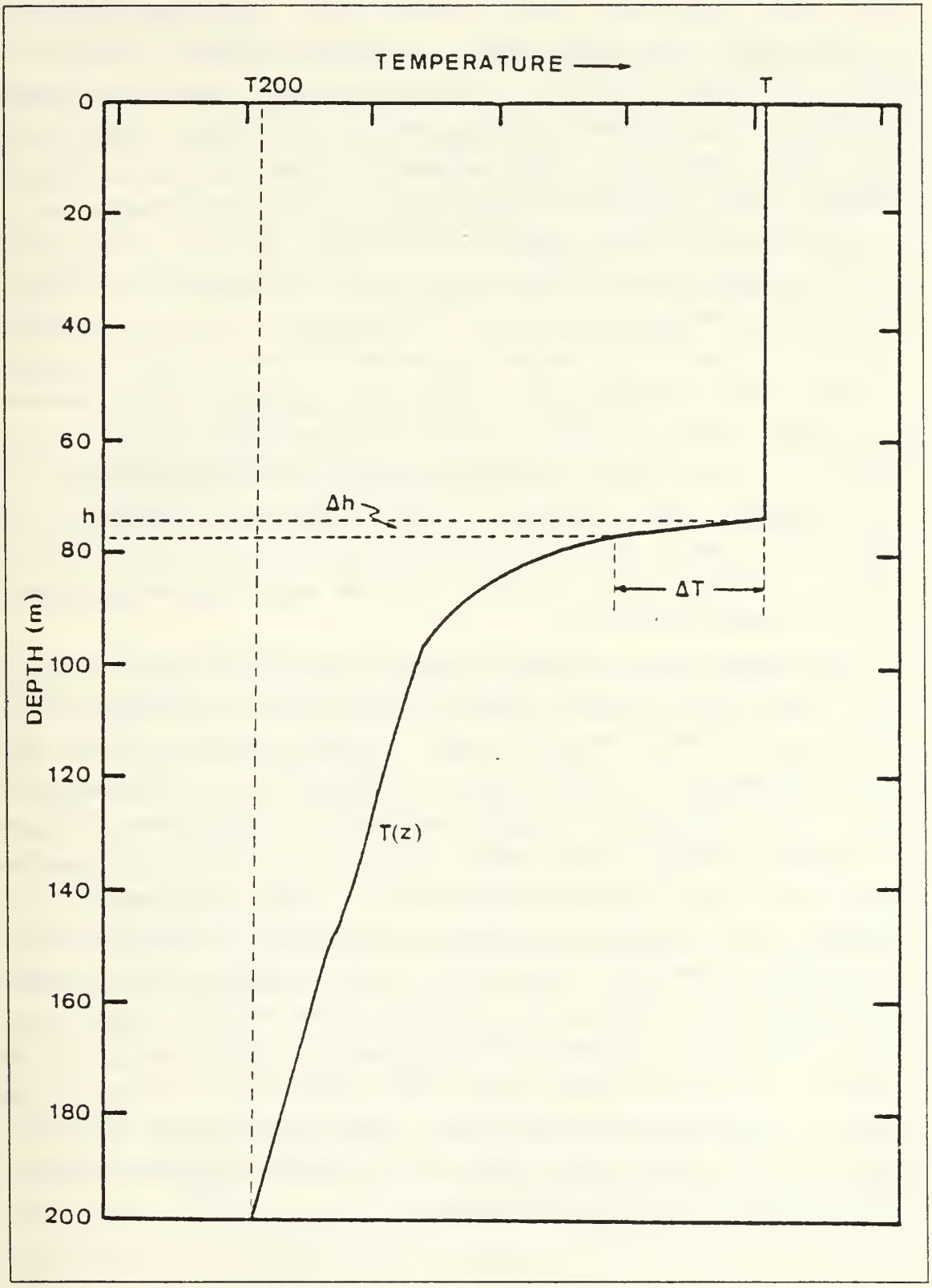

Fig. 3.1 Idealized Thermal Profile (Warrenfeltz, 1980).

layer that has small static stability. At times the water in the mixed layer is weakly unstable (Pickard and Emery, 1982), and this allows vertical motion and turbulent mixing to exist. The changes in the density profile are determined to a large extent by the changes of the salinity flux and diabatic heat exchange through the air-sea interface.

The mixed layer depth fluctuates on two major time scales, diurnal and annual; but it is perturbed by synoptic atmospheric events such as tropical and extra-tropical cyclones. The mixed layer characteristically shallows most at noon when maximum solar radiation occurs and it deepens at night when surface water cools and mixes down. Seasonally, the mixed layer shallows in the late spring and early summer and deepens in the autumn and winter. The mixed layer depth is most variable in the spring when there exists a competition between spring warming and vigorous spring storm activity.

The mixed layer rarely extends below 200 meters because below this level the two most important factors which determine its existence are reduced. In the clearest water, 88% of incoming solar radiation is absorbed in the upper 10 meters of depth and 99.5% is absorbed by 100 meters (Pickard and Emery, 1982). In more turbid water the absorption occurs at even shallower depths. The attenuation of sunlight as described by Beer's law would suggest that a thermocline from the surface down should occur with no homogeneous mixed layer. To explain the mixed layer as a "slab," one must assume turbulent mixing. The source of the turbulent kinetic energy that mixes the upper ocean is the result of wind-shear production. The formation of the mixed layer was explained by Kraus and Turner (1967) using a turbulent kinetic energy equation.

C. SURFACE FLUXES

The Kraus and Turner model has provided the basis for a number of mixed layer models. The most important idea of Kraus and Turner was the suggestion that the mixed layer could be described without the need for models with three dimensional eddy resolving power. The advantage of this assumption is that it permits the use of less costly one-dimensional models. The assumption of one-dimensionality hinges on the validity of two hypotheses as stated by Garwood (1979):

- vertical mixing within the mixed layer is in response to *local forcing*.
- the mechanical energy budget is the key to understanding mixed layer dynamics.

The heat flux across the sea surface, Qt, is given by:

$$Qt = Qs + Qb + Qe + Qh \qquad (3.1)$$

where Qs is incoming solar radiation, Qb is outgoing long-wave radiation, Qe is the latent or evaporative heat flux, and Qh is the sensible heat flux. Qs is essentially described by an astronomical model but is complicated by the need for knowledge of cloud amount, thickness and optical properties. Qb is governed by the Stephan-Boltzman law which must be modified to include a radiative transfer equation for the presence of clouds which absorb and re-radiate long wave radiation. The turbulent fluxes, Qe and Qh, are important terms but difficult to measure. Bulk aerodynamic formulas are used to compute these quantities for ocean models.

Wind mixing can cause penetrative convection of thermal energy through some or all of the mixed layer. Forced downward flux of heat will cause significant changes to the mixed layer by entrainment mixing at the base of the mixed layer. Wind stress, τ may be related to the friction velocity in the air (u*) and ocean (U*), respectively:

$$\tau = \rho\, u^{*2} = RU^{*2} \qquad (3.2)$$

Here ρ and R are the densities of the air and water. The values of friction velocity characterize the scales of turbulent velocities. The stress is itself continuous across the air-ocean interface. Friction velocity in the air is related to wind speed by the bulk aerodynamic formula 3.3,

$$u^{*2} = C\, u^2, \qquad (3.3)$$

where u is the wind speed, and C is the momentum drag coefficient. The cube of the friction velocity in the ocean is used to parameterize the shear production of turbulent kinetic energy in the ocean's mixed layer.

D. NUCLEAR WINTER CONSIDERATIONS

For a nuclear winter scenario, it can be expected that ocean temperatures will decrease because of reduced solar radiation (Qs reduced in 3.1). While Qs may be reduced, the magnitude of Qb, (a heat loss term) is also reduced, thus partially countering the effect of reduced sunlight. For a summer situation, however, the net effect is always a *reduction* of the net downward heat flux into the ocean. This should not only serve to cool the mixed layer directly, but it should increase the amount of vertical turbulent mixing by convective motions, and this will tend to enhance further the cooling of the mixed layer through increased entrainment of cold water from below the mixed layer.

In a wintertime situation the effects on the mixed layer from a nuclear winter will be less significant than in a summertime situation. First, the amount of Qs reduced by smoke will be smaller in winter simply because the days are shorter (assuming war in the winter hemisphere). Secondly, for equal wind stresses on the ocean and, therefore, equal production of turbulent kinetic energy, the effect will be

greater in summer than in winter because the mixed layer is characteristically shallower in summer and less turbulent kinetic energy is needed to penetrate below the mixed layer and entrain colder water. For these reasons, a summertime ocean structure is studied here.

IV. THE EXPERIMENT

A. THE ATMOSPHERIC DATA

The atmospheric forcing data for the "nuclear winter" and "control" cases came from model simulations using a version of the Oregon State University (OSU) two-level GCM model documented by Ghan et al. (1982). This model has a modified solar radiation package and is coupled to a particle transport model known as GRANTOUR developed by Walton and MacCracken (1984). The OSU model is a development of the Mintz-Arakawa GCM formulated in the early 1960's at UCLA.

The model uses prescribed orography, ground surface type, SST and sea ice on a four degree latitude by five degree longitude grid. SST is held constant. The surface is categorized into nine types:

- woodland, grassland and cultivated areas
- forest land
- steppe and grasslands
- steppe desert
- desert
- tundra, mountain, taiga and land ice
- sea ice
- water

The principle variables of the boundary layer used for this study are

- Qs, solar radiation reaching the surface
- Qb, long wave radiation given up by the ocean surface
- Qh, sensible heat flux
- Qe, latent heat flux
- τ, wind stress
- P, precipitation rate

The turbulent flux of momentum, sensible heat, and moisture in the atmospheric boundary layer of the model are parameterized by bulk aerodynamic formulas. These are

$$\tau = \rho \, C1 \, u \, v \tag{4.1}$$

$$Qh = \rho \, C2 \, Cp \, u \, (Ts - Ta) \tag{4.2}$$

$$Qe = \rho \, L \, C3 \, u \, (q^*(Ts) - q) \tag{4.3}$$

- ρ is air density
- v is the surface wind speed
- u is an effective surface wind speed which includes a gustiness parameter
- C1, C2 and C3 are a drag coefficients which are a function of v. In this version of the model C1 = C2 = C3.
- Cp is the heat capacity of water
- q is the water vapor mixing ratio (q* is saturated and a function of Ts)
- Ts is the sea-surface temperature (SST)
- L is the latent heat of vaporization

The surface wind is computed as a function of the predicted large scale wind components at the bottom of the two model layers. Boundary processes are modified by both penetrating and low-level convection such that the moist static energy at the lower model layer becomes the moist static energy of the boundary layer when convection conditions are met.

Both large scale, frontal-type precipitation and convective-type precipitation are simulated by the model. Large scale precipitation occurs whenever the water vapor mixing ratio exceeds the saturation mixing ratio. The increase in temperature due to latent heat is accounted for

when condensation occurs. Precipitation which falls through the upper layer may evaporate as it passes though the lower layer. Precipitation which is formed in the lower layer falls to the ground.

Long wave radiation emitted from the ocean surface is given by the black body flux at the surface using the Stephan-Boltzman law. The model takes into account the long wave radiation that is emitted downward from clouds into the ocean.

The solar radiation routine within this version of the model uses a delta-Eddington model to allow the inclusion of massive amounts of smoke for nuclear winter simulation. For solar transmitance and absorption calculations two representative wavelengths, 0.51-μm and 1.55-μm, were used to allow computational efficiency. The 30-day experiment used perpetual July conditions with no change in the solar declination due to the Earth's orbit around the sun.

GRANTOUR is a Lagrangian trace species transport model which was coupled to the atmospheric model. The model accounts for dry deposition, coagulation, precipitation scavenging and transport of the smoke injected into the atmosphere.

The nuclear winter simulation which provided the atmospheric data used in this study, reported by Ghan et al. (1985), was performed at Lawrence Livermore National Laboratory. A 150 Tg summertime injection of smoke from fires following nuclear attacks in Europe, Asia and North America was used to initialize the nuclear winter (or "smoke") simulation. A control run, with no smoke injection, was also made. The initial distribution of smoke in terms of optical depth is shown in Fig. 4.1. Two types of particles were used in the experiment; 2/5 of the particles were larger than 1-μm in diameter and 3/5 were submicron. The vertical distribution is initially one of constant mixing ratio with height.

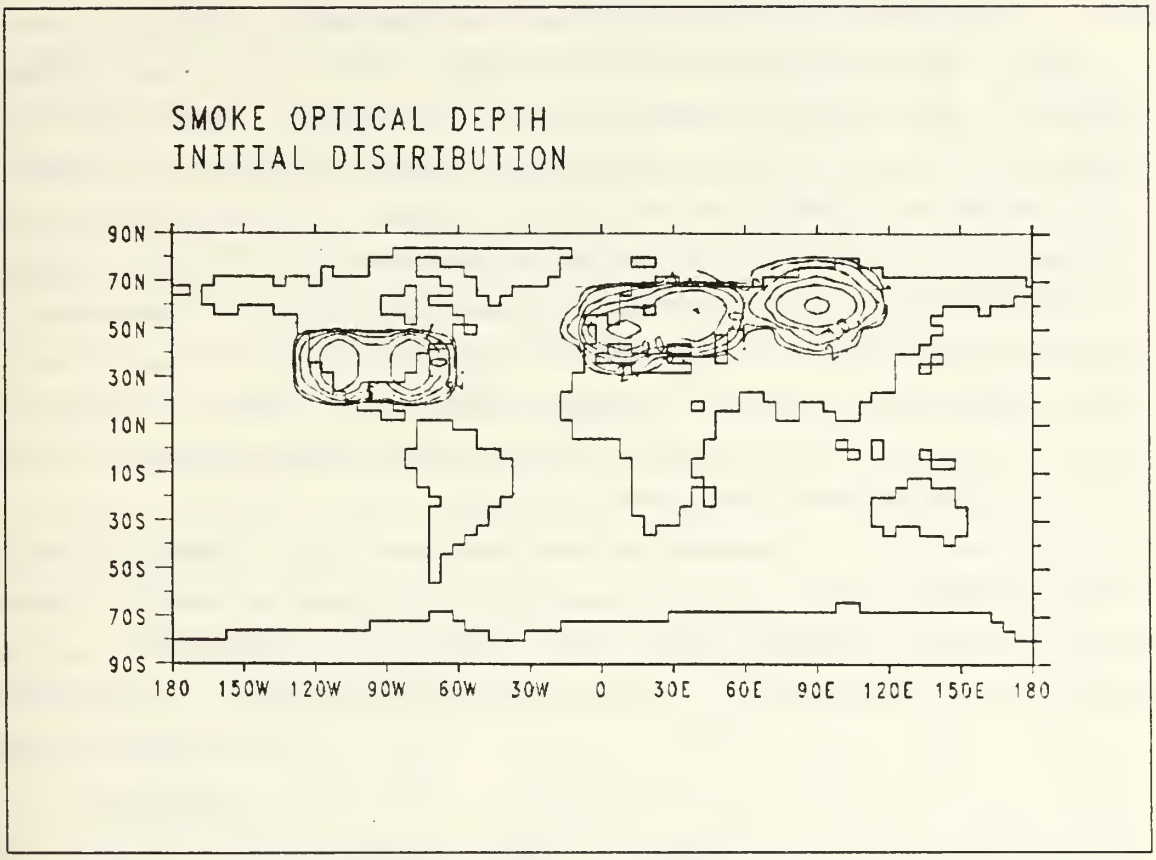

Fig. 4.1 Initial Optical Depth (from Ghan et al., 1985).

Six-hourly values of Qs, Qb, Qe, Qh, τ, and P for control and smoke runs for the 30-day simulation period at six locations are the basic forcing data for this oceanic "nuclear winter" experiment. These values were directly input into the ocean model. As might be expected, the fluxes (heat and stress) generated by the atmospheric model during the control run showed some disagreement with July climatological values at some of the oceanic locations used in the ocean experiment. In order to provide a more realistic control *and* nuclear winter simulation in the ocean, "biased" surface fluxes were developed and used in a separate set of experiments described below. A total of 24 separate ocean runs were done: control and smoke at six locations with biased and unbiased fluxes.

B. THE OCEAN PLANETARY BOUNDARY LAYER MODEL (OPBL)

The OPBL model used for this study is from Garwood (1977). The Garwood model uses a turbulent kinetic energy budget to describe the generation and dissipation of turbulent kinetic energy in the upper ocean. It is a vertically integrated or bulk model that diagnoses the flux of energy at only the top and bottom of the mixed layer. The model is closed by parameterizing the second and third order terms of the turbulent kinetic energy equation. The inclusion of higher order terms enables realistic parameterizations of dissipation and entrainment mixing.

The model is characterized by two important features. First, the amount of wind energy that goes into the turbulent kinetic energy used for mixing is dependent on the stability of the layer. That is, wind mixing is a function of the ratio, h/L, where h is the depth of the mixed layer and L is the Obukov length scale. Secondly, dissipation of turbulent kinetic energy is based on the value of a local Rossby number, Ro,

$$Ro = U^*/hf, \qquad (4.4)$$

where f is the Coriolis parameter, and U^* is the ocean friction velocity. Garwood has pointed out that f is an important time scale in the internal structure of the mixed layer. The model uses separate equations for the vertical and horizontal components of turbulent kinetic energy. This allows explicit control of the relative distribution of turbulent kinetic energy between the three turbulent velocity components in the mixed layer.

For this experiment, the Garwood model was initialized with a temperature and salinity profile for the upper 200 meters. A different thermal and salinity profile was used at each location. The profiles were obtained from the Fleet

Numerical Oceanography Center (FNOC), Monterey, CA. The FNOC profiles are operational climatological profiles derived from the Navy's Extended Ocean Thermal Structure (EOTS) analysis system which consists of 26 global horizontal temperature fields between 0 and 400 meters depth for each month of the year. The salinity profiles were also obtained from FNOC and are based on a digitized version of the U.S.S.R Navy *World Ocean Atlas* (1974). No climatological salinity profile was available for point six (10°N 150°W), so a simple isohaline salinity profile was used. Each thermal profile was modified to have an explicit jump discontinuity in temperature to represent an entrainment zone. The temperature jumps were taken from climatological mixed layer depth fields for July from Bathen (1972) and Robinson (1976). FNOC data were used exclusively at point three (50°N 50°W).

C. PROCEDURE

The six-hourly biased (below) and unbiased values of the fluxes, the wind stress, and the precipitation rate from the GCM data were used to force the Garwood model. The Garwood model was run with one-hour time steps for six hours when it was then updated with the next six-hourly GCM data. This procedure was carried out for 720 hours.

Control (no smoke) and smoke (nuclear winter) runs were made at the six locations shown in Fig. 1.1.

- Point one : 50°N 150°W
- Point two : 50°N 150°E
- Point three : 50°N 50°W
- Point four : 30°N 150°W
- Point five : 10°N 150°W
- Point six : 30°N 125°E

These points were chosen to give mid-latitude, subtropical, and tropical representations as well as to give some indication of changes under different amounts of smoke, and between coastal and open ocean areas.

The GCM fluxes (Qs, Qb, Qe, Qh, τ) were analyzed and compared with typical climatological values from Esbensen and Kushnir (1981). Ocean model "biased fluxes" were constructed such that the average values of the fluxes from the control run were the same as the climatological values of Esbensen and Kushnir. Using the fluxes from the control run, the bias factor B was computed from 4.5,

$$B \cdot GCM = CV, \tag{4.5}$$

where GCM denotes a 30-day time average of the appropriate GCM flux (heat or stress), and CV is the climatological value. One disadvantage of this technique is that the variability of the GCM data is affected in addition to the mean. The bias factors obtained are shown in Table 1. Thus, for example, in the "bias" ocean run the fluxes from the GCM runs (control and nuclear winter cases) were multiplied by the factors shown in Table 1. Most of the values are fairly close to unity, indicating that, in general, the GCM fluxes are close to the climatological values.

TABLE 1
BIAS FACTORS USED

Point	Qs	Qb	Qe	Qh	τ
1	0.54	1.00	1.00	1.00	2.10
2	0.68	1.67	1.50	0.45	0.90
3	0.67	0.83	5.00	0.45	0.42
4	0.72	1.06	1.62	1.00	2.08
5	0.96	0.95	0.73	0.38	1.02
6	0.75	0.49	0.59	1.00	0.84

The Garwood model requires several input variables including Qs, Qb, Qe, Qh, τ, P and E (evaporation rate), as well as the multiplicative biases for Qs, Qb, Qe, Qh and τ.

as necessary. An extinction coefficient and a value which represents the fractional amount of solar radiation that penetrates the first meter of the ocean were also specified to be 0.10/m and 0.05 respectively for each point for all runs. A minimum stress value of either 0.010 N/m^2 or 0.005 N/m^2 was used to override and replace any stress that was less than this value. This is justified as an rms gustiness factor. A value of 0.010 N/m^2 corresponds to a wind speed of 2.5 m/s. The minimum value was 0.005 N/m^2 for all points except points four and six which had long periods of low wind stress which caused unrealistic shallowing of the mixed layer depth (MLD) and warming of SST. Evaporation rate at each time step was computed from the value of Qe at the same time step using the conversion in 4.6, where $R = 1.21 \cdot 10^3$ kg/m^3 and $L = 2.5 \cdot 10^6$ J/kg.

$$E = Qe/ R L \qquad (4.6)$$

D. THE GCM DATA

The unbiased GCM fluxes are shown in Figs. 4.2 through 4.13. The values above the zero line represent a flux of energy into the ocean. The unbiased GCM wind stress data are shown in Figs. 4.14 through 4.19.

At all six points, the 30-day time average of Qs, biased and unbiased, is smaller in the smoke case than in the control case. The maximum reduction in average Qs is 67% at point three (50°N 50°W). The effect of this reduced sunlight at point three in lowering SST and deepening the mixed layer however is offset slightly by the decrease in average wind stress from control to smoke.

The difference in Qb for smoke and control cases is independent of SST because SST is a prescribed constant in the GCM used. The difference, Qb(smoke) - Qb(control) is a function of the downward longwave radiation from clouds.

Consequently, a larger Qb in the smoke case compared to the control case indicates a decrease in cloud cover, i.e., the control case is cloudier, over a 30-day time average, than the smoke case. This happens at points one (50°N 150°W) and two (50°N 150°E). In the opposite sense, extensive cloudiness occurs over the the remaining four points in the smoke case, which allows less upward flux of longwave radiation.

Upward latent heat flux is greater in the smoke case than in the control run at points one, two, three, and six presumably due to the flow of colder drier air over these locations. The greatest value of Qe(smoke) - Qe(control) is 236 W/m^2 at point six. This is most likely due to a monsoonal type flow of extremely colder drier air off Asia into the western Pacific in the smoke case for these locations (Fig. 1.1).

The same argument holds for the significant increase in Qh of 119 W/m^2 also at point six. Simple bulk aerodynamic considerations, with a wind speed of 10 m/s, imply an average temperature difference between the air and the water to be 12°C (water warmer).

A summary of the 30-day average total heat flux, Qt, across the ocean surface for each point in the biased/unbiased and control/smoke cases is shown in Table 2. Negative values denote a net loss of energy by the ocean. In all cases the smoke scenario shows less energy flux into the ocean than in the control case or more energy flux out of the ocean than in the control case.

The average wind stress was found to be dependent on the type of run, i.e., control, smoke, biased, or unbiased. The wind stress had a tendency to be higher during the smoke run and when the control wind stress was greater than the smoke case it was not significantly greater. Table 3 shows the 30-day time averaged wind stress values. Together, Tables 2 and 3 show the two most important factors in control of the mixed layer even though, in a strict sense, the

TABLE 2

30-DAY AVERAGE TOTAL ENERGY FLUX

Point	UNBIASED		BIAS	
	control	smoke	control	smoke
1	181*	102	83	28
2	186	20	95	-44
3	244	94	138	12
4	149	96	18	-2
5	-51	-99	0	-36
6	114	-347	122	-220

* All values in units of W/m^2

representation of wind stress should be made in a different way. The production of turbulent kinetic energy into the mixed layer is proportional to the the cube of the friction velocity, which implies that u^{*3} is proportional to $\tau^{3/2}$.

TABLE 3

30-DAY AVERAGE WIND STRESS

Point	UNBIASED		BIAS	
	control	smoke	control	smoke
1	.36*	1.02	.76	2.14
2	.50	.99	.45	.90
3	1.07	.85	.45	.36
4	.36	.81	.75	1.69
5	1.28	1.22	1.30	1.25
6	.89	1.71	.75	1.44

* All values in units of N/m^2

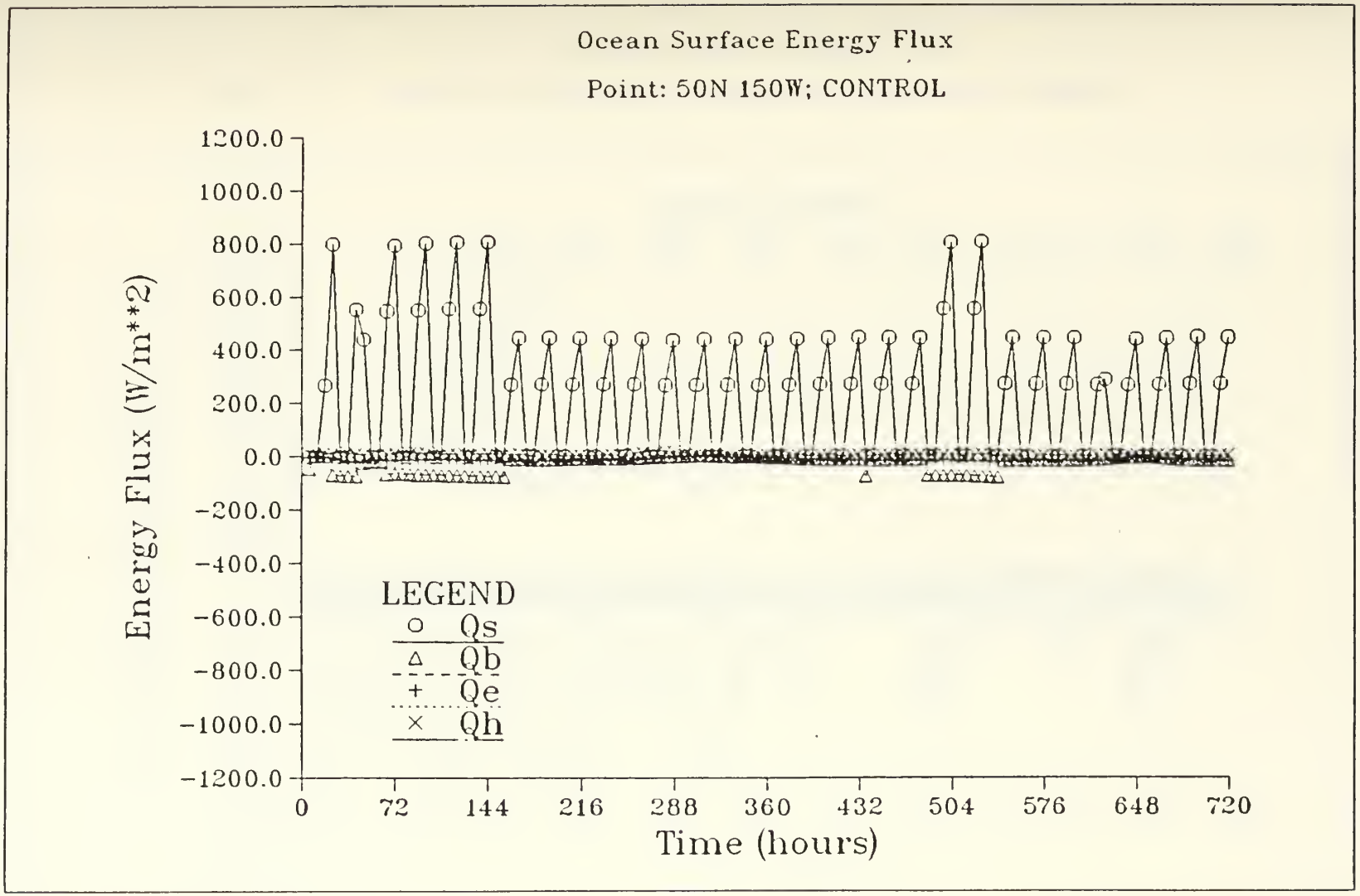

Fig. 4.2 Energy Fluxes at Point One (50°N 150°W) CONTROL.

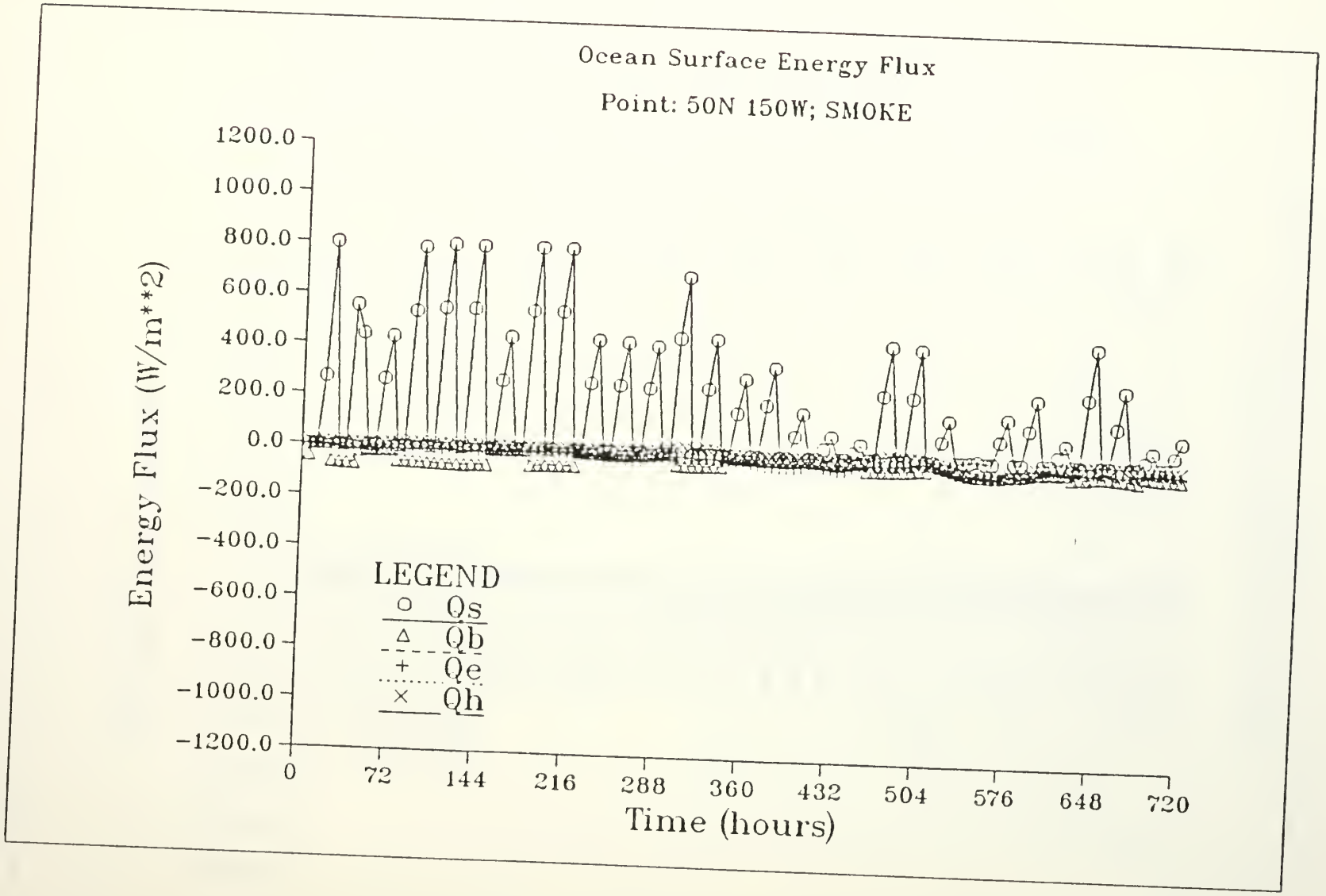

Fig. 4.3 Energy Fluxes at Point One (50°N 150°W) SMOKE.

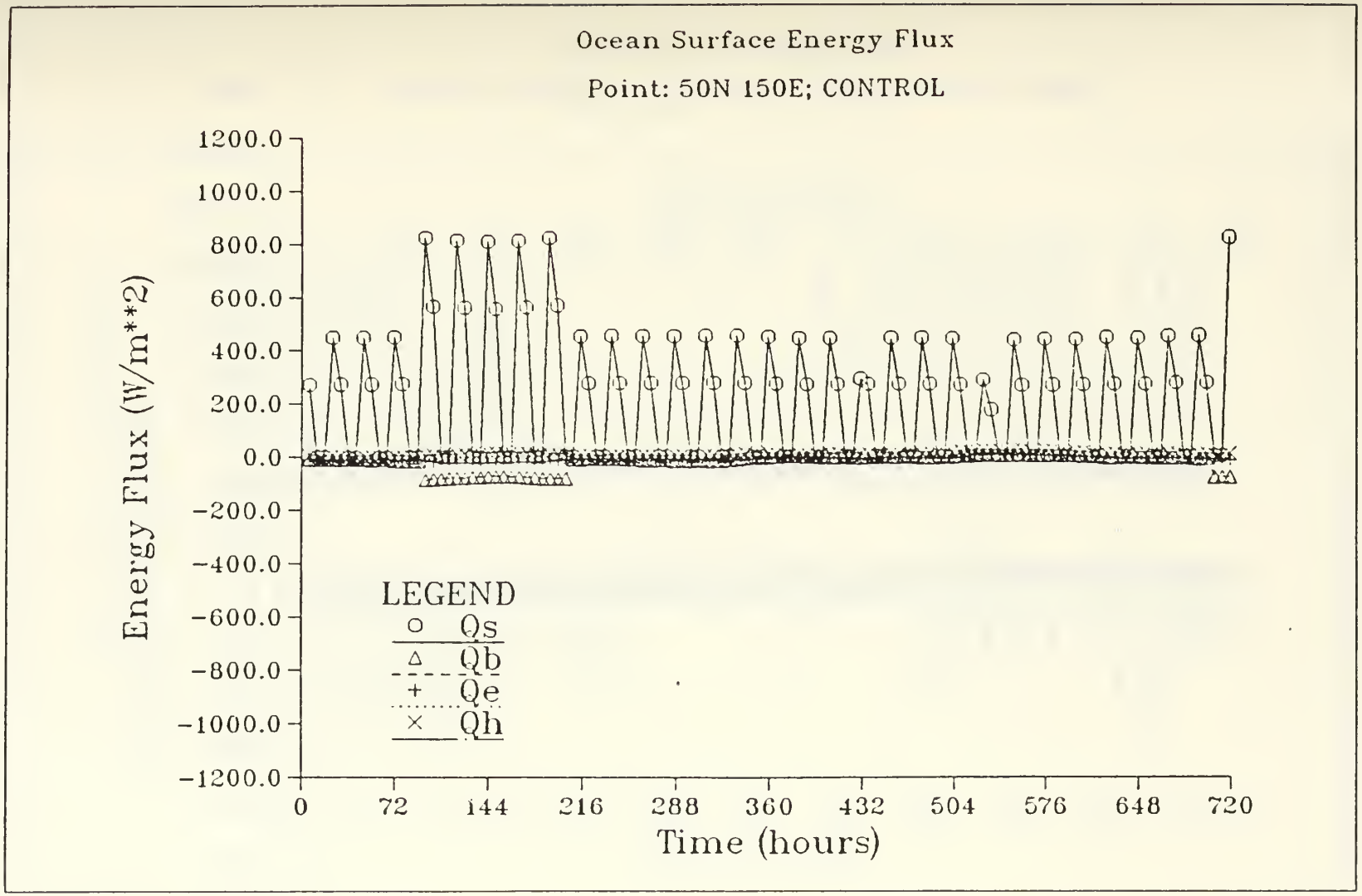

Fig. 4.4 Energy Fluxes at Point Two (50°N 150°E) CONTROL.

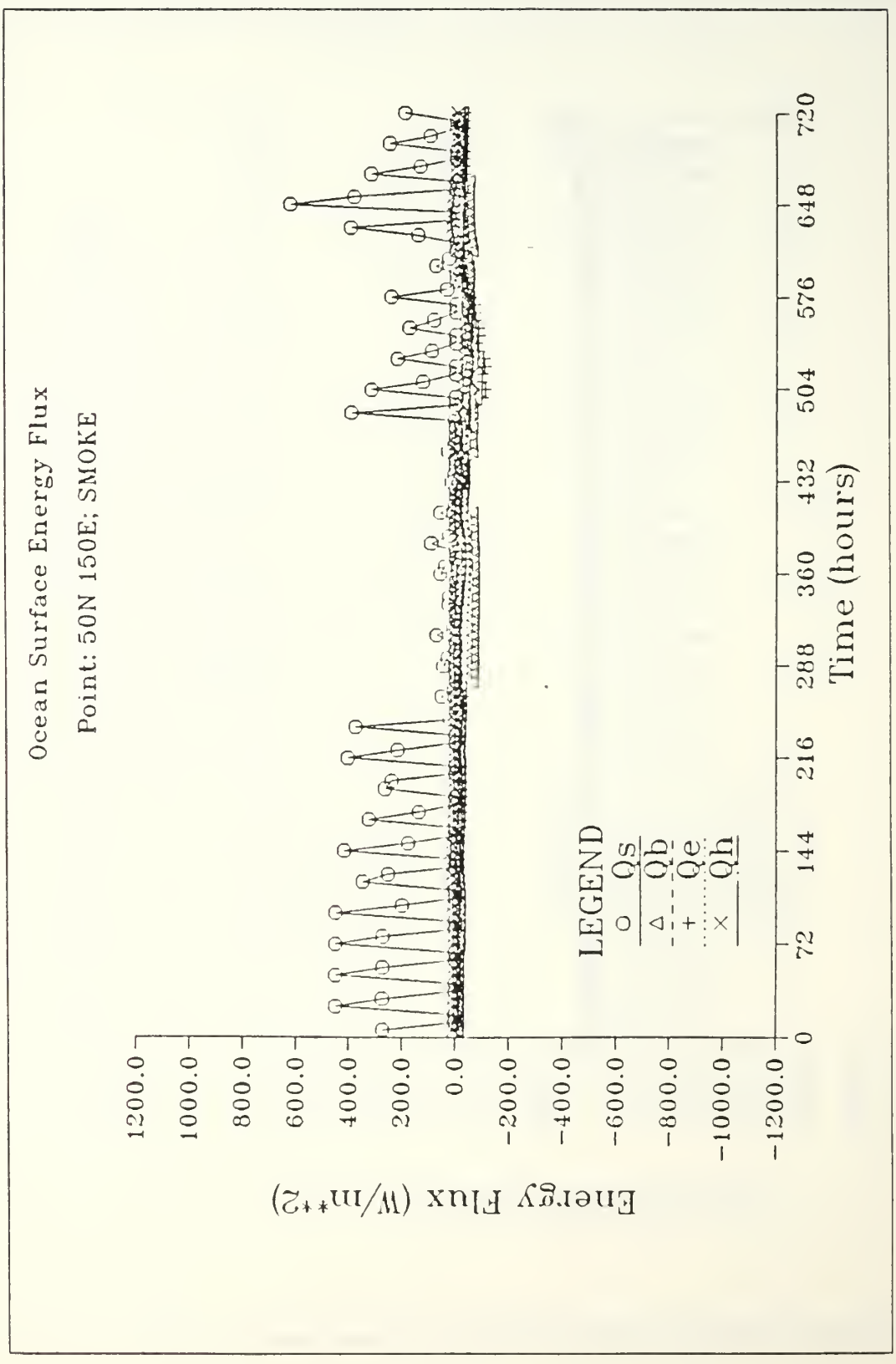

Fig. 4.5 Energy Fluxes at Point Two (50°N 150°E) SMOKE.

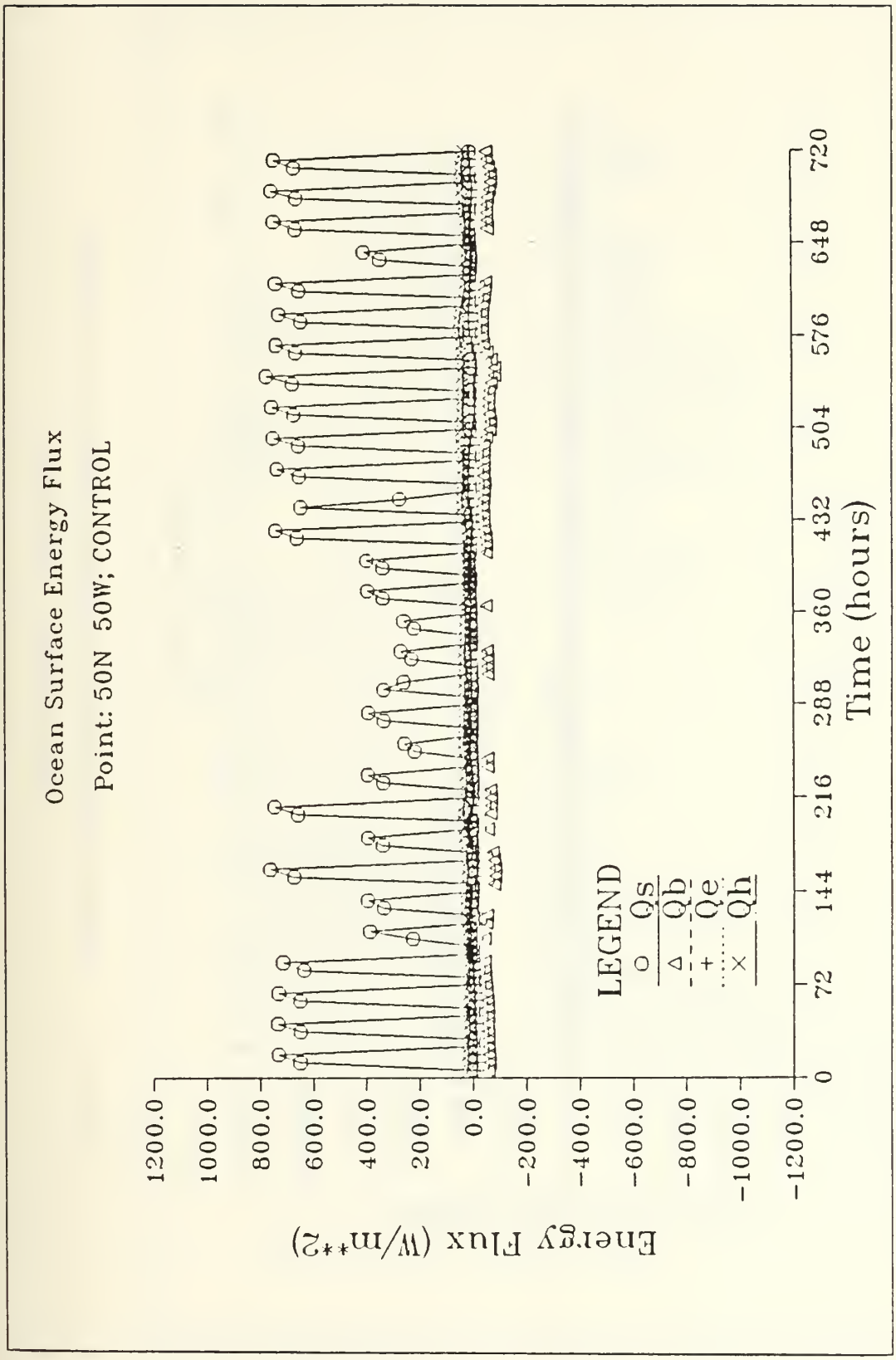

Fig. 4.6 Energy Fluxes at Point Three (50°N 50°W) CONTROL.

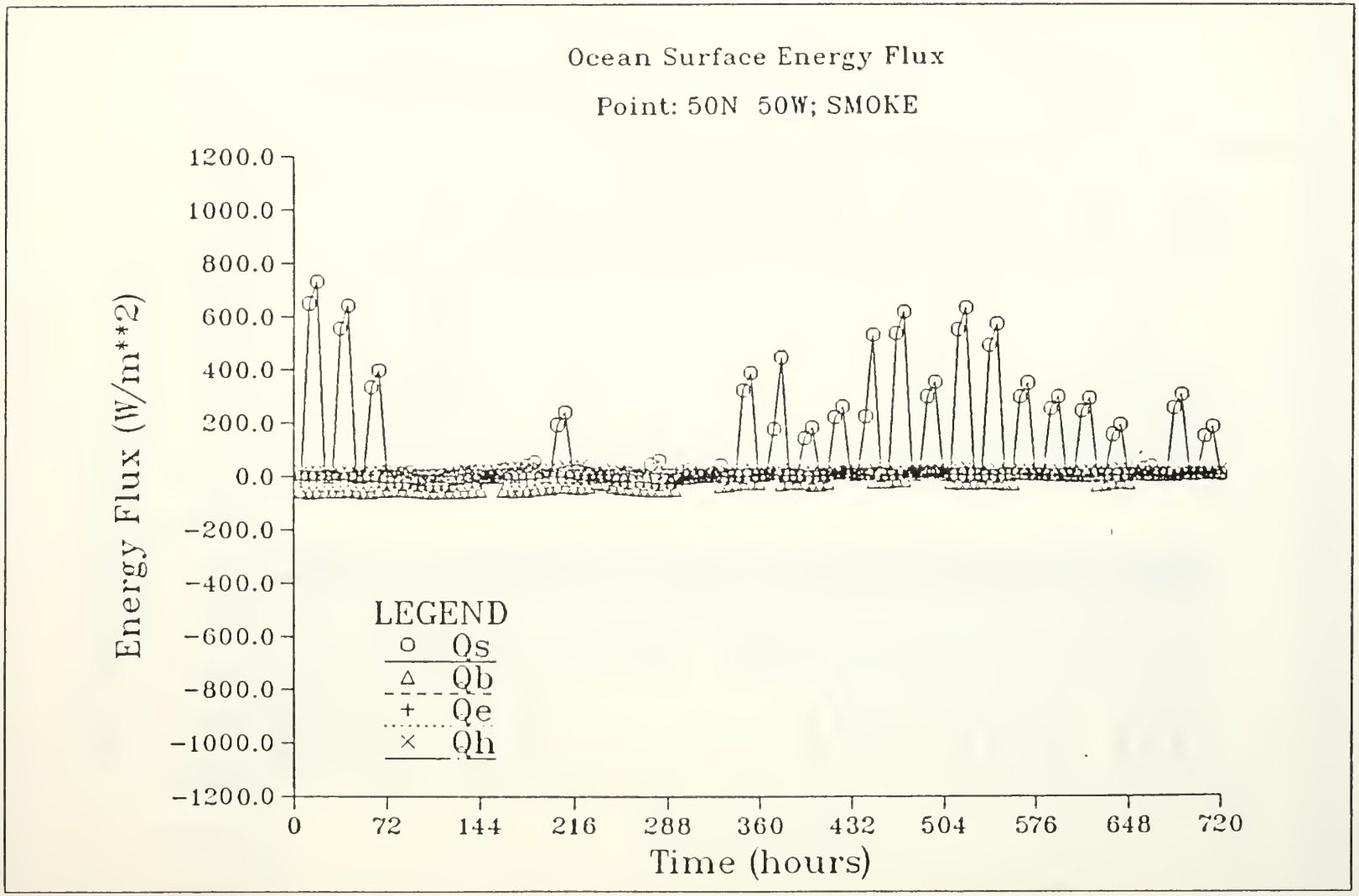

Fig. 4.7 Energy Fluxes at Point Three (50°N 50°W) SMOKE.

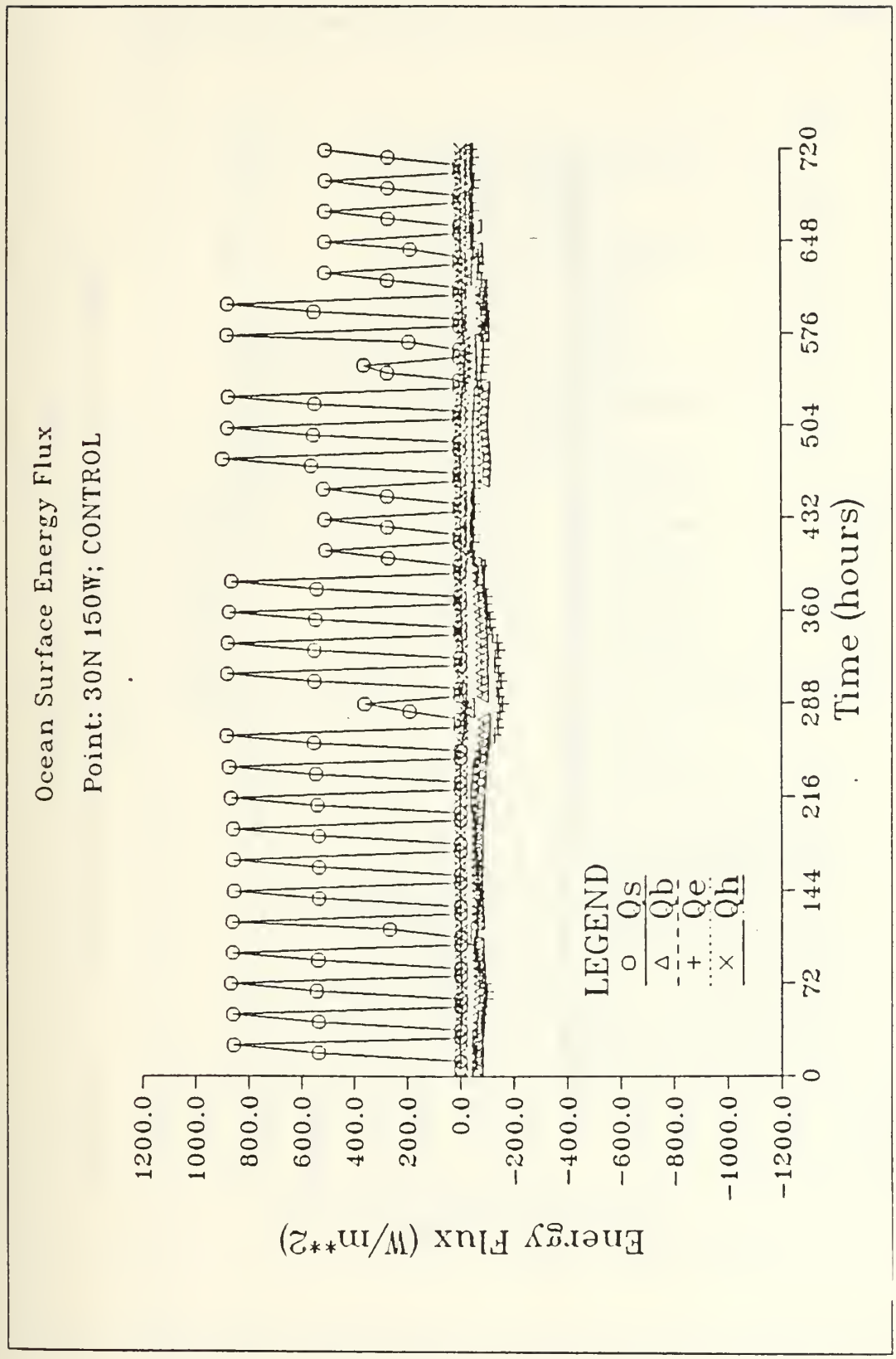

Fig. 4.8 Energy Fluxes at Point Four (30°N 150°W) CONTROL.

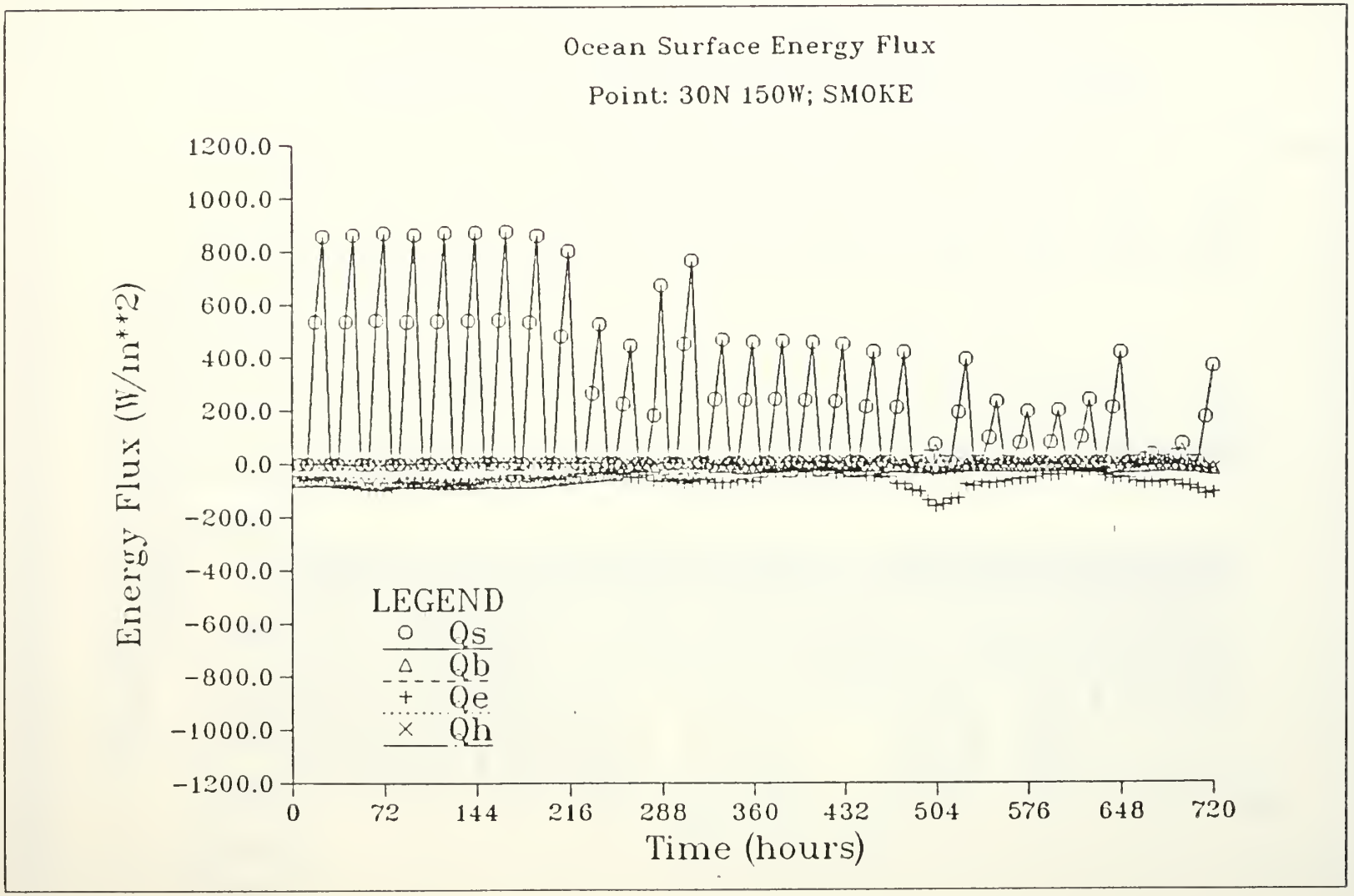

Fig. 4.9 Energy Fluxes at Point Four (30°N 150°W) SMOKE.

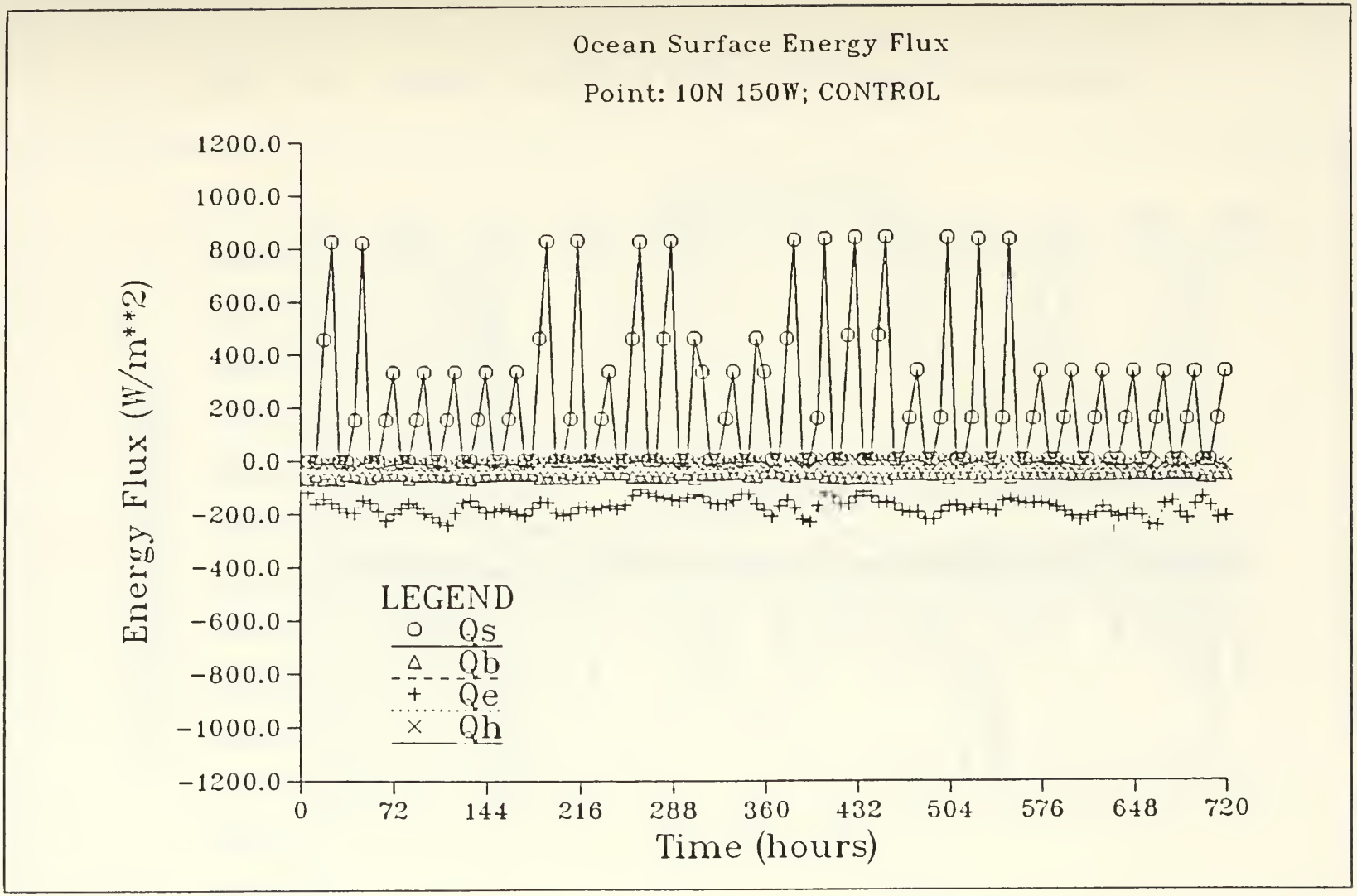

Fig. 4.10 Energy Fluxes at Point Five (10°N 150°W) CONTROL.

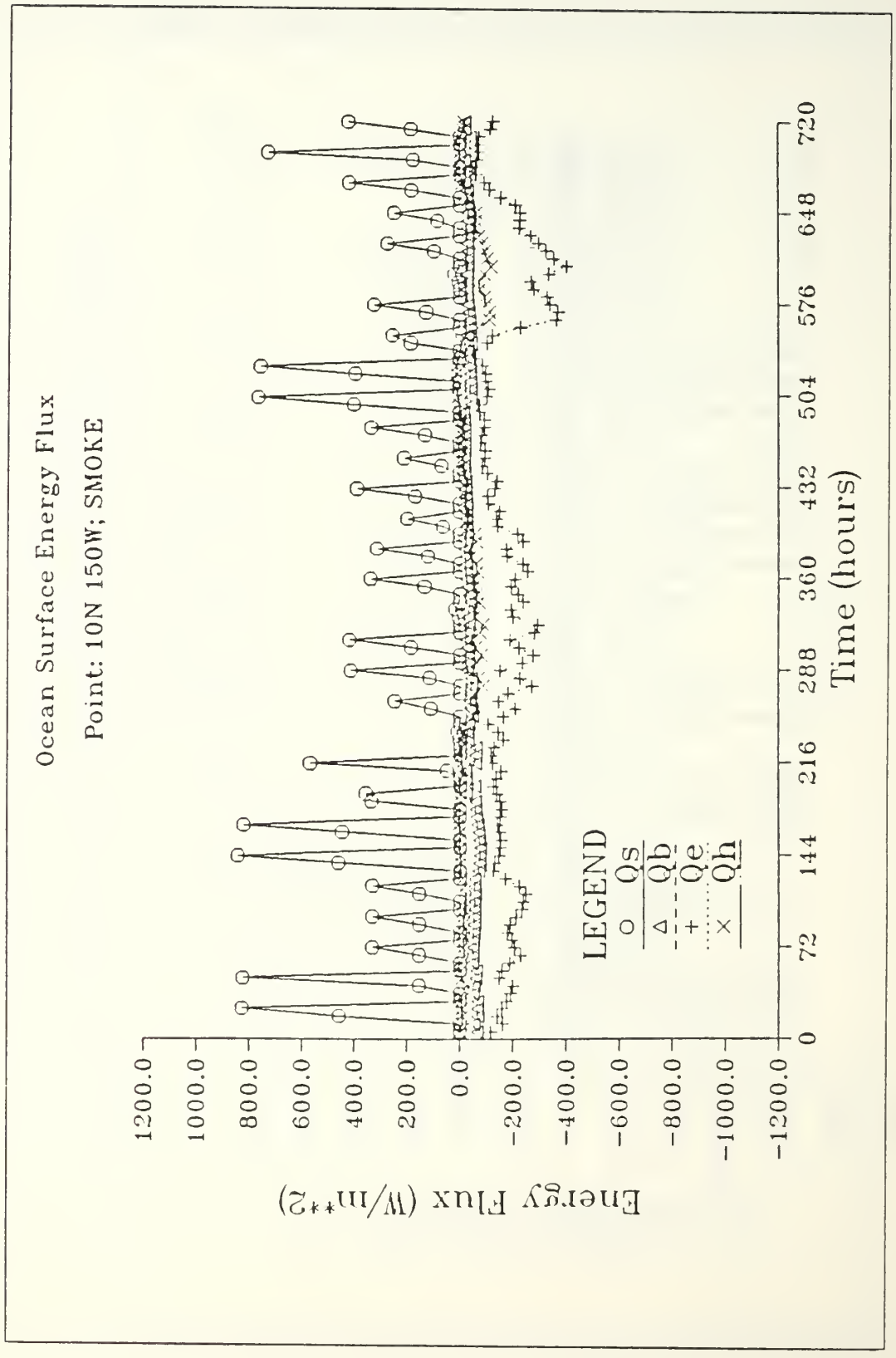

Fig. 4.11 Energy Fluxes at Point Five (10°N 150°W) SMOKE.

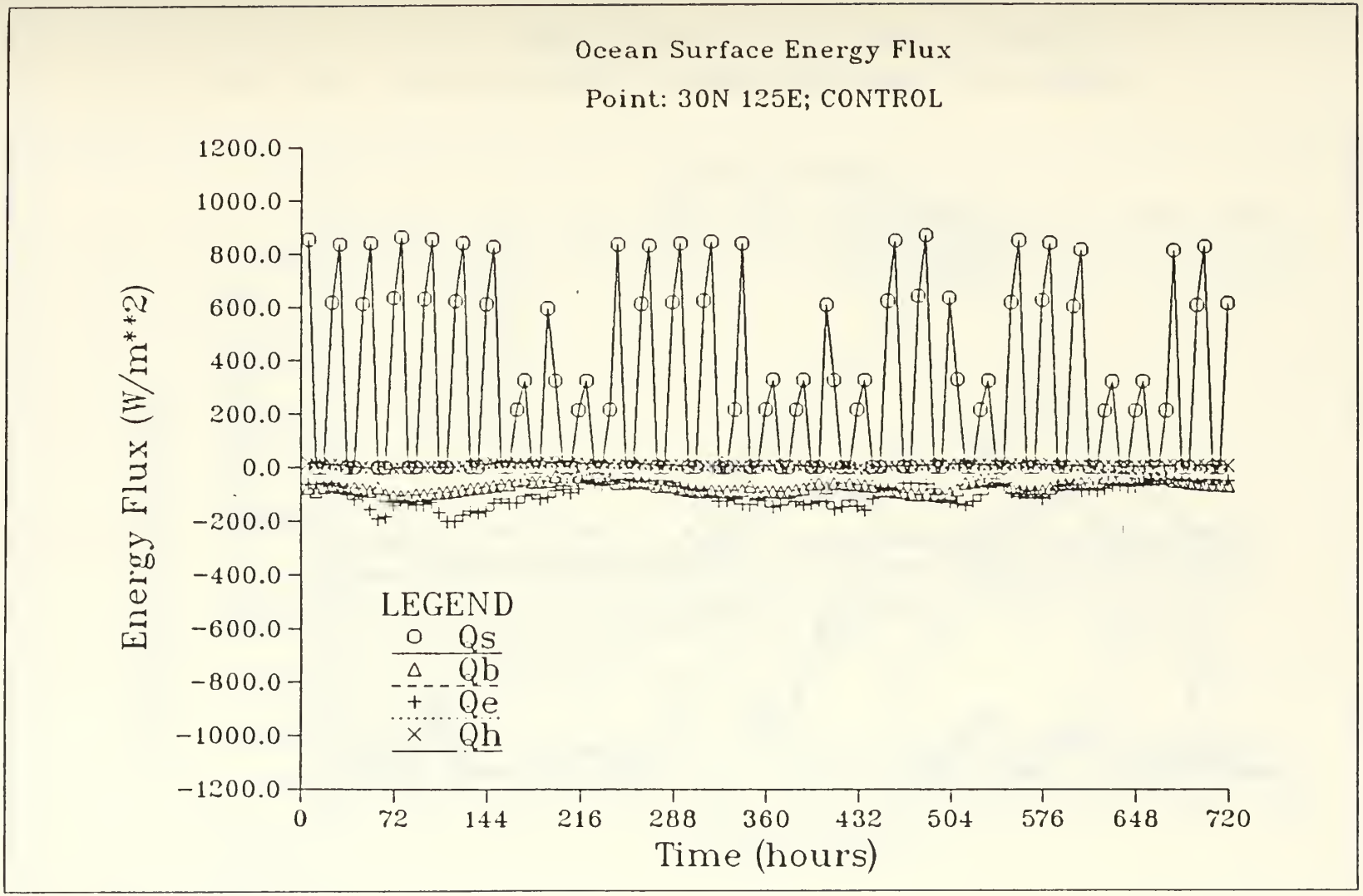

Fig. 4.12 Energy Fluxes at Point Six (30°N 125°E) CONTROL.

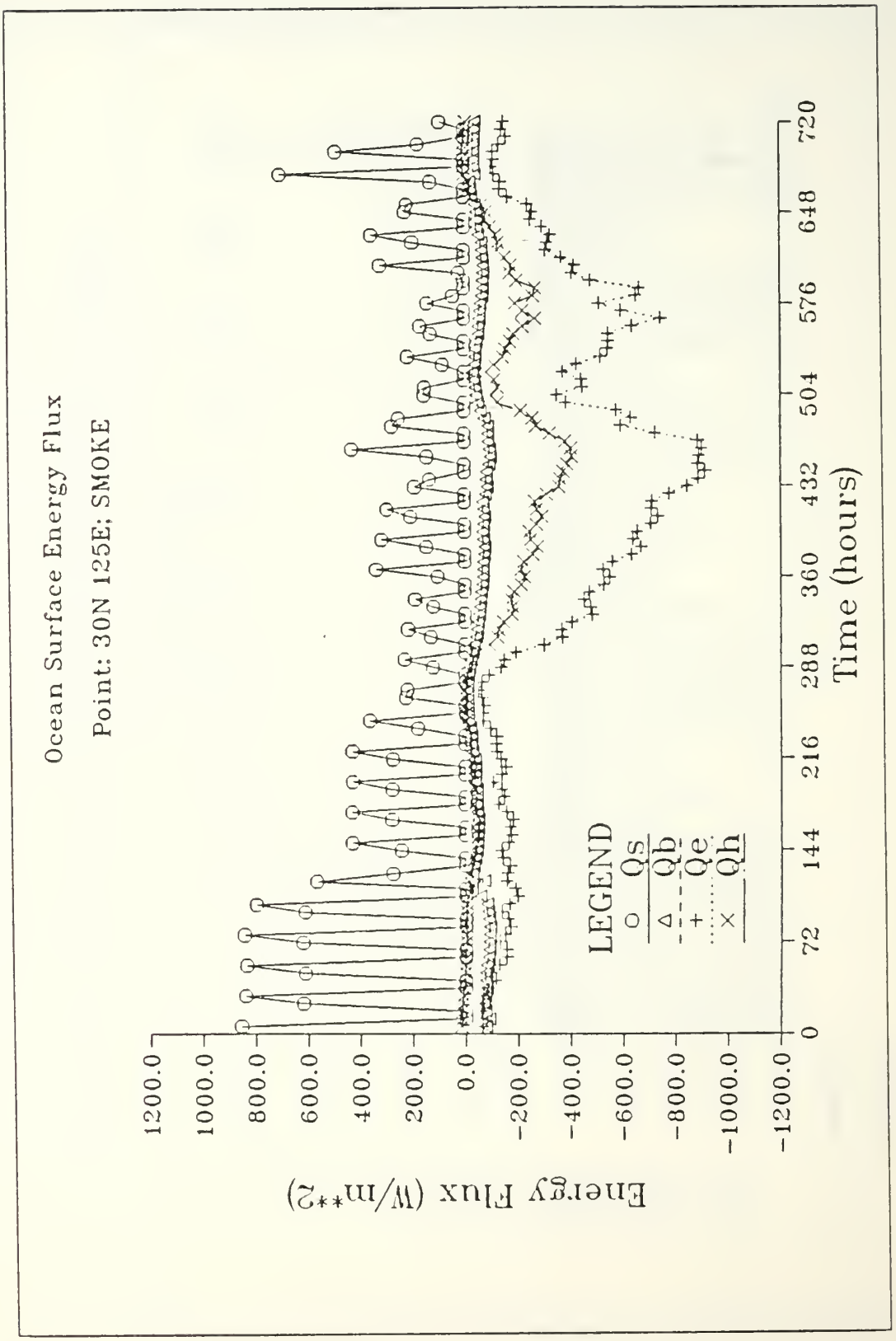

Fig. 4.13 Energy Fluxes at Point Six (30°N 125°E) SMOKE.

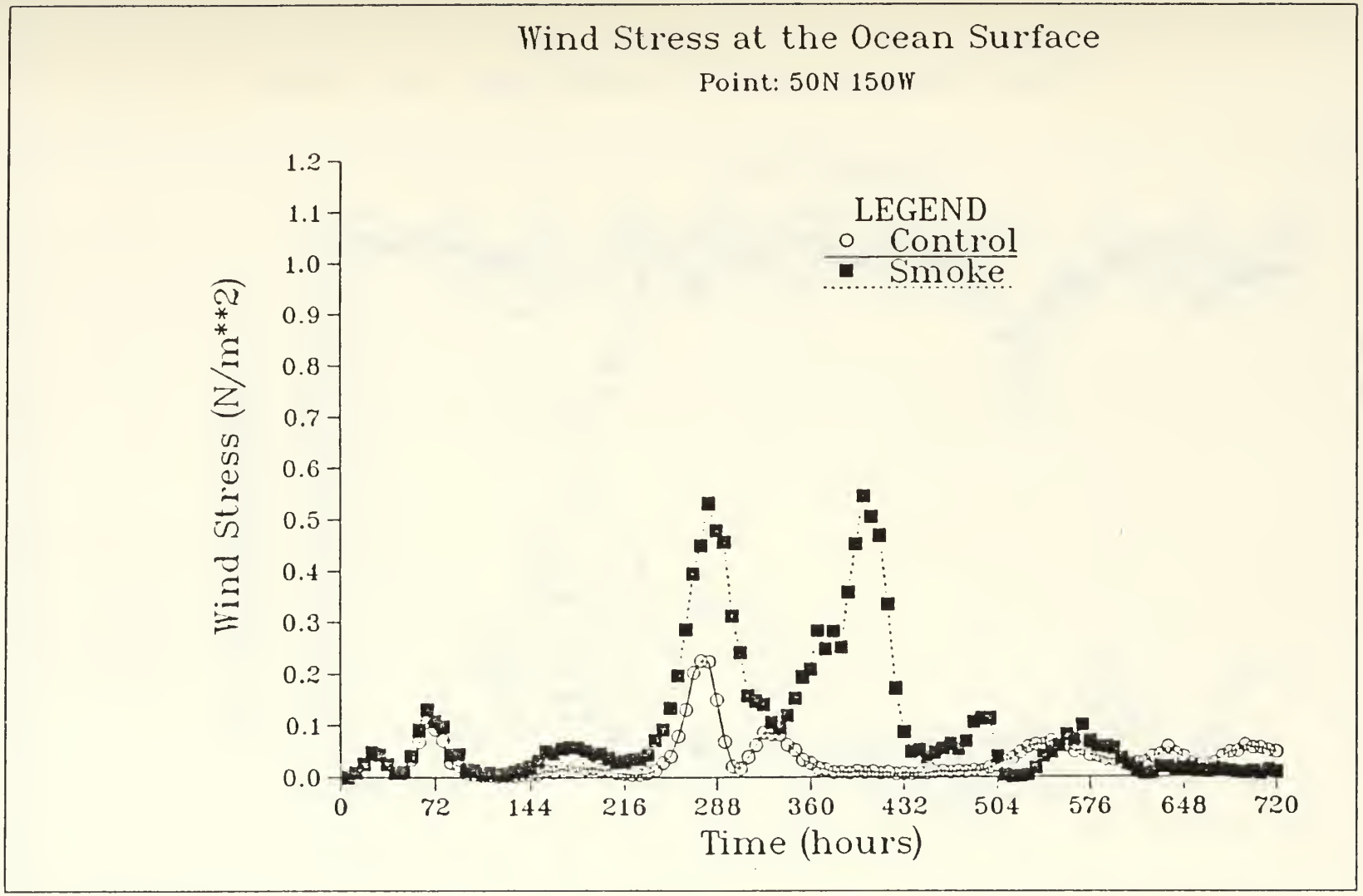

Fig. 4.14 Wind Stress at Point One (50°N 150°W).

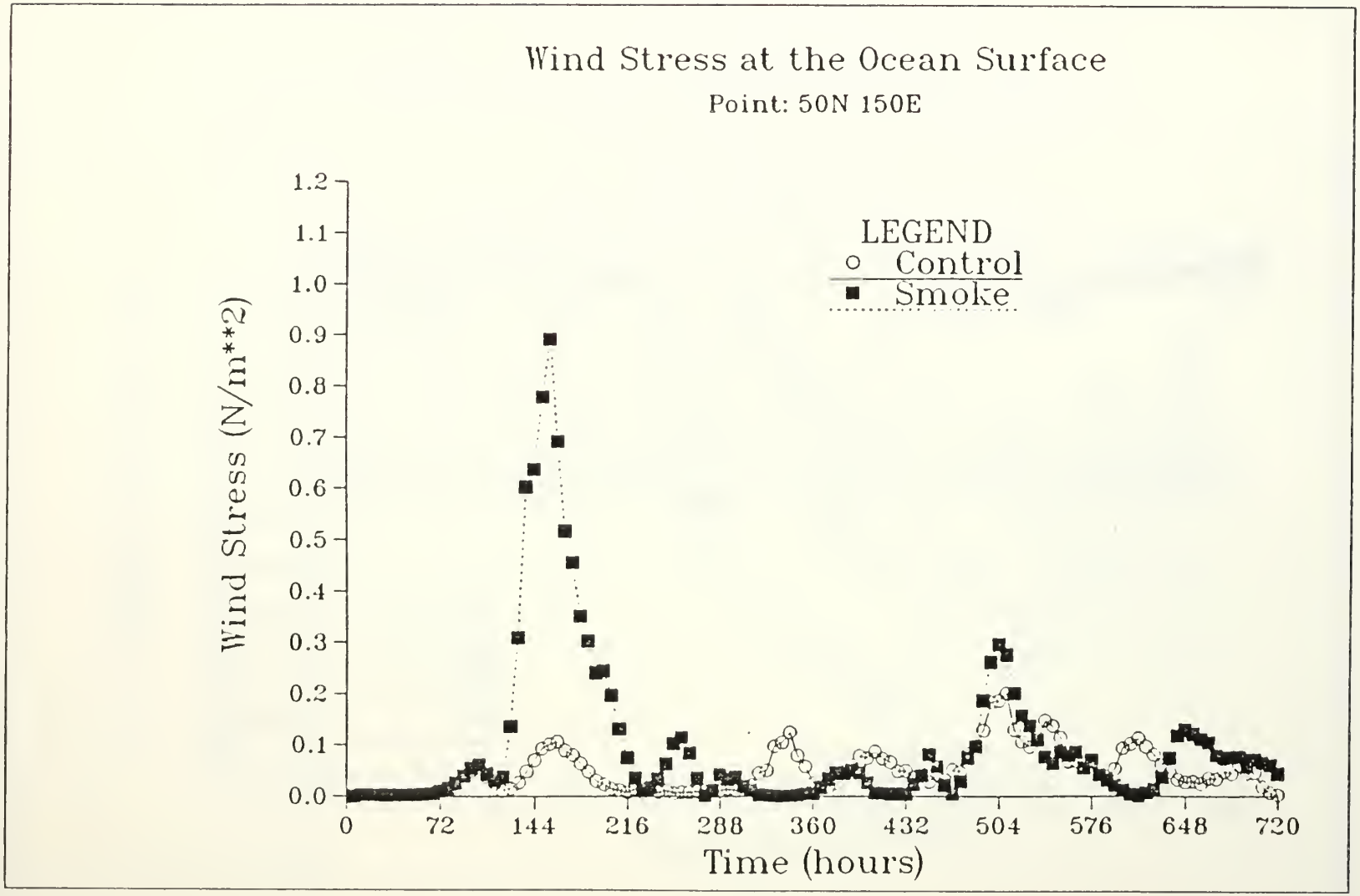

Fig. 4.15 Wind Stress at Point Two (50°N 150°E).

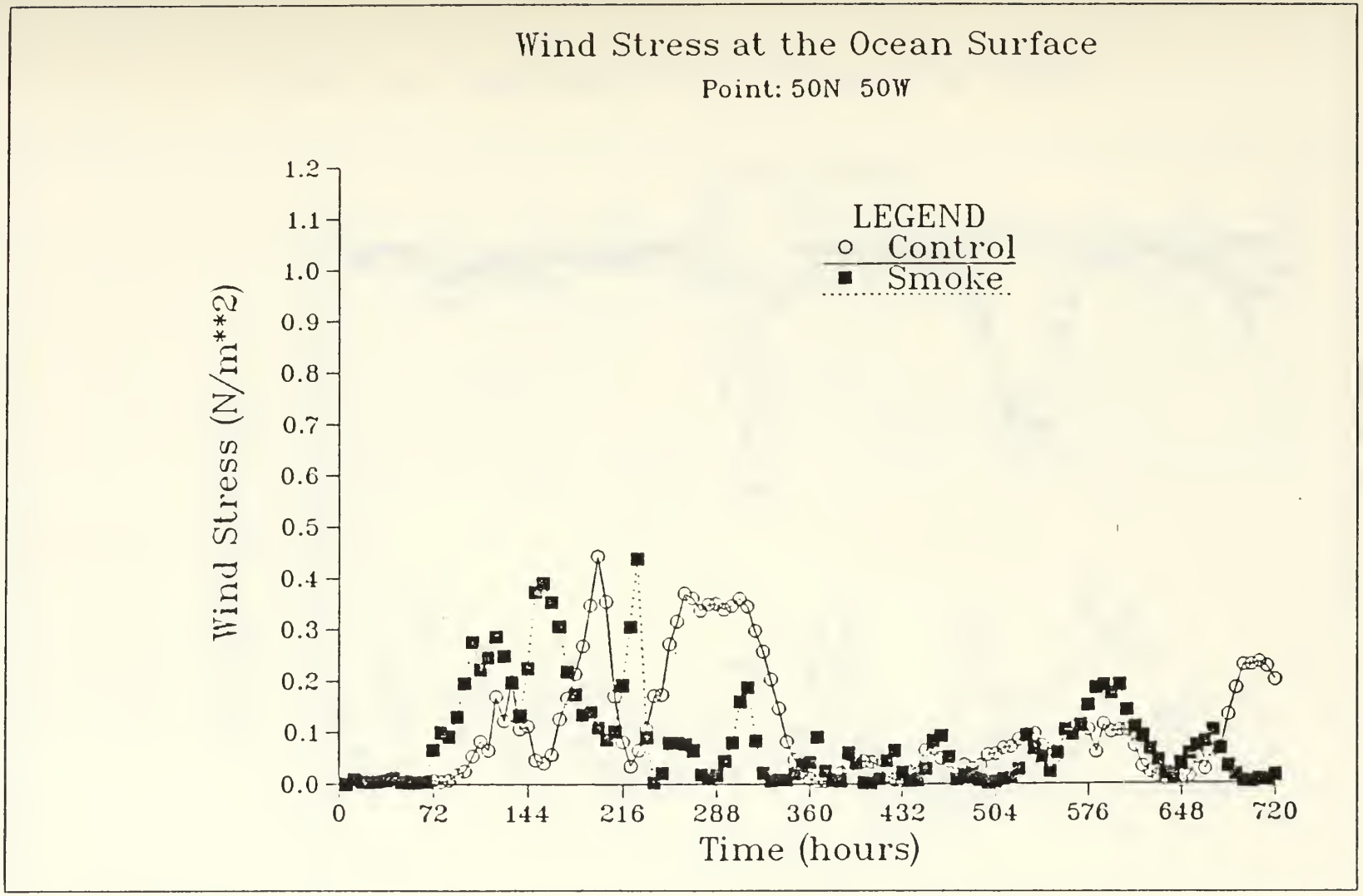

Fig. 4.16 Wind Stress at Point Three (50°N 50°W).

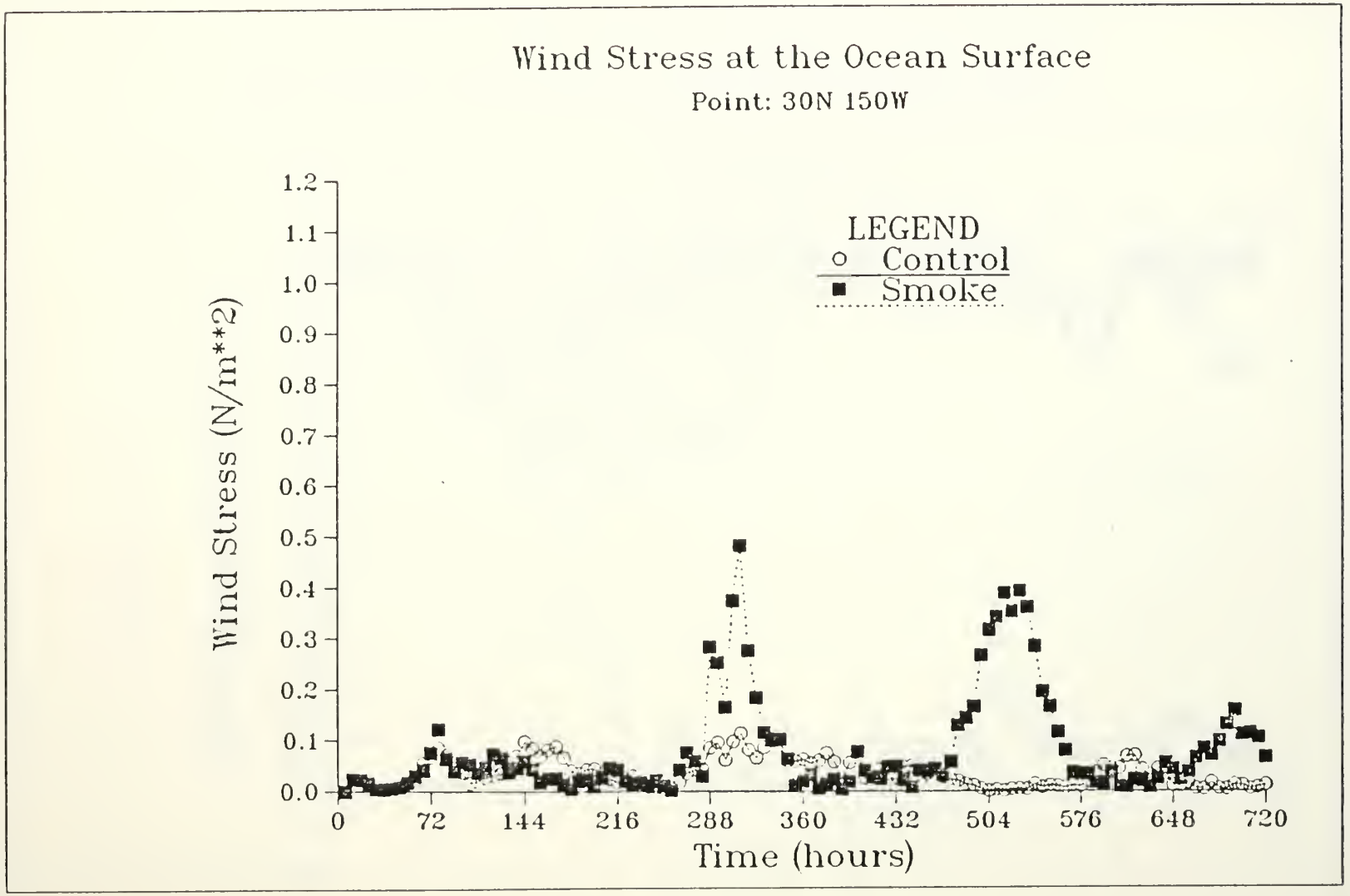

Fig. 4.17 Wind Stress at Point Four (30°N 150°W).

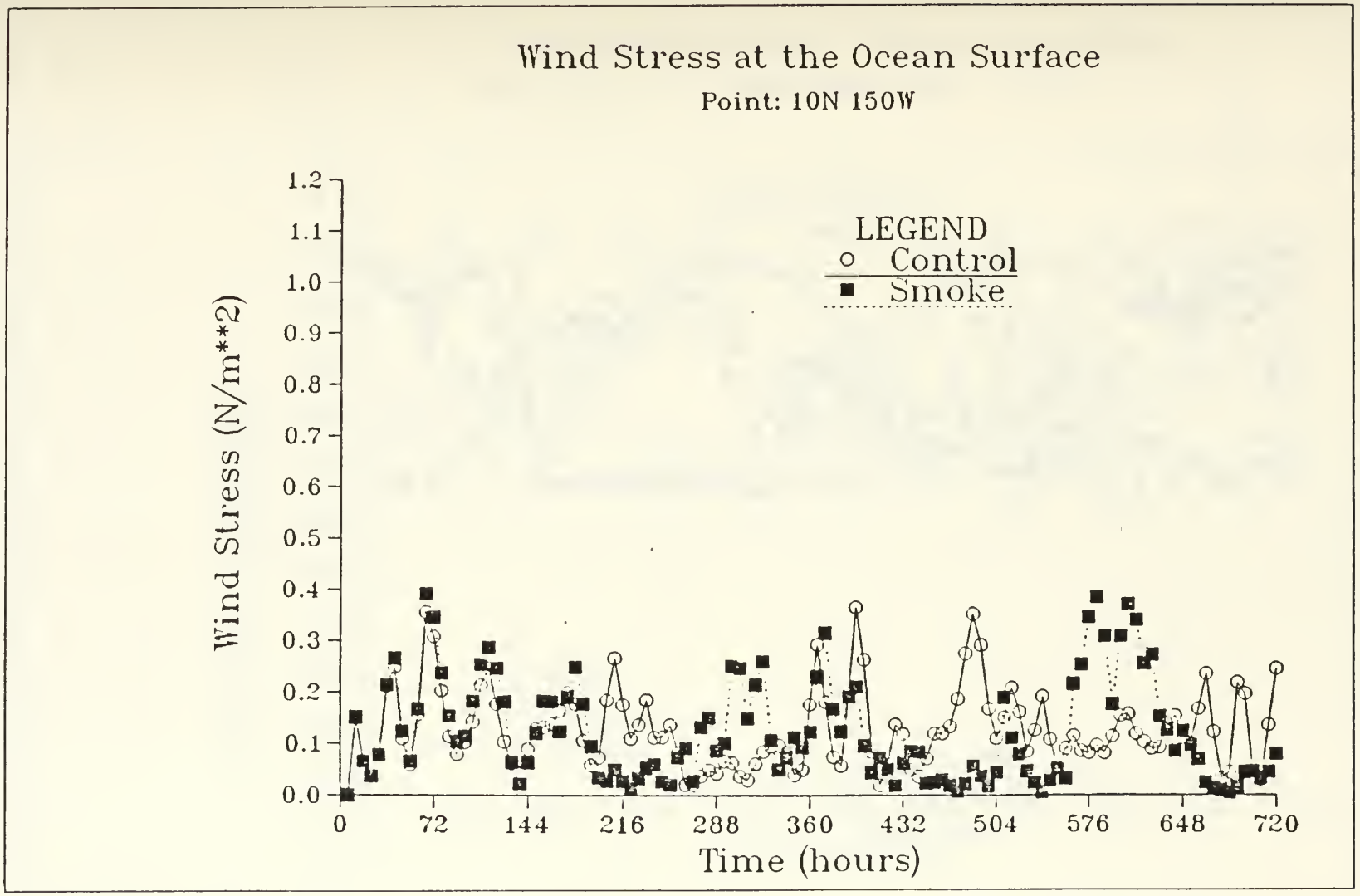

Fig. 4.18 Wind Stress at Point Five (10°N 150°W).

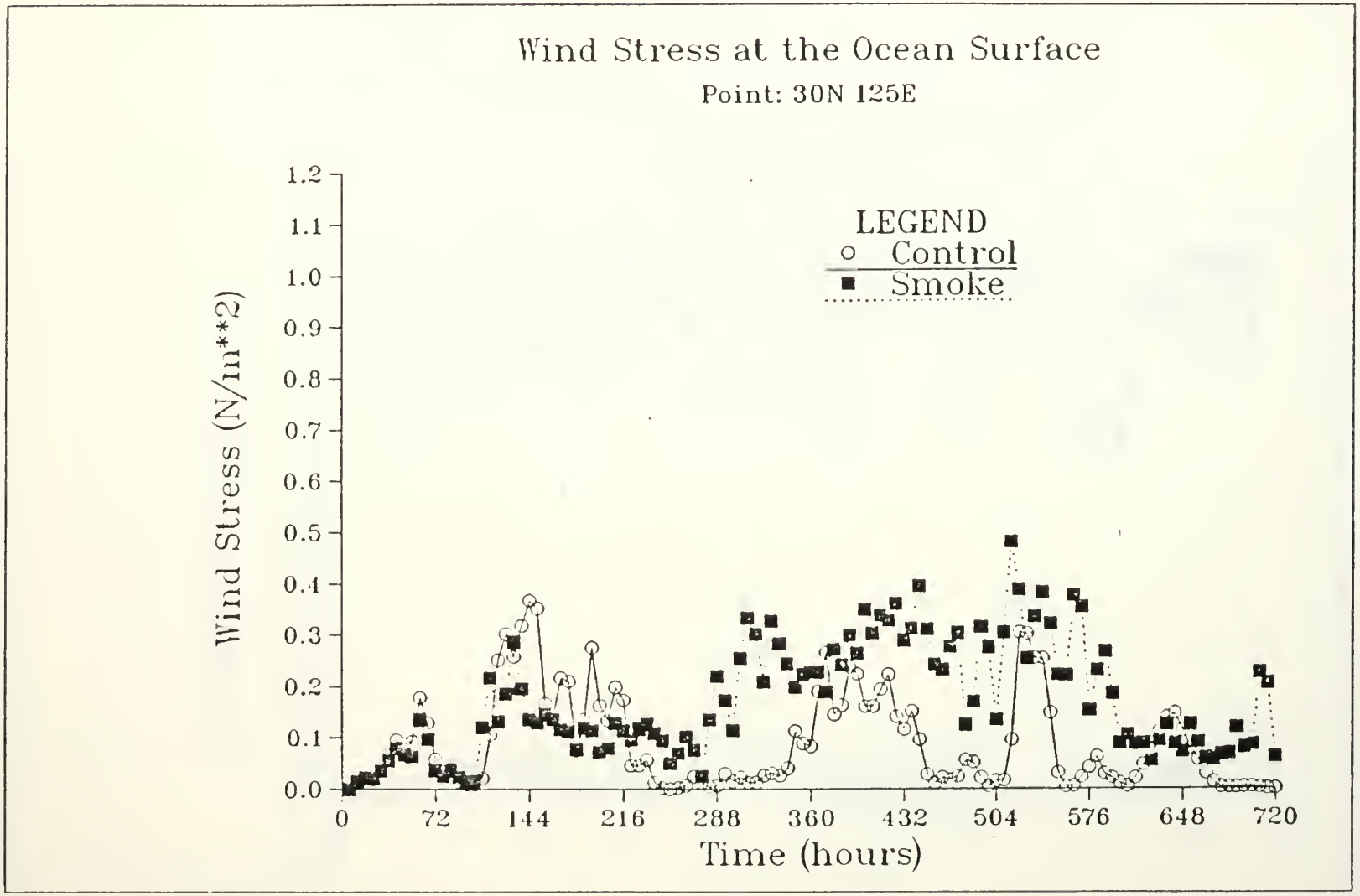

Fig. 4.19 Wind Stress at Point Six (30°N 125°E).

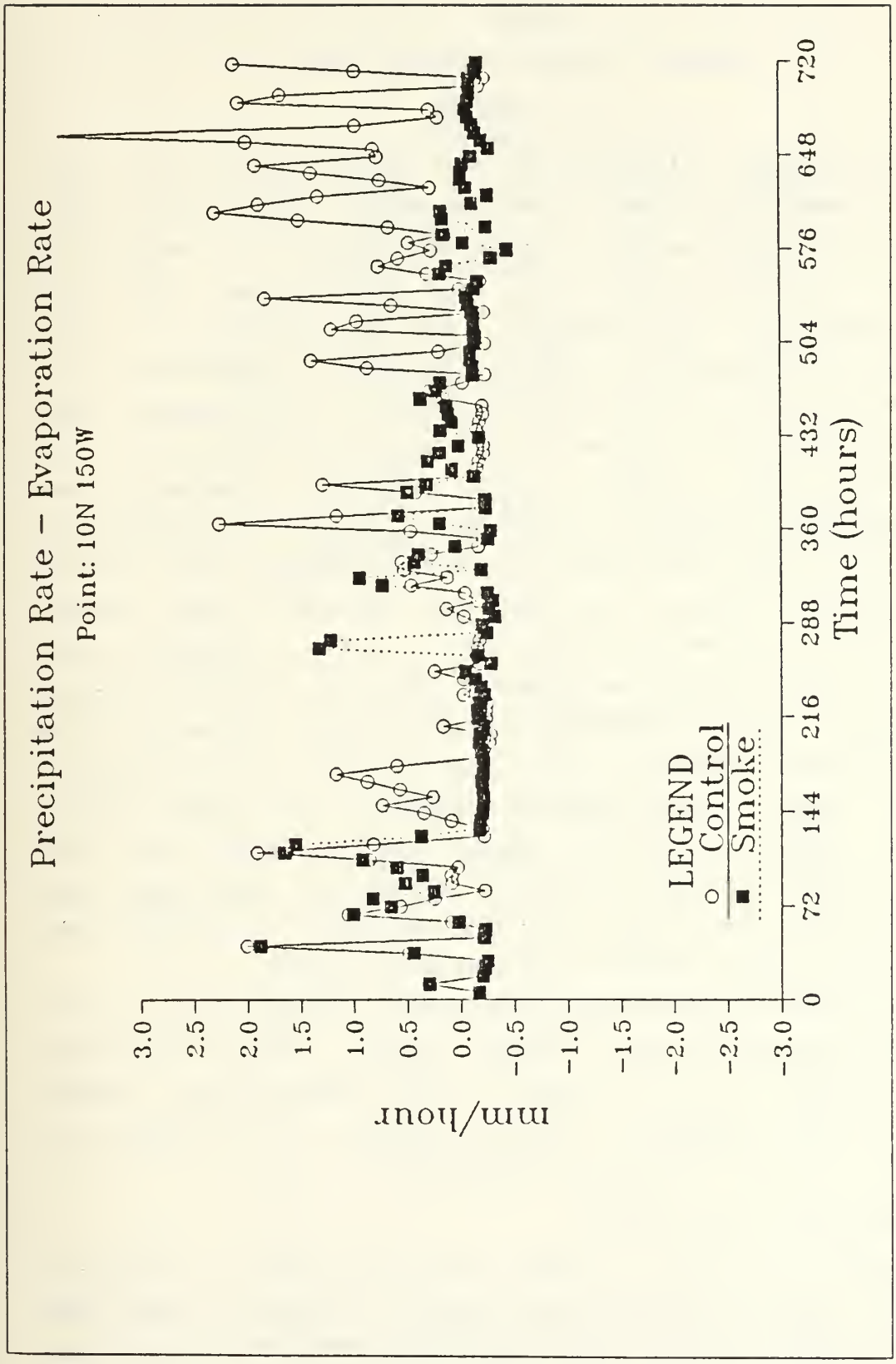

Fig. 4.20 Salinity Flux at Point Five (10°N 150°W).

V. RESULTS

This chapter will discuss the evolution of the sea-surface temperature (SST) and the mixed layer depth (MLD) through the 30-day period of both the control and smoke runs at each of the six locations. Only the "biased" runs will be discussed in this chapter. For the purposes of this analysis the "change" in SST or MLD will be defined as the difference between the hourly average of the quantity over the last three days of the run and the hourly average of the first three days of the run. The advantage of using three-day averaging intervals is that the periods are separated by a length of time that ensures that the averages are a result of unrelated synoptic forcing and secondly that diurnal variability has been filtered out. Table 4 summarizes the change in SST and MLD at each of the six locations during the control runs. Also included in this table are the corresponding averages in wind stress and Qt (from Tables 2 and 3). Table 5 summarizes the average wind stress and Qt and also the SST and MLD changes in the smoke run. The general result of less ocean heating in the smoke cases and consequently a cooler and deeper mixed layer is evident from a comparison of the results of Tables 4 and 5.

The values of the fluxes (heat and stress) cited in the following discussion are "biased" fluxes. These values may not correspond to the values on the appropriate figures which are the graphs of these stresses. The figures in chapter IV. depict "unbiased" values.

A. POINT ONE (50°N 150°W)

The SST evolution at point one (50°N 150°W) is shown in Fig. 5.1, and the mixed layer depth evolution for the same point is shown in Fig. 5.2. In the control case, a normal 30 days in July, the SST warmed slightly and the MLD

TABLE 4

SST AND MLD CHANGES:CONTROL

CONTROL (Biased)

Point	Wind Stress avg. (N/m^2)	Qt avg. (W/m^2)	SST change (°C)	MLD change (m)
1	.76	83	0.4	-15*
2	.45	95	0.1	-12
3	.45	138	2.4	-6
4	.75	18	-0.4	0
5	1.30	0	-0.5	-32
6	.75	122	2.2	0

* A positive value denotes shallowing of the mixed layer

TABLE 5

SST AND MLD CHANGES:SMOKE

SMOKE (Biased)

Point	Wind Stress avg. (N/m^2)	Qt avg. (W/m^2)	SST change (°C)	MLD change (m)
1	2.14	28	-2.3	-41
2	.90	-44	-4.3	-46
3	.36	12	-0.9	-5
4	1.69	-2	-1.3	-50
5	1.25	-36	-1.1	+2
6	1.44	-220	-4.9	-40

deepened 15 meters. The location of point one is very close to the site of Ocean Weather Station Papa (50°N 145W) which has a climatological mixed layer depth of approximately 20

meters (Adamec and Elsberry, 1984; Bathen, 1972; Robinson, 1976, Pickard and Emery, 1982). The 30-day hourly averaged MLD of 21 meters for the control run (Fig. 5.2) agrees closely with this climatological value. The control temperature curve has two significant features. The first feature is the series of distinctive temperature peaks between hour 72 and hour 144. This is associated with a period of reduced wind stress (Fig. 4.14) that causes the mixed layer to shallow and warm markedly. The second feature of the control SST curve is the gradual reduction in SST just prior to hour 288 that is associated with a corresponding wind stress peak (Fig. 4.14).

This point, at 50°N 150°W is located about 400 n mi south of Kodiak, a coastal island south of the mainland of Alaska. This location is relatively unaffected by the spread of smoke in the nuclear war scenario until day 10. This is evident in Figs. 4.2 and 4.3. The smoke which affects this point is from a hypothetical attack centered near 60°N 190°E, near Krasnojarsk, in Siberia (Fig. 4.1). As a result of the smoke coverage, the SST and MLD evolutions in the smoke run are very different from the control run. Fig. 5.1 reveals a steady but gradual departure of the smoke SST curve from the control SST curve commencing just prior to hour 72. The maximum difference in temperatures is at the end of the run. However the difference is fairly constant during the last ten days (after hour 480). This is consistent with the occurrence of maximum smoke coverage prior to about day 20. Tables 6 and 7 show that point one undergoes moderate cooling of 1.5°C and a substantial deepening of the mixed layer of 28 meters (compared with the control run averages). The difference in MLD between the smoke and control runs is the greatest of the six locations. The reason for this enhanced deepening is the two periods of high wind between days 9 and 18 (see Fig. 4.14.). These

maxima in wind stress correspond to wind speeds of approximately 18 and 19 m/s respectively. Both wind peaks follow reductions in Qs. The timing of the wind stress maxima and onset of smoke suggest that point one is influenced by a strong monsoon type flow.

TABLE 6

30-DAY TIME AVERAGED SST (°C) AND MAXIMUMS

(Biased)
(standard deviation of mean is in parentheses)

Point	Smoke	Control	Smoke-Control	Hourly Max
1	9.1 (0.2)	10.6 (1.1)	-1.5	-2.7
2	5.7 (0.2)	8.4 (1.4)	-2.7	-5.0
3	7.4 (0.9)	9.8 (0.8)	-2.4	-4.6
4	22.4 (0.2)	22.8 (0.6)	-0.4	-1.3
5	25.9 (0.2)	26.2 (0.4)	-0.3	-0.8
6	25.0 (0.9)	27.9 (1.9)	-2.9	-9.2

B. POINT TWO (50°N 150°E)

The SST evolution at point two (50°N 150°E) is shown in Fig. 5.3, and the the mixed layer evolution is shown for the same point in Fig. 5.4. In the control run, the SST remained nearly constant and the MLD deepened a total of 12 meters. The variability of the mixed layer in the control case is a result of periodic wind events clearly seen in Fig. 4.15. The 30-day average value of MLD (Table 7) is 12 meters which compares acceptably with the climatological value given by Bathen (1972) of around 20 meters. The SST curve is realistic; it shows no tendency to warm or cool and it exhibits the typical diurnal and synoptic fluctuations of the mixed layer temperature in a summertime shallow layer regime.

TABLE 7

30-DAY TIME AVERAGED MLD (METERS)

(Biased)
(standard deviation of mean in parentheses)

Point	Smoke	Control	Smoke-Control
1	49.1 (27.6)	20.6 (11.7)	28.5
2	33.4 (14.4)	12.4 (7.4)	21.0
3	15.9 (12.3)	9.3 (7.9)	6.6
4	54.6 (19.8)	29.0 (15.3)	25.6
5	39.8 (20.6)	37.4 (15.3)	2.4
6	34.6 (19.8)	10.6 (9.3)	24.0

This point, at 50°N 150°E, is located approximately 150 n mi west-northwest of the southern tip of the Kamchatka Peninsula in the Sea of Okhotsk. This location is affected by the same cloud of smoke which affected point one, except, it is affected much earlier. The obscuration of sunlight is practically total for a period of nine days following the arrival of the smoke. The blockage of sunlight is much greater at the Kamchatka location then at the Alaska location because the smoke cloud which originates in Siberia is thicker over Kamchatka. The evolution of MLD and SST at point two in the smoke case shows a severe drop in SST about day 5 with a corresponding drop in MLD. The reason for this abrupt change in the mixed layer is because of a very strong wind stress period beginning near day 5, peaking at day 7, and then ending near day 9 (Fig. 4.15). The maximum wind stress during this event is equivalent to a wind speed of 23 m/s (gale force) preceded and followed by a day of strong winds. This event suggests a very important point: ocean waters can be affected significantly (in addition to any

smoke obscuration) by the remote effects of nuclear winter-generated extra-tropical cyclones and monsoon-type circulations.

The departure of SST in the smoke run from the control SST curve averages 2.7°C and reaches a maximum value of 5.0°C. The result shows that oceanic regions within the borders of the continental shelf can be severely and suddenly affected following a nuclear exchange.

The time evolution of the thermal structure of the water column at point 2 for the control run is shown in Fig. 5.13. The corresponding smoke run thermal structure for the same point is shown in Fig. 5.14. The evolution of the isotherms for both the control and smoke runs below 65 meters are essentially identical. The dicothermal layer, characteristic for this location, near 95 meters, weakens in both the control and smoke cases. The weakening is an indication that the Garwood model is adjusting to a "natural" temperature profile more consistent with the GCM data. However, the differences are slight. The differences between the smoke and control runs are very evident above 65 meters. In the smoke run, the effect of the strong wind stress at day 5 is a deepening of the mixed layer as well as a significant strengthening of the thermocline by day 7. By day 7 the temperature changes 9°C within a 2-meter interval near 40 meters depth.

This location experienced a 4.3°C reduction in SST during the course of the smoke simulation.

C. POINT THREE (50°N 50°W)

The SST evolution at point three (50°N 50°W) is shown in Fig. 5.5, and the mixed layer evolution is shown in Fig. 5.6. In the control case, the SST warmed by 2.4°C and the mixed layer deepened 6 meters. The warming of the SST occurred under the influence of a positive average Qt (Table 2). The mixed layer depth increased during the first part of the month due to synoptic variability in the winds (Fig.

4.16) after which it shallowed until near the end of the month when several other wind events occurred. The control SST and MLD curves reveal a tendency for the Garwood model to shallow and warm the mixed layer under reduced wind stress conditions. The minimum wind stress allowed at this location was, 0.005 N/m^2, the smaller of the two values used in the experiment. It is possible that the intense SST peaks during the first 5 days of the control run and in the period from day 15 to day 20 would have been eliminated had a larger minimum been used. However, the climatological record at this location indicates that a high variability of SST is normal. The standard deviation of the hourly SST about the monthly mean in the control run was 0.9°C while Tucker and Barry (1984) have shown that the observed standard deviation of daily SST about the monthly July mean is much higher: 1.6°C. Although the exact mechanism by which air-sea interactions at this location produce such variability is not known, it is encouraging that a one dimensional ocean model can reproduce that variability from GCM data. This suggests that local processes are an important cause for the variability of SST off the coast of Newfoundland in July.

Point three, at 50°N 50°W, is located about 180 n mi northeast of Gander, Newfoundland. Of the six locations, this is the first to be covered with smoke. The source of this smoke is centered in the Washington D.C. area. By day 2 there is almost total blockage of sunlight and the smoke persists for about ten days. However, less severe patches of smoke also blanket the area during the second half of the smoke run (Fig. 4.7) As happened at points one (Alaska) and two (Kamchatka), there is an attendant increase in wind stress with the smoke, but the wind stress is much less severe than at the other two locations. The difference between this location and the other two is that the smoke arrives at the same time as the wind stress maximum. This

is probably due to the fact that Newfoundland is relatively close to the eastern U.S. and that by the time the smoke reached Newfoundland the North American continent had not had enough time to cool significantly and to set up a monsoon type circulation. The average wind stress at this location during the smoke case is actually less than in the control case and explains why the average MLD in the smoke case is only moderately deeper (6.6 meters) than in the control case. hy off At this location, the extra deepening of the mixed layer in the smoke case is due entirely to the turbulence generated by the extra surface cooling.

The -0.9°C change in SST in the smoke run (Table 5) compared with the +2.4°C change in SST in the control run (Table 4) implies a 3.3°C *reduction* in SST due to the smoke. The *actual* drop of SST due to smoke over the 30-day period is about 4°C, with much of it occurring during the first five days (Fig. 5.5).

D. POINT FOUR (30°N 150°W)

The SST evolution at point four (30°N 150°W) is shown in Fig. 5.7, and the mixed layer evolution for the same point is shown in Fig. 5.8. In the control case the SST cooled by 0.4°C and the mixed layer deepened less than one meter. The changes which occurred were due to the competing influences of a moderate average wind stress of 0.75 N/m^2 and a small positive net heat flux into the ocean. At this location in the center of the North Pacific Ocean High, there is little variation of SST or MLD during the peak of summer.

This point is located about 600 n mi northeast of Oahu. The smoke cloud which affects this location is initially centered over the southwest U.S., and it spreads westward under the influence of the northeast trade winds. The obscuration of sunlight is much less than at the Alaska, Kamchatka, or Newfoundland locations. In the 30-day period of the smoke case (Fig. 4.9) the blockage of sunlight is represented by only two relatively short periods during

which Qs falls below 70 W/m^2: at day 20 and from day 27 to day 29. The decrease in SST in the smoke case compared to the control is therefore rather small and confined to the second part of the month. The wind stress (Fig. 4.17) in the smoke case has three significant maxima at about day 13, 22 and 29. The effect of these wind stress maxima in the smoke case is significantly deepening of the mixed layer. The first wind peak in the smoke case occurs at day 12. This is later than the corresponding wind peaks at points one and two (Alaska and Kamchatka) and can be explained by this location being much further from a continental land mass than the other locations previously discussed. However, it should be noted that a pronounced wind stress maximum follows the arrival of the main cloud of smoke. This lends further support to the notion that over the ocean the effect of a nuclear winter goes beyond the local effects of smoke. The changes in *wind* are important.

E. POINT FIVE (10°N 150°W)

The SST evolution at point five (10°N 150°W) is shown in Fig. 5.9, and the mixed layer evolution for the same point is show in Fig. 5.10. In the control case, the SST cooled 0.5°C, and the mixed layer deepened 32 meters. The excessive deepening may be a result of using an initially isohaline salinity profile. Table 2 shows that at point five there is essentially no change in the net heat flux into the ocean over the 30-day period, so the cooling of 0.5°C is due entirely to entrainment of cold water from below during the deepening. It is assumed that during much of the early period of the control run the ocean model was adjusting to the initial imbalance of wind and mixed layer depth. The climatological July MLD at this location according to Bathen (1972) is about 60 meters. It is assumed that the control run was deepening to achieve this.

Despite this flaw in this control run, the smoke runs provide some interesting insights. This point, at 10°N

150°W, is located about 780 n mi southeast of Oahu and about 180 n mi north of Truk in the Caroline Islands. This location is the farthest of the six experiment locations from a continental land mass. In the smoke case, it receives the least amount of smoke of all six locations. The average wind stress at this location was essentially unchanged by the smoke. In the control case there is no net heat flux across the ocean surface but in the smoke case there is an average heat loss of 36 W/m^2 (Table 2). These are not big changes and this is somewhat expected since the location is tropical and distant from any war center. What is significant is the reduction in precipitation rate in the smoke case compared with the precipitation rate in the control case (Fig. 4.20).

F. POINT SIX (30°N 125°E)

The SST evolution at point six (30°N 125°E) is shown in Fig. 5.11, and the mixed layer evolution for the same point is shown in Fig. 5.12. In the control case the SST warmed 2.2°C, and the mixed layer depth remained nearly constant. The changes were due to a large positive value (Table 2) of Qt. The SST curve for the control run was very similar in character to the control run SST curve at point three (50°N 50°W, Newfoundland). Both curves show high variability and warming. The GCM wind stress becomes so low at times that the higher wind stress minimum of 0.010 N/m^2 was used to prevent excessive SST warming in the second half of the run.

This point, at 30°N 125°E, is located in the central Tung Hai (East China Sea) about 180 n mi east-southeast of Shanghai. The smoke from the war does not affect this location until after day 6, as can be seen from Fig. 4.13. The obscuration is not as severe as the obscuration experienced at the three points located along 50°N (Newfoundland, Alaska, Kamchatka) since the daily Qs values in the smoke run are never less than 125 W/m^2. The wind stress for the smoke run does not have any exceptional storm maxima.

Rather, it is a nearly continuous period of high wind stress greater than 0.13 N/m^2 from day 12 until day 26. A wind stress of 0.13 N/m^2 is equivalent to a wind speed of around 10 m/s. The effect of this moderate wind stress during the smoke run is to *deepen* the mixed layer in the smoke run from 14 meters in the first ten days of the run to 55 meters in the last ten days. This high wind stress has probably the most important influence in such a significant deepening, although the rapid increase in heat loss is also a significant factor. The average heat loss at the surface in the smoke run is 342 W/m^2 greater than the heat loss in the control run (Table 2).

The most interesting thing about the smoke run for this location is the phenomenal loss of heat due to evaporation and conduction. Bulk aerodynamic considerations (4.2) suggest that there is a large air-sea temperature difference at this location following the war. The maximum Qh value occurs at about day 20 and is approximately 300 W/m^2. At this time, the wind stress is approximately 0.13 N/m^2. These values imply an air-sea temperature difference of approximately 17°C. At the time of the Qh maximum the SST was approximately 23°C. This suggests that a continental air mass with surface air temperatures of the order of 5°C was influencing this location. The long period of continuously high wind stress from day 12 to day 26 and the implied air temperature suggest a vigorous circulation from land to sea that had significantly changed the mixed layer.

G. SUMMARY

In summary, the ocean experiment showed the following:

- At each of the six locations, the 30-day average SST in the smoke run was less than the 30-day average SST in the control run. These differences were due to a combination of reduced incoming solar radiation and high wind stress, except at two locations where cooling was due only to reduced incoming solar radiation. For the six cases considered, the greatest monthly average difference between the smoke and control cases was 2.9°C off the coast of Shanghai. The actual change in SST during the month at this location due to smoke was over 7.1°C.

- At all locations, the 30-day average MLD in the smoke case was deeper than in the control case. This was due to a combination of reduced incoming solar radiation and increased wind stress except at two locations where the deepening was due to reductions in incoming solar radiation only. The greatest difference between the monthly averaged MLD of the smoke and control runs was 28.5 meters south of Alaska.
- At the four locations relatively close to continental land masses there occurred significant increases in wind stress probably associated with "nuclear winter-generated" monsoonal circulations. At each of the four locations the increases in wind stress occurred simultaneously with or shortly after the arrival of large quantities of smoke.
- The Garwood ocean model adequately simulated realistic climatological conditions using the control GCM data at all the locations except point five (10°N 150°W). The reason that climatological conditions were not adequately simulated there was because of a poor initialization using an isohaline salinity profile. At the five other locations it can be assumed that nuclear winter effects on the ocean were simulated with some skill.

H. RECOMMENDATIONS FOR FURTHER RESEARCH

The Garwood model has been shown to be capable of adequately simulating the ocean thermal structure in normal or control summertime regimes. The smoke runs have shown that there is, indeed, significant cooling of the ocean 10 to 20 days following a "nuclear winter." Further research in this subject should include an extended areal study of regions using a 3D GCM run, FNOC EOTS fields as initial conditions and the Garwood model. Seasonal, (i.e., winter and transiton) times should also be investigated. A horizontal area study may show that a 1D OPBL designed for operational mixed layer forecasting may not be suitable when used with a 3D GCM.

The nuclear winter concept is to date built on solid scientific principles. The next important step will be to develop and test a coupled 3D GCM/ocean model/smoke transport model. The results may show that the large temperature drops found in this study may be too large because of the ameliorating effects of land-sea temperature differences along the coasts of continents. An investigation of the air-sea interaction along the east coasts of continents may

suggest that nuclear winter effects could play a vital role in affecting the ocean current systems.

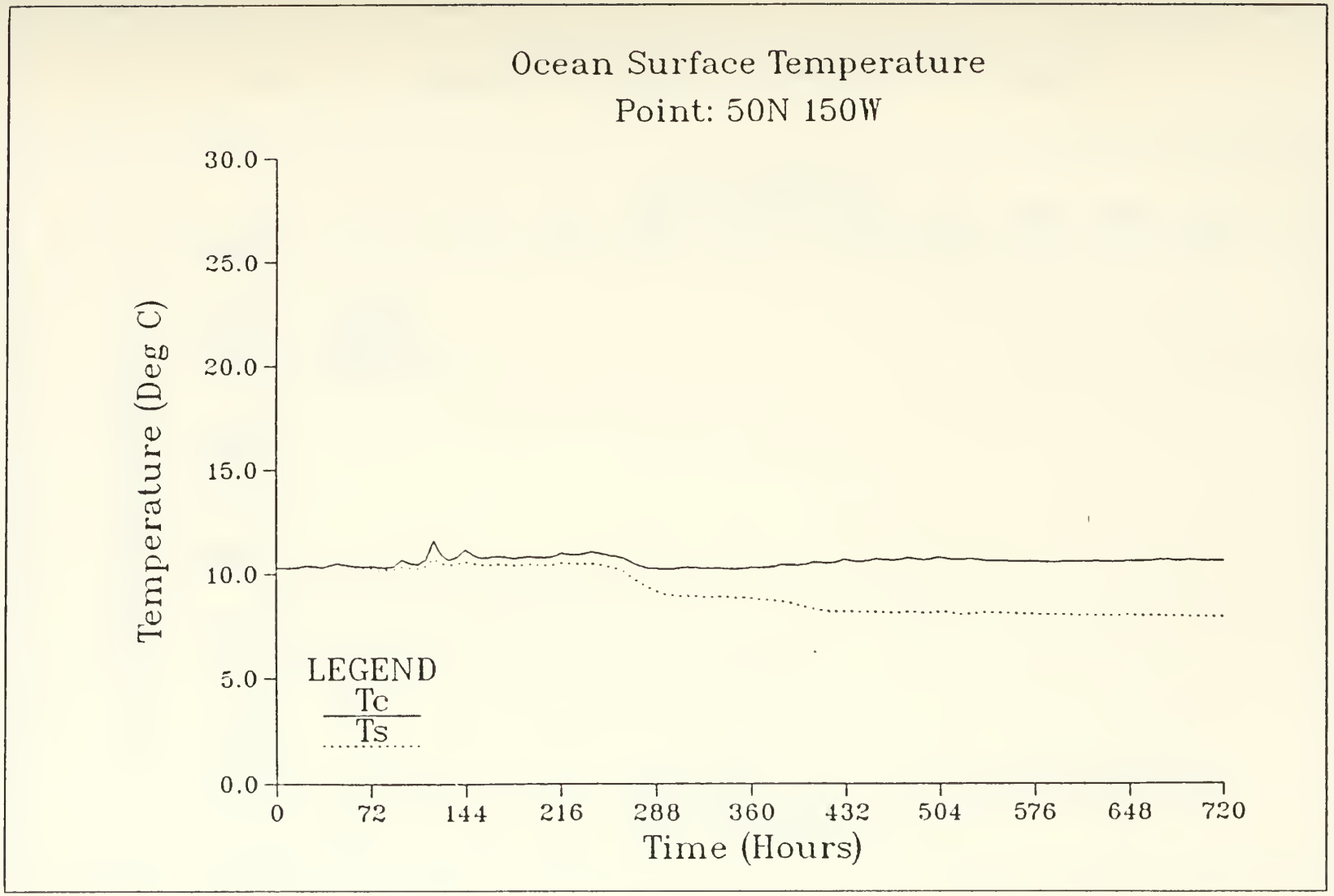

Fig. 5.1 Sea Surface Temperature at Point One (50°N 150°W).

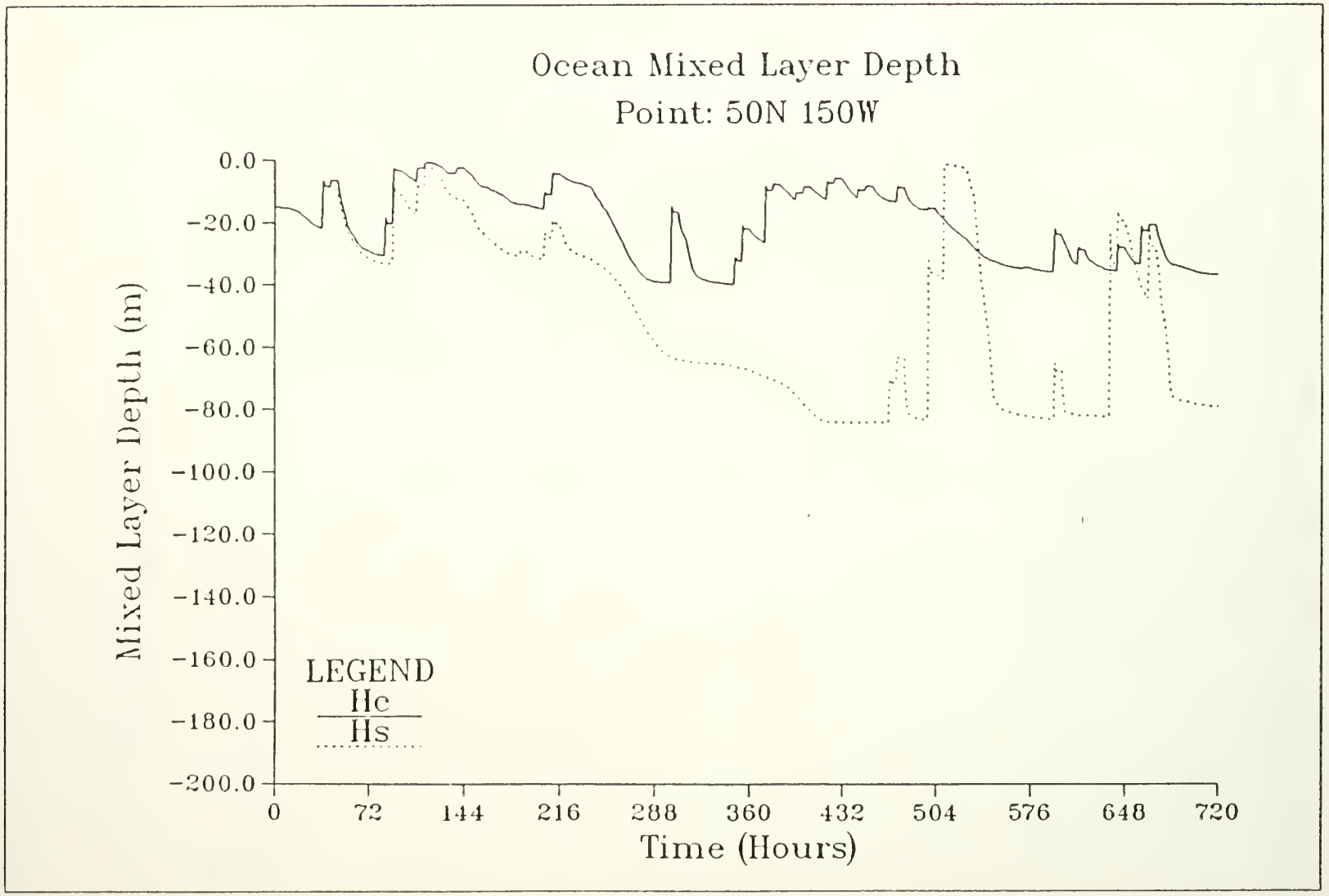

Fig. 5.2 Mixed Layer Depth at Point One (50°N 150°W).

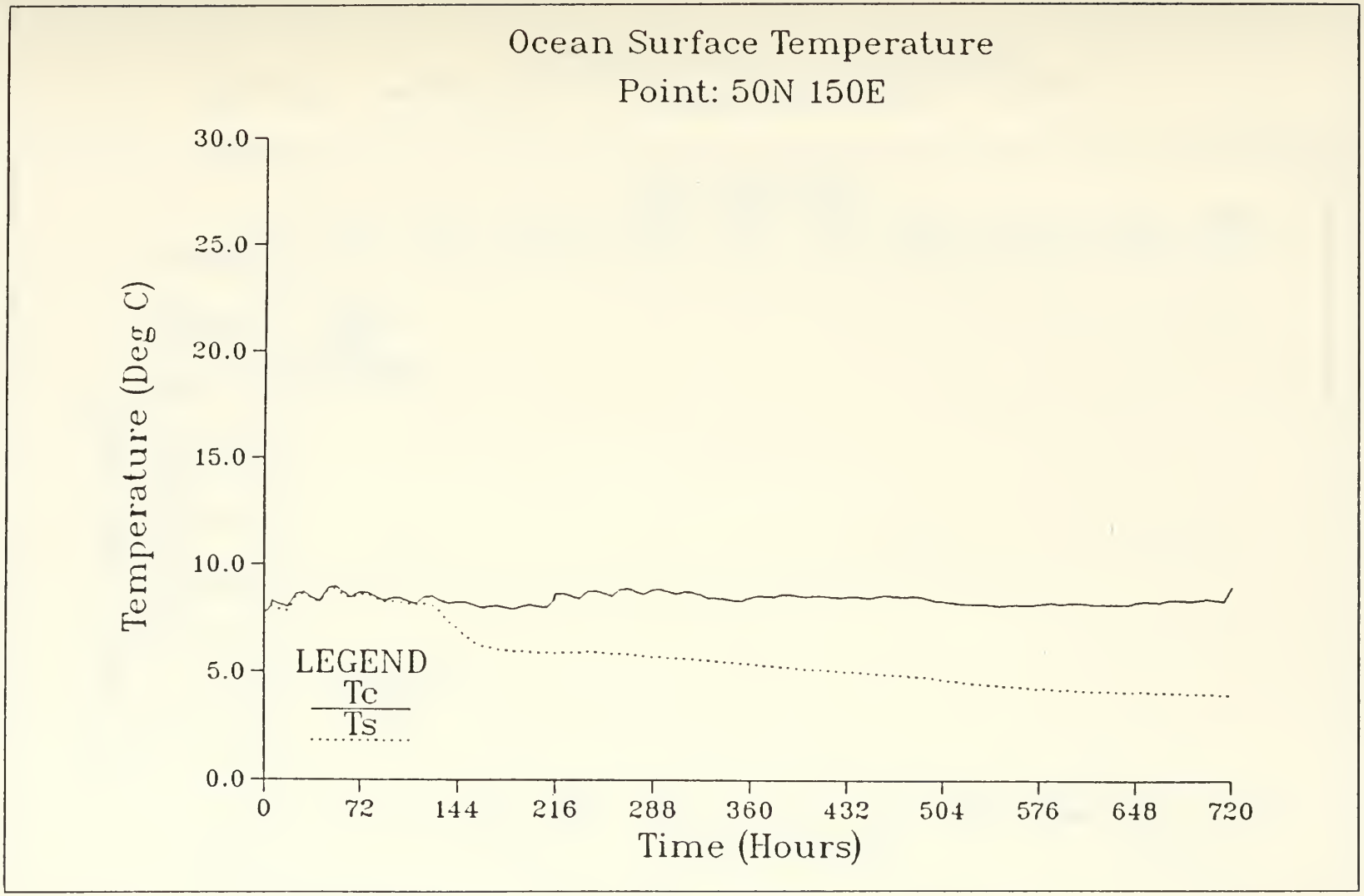

Fig. 5.3 Sea Surface Temperature at Point Two (50°N 150°E).

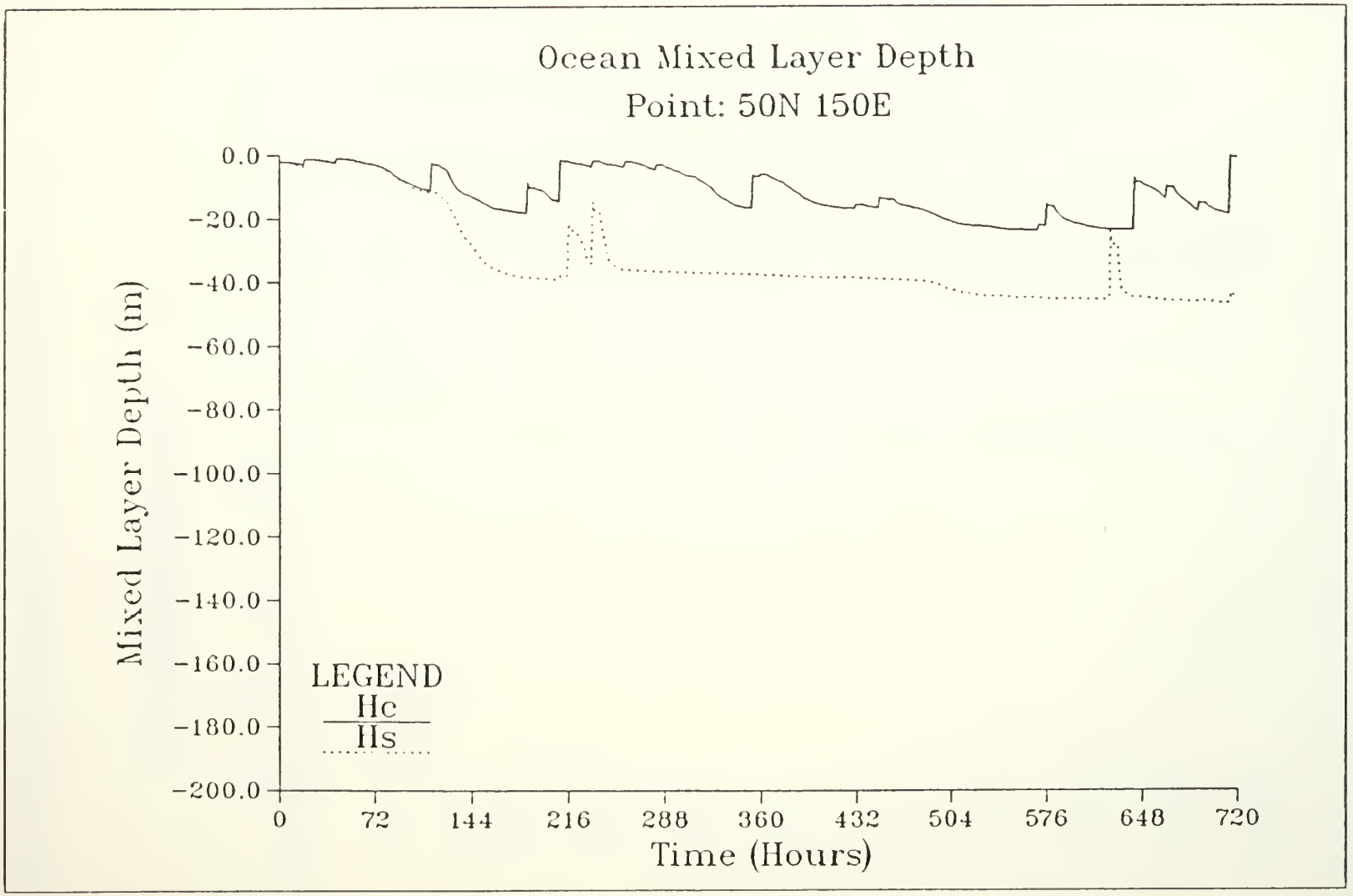

Fig. 5.4 Mixed Layer Depth at Point Two (50°N 150°E).

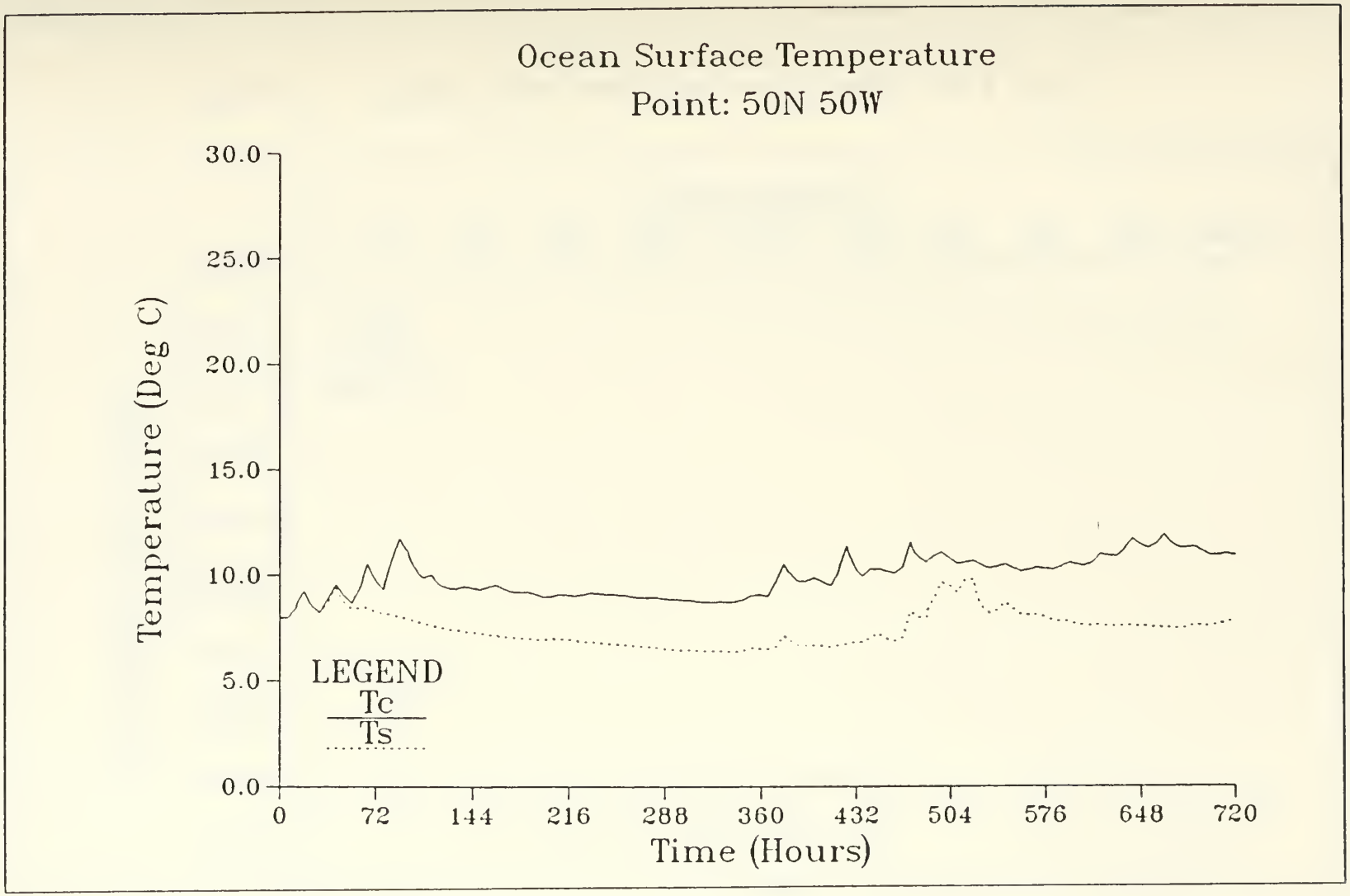

Fig. 5.5 Sea Surface Temperature at Point Three (50°N 50°W).

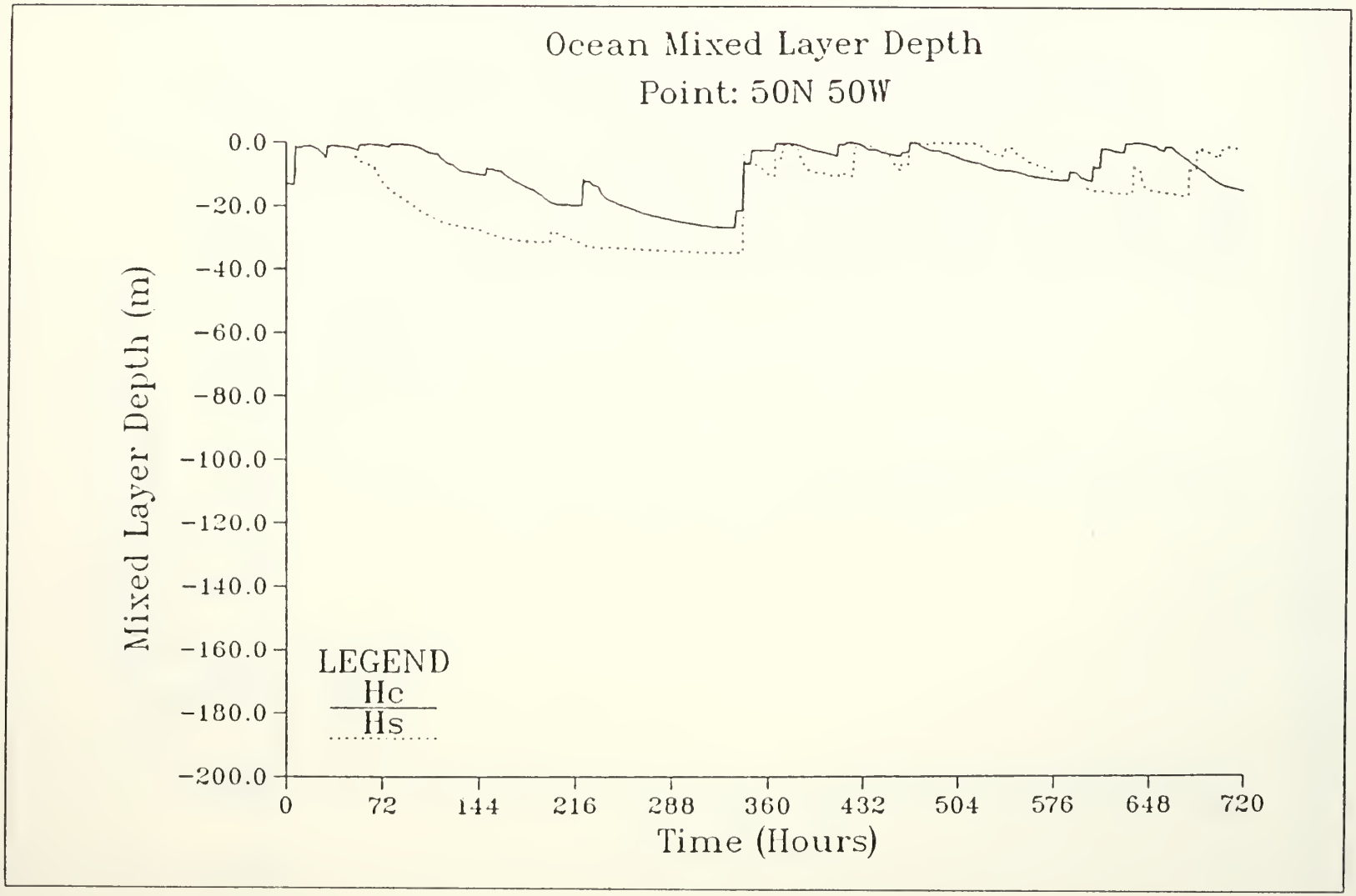

Fig. 5.6 Mixed Layer Depth at Point Three (50°N 50°W).

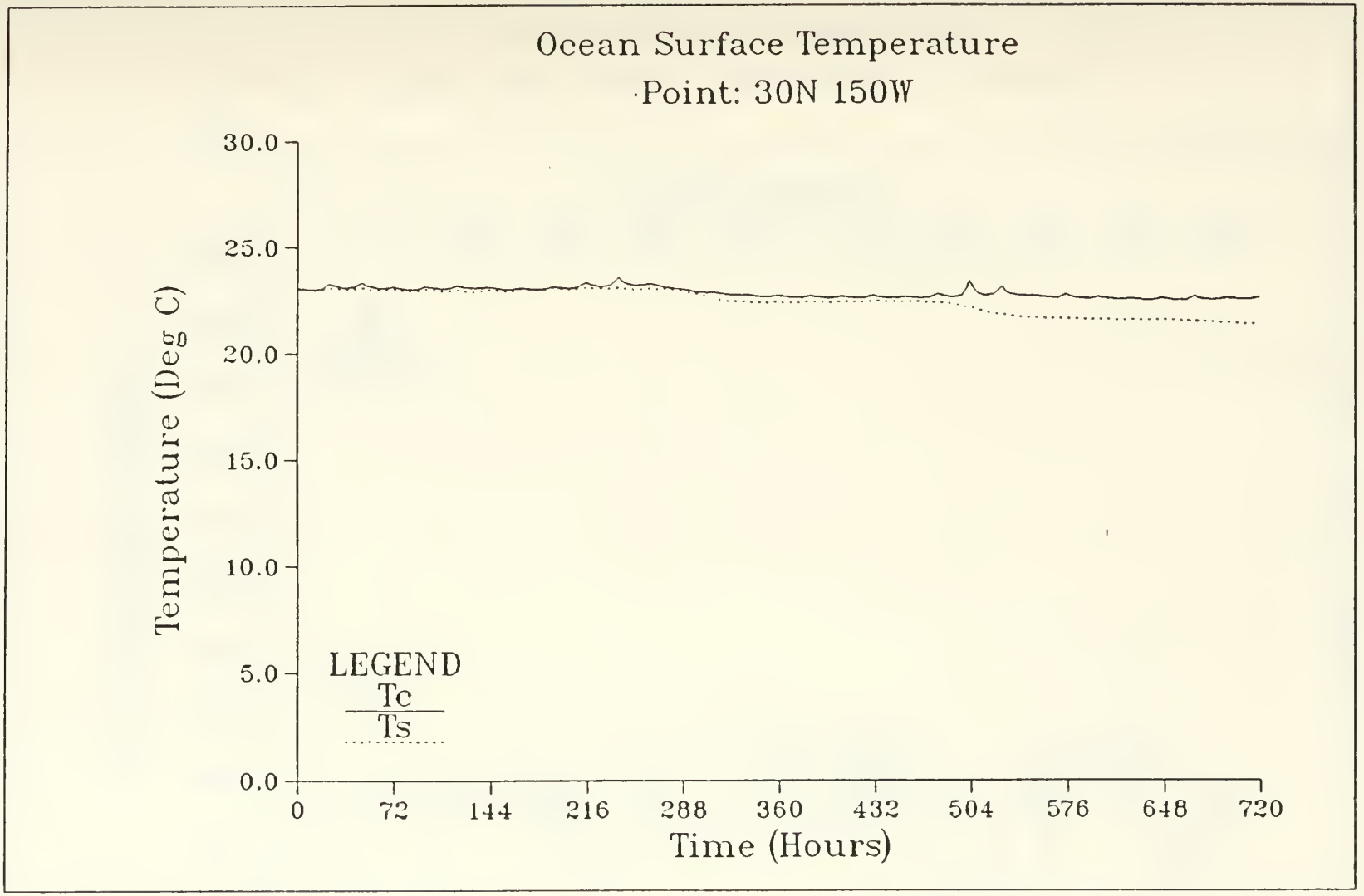

Fig. 5.7 Sea Surface Temperature at Point Four (30°N 150°W).

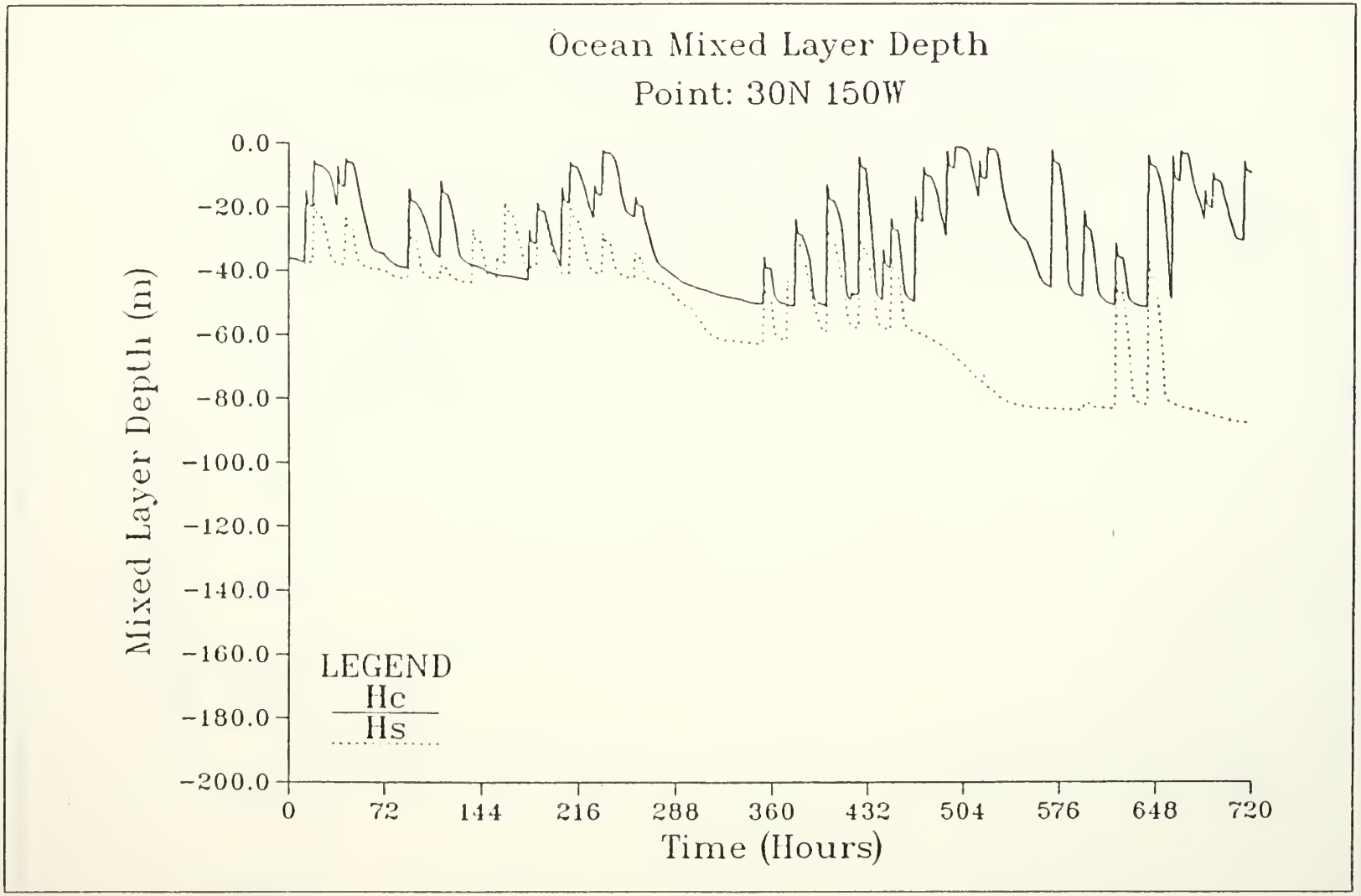

Fig. 5.8 Mixed Layer Depth at Point Four (30°N 150°W).

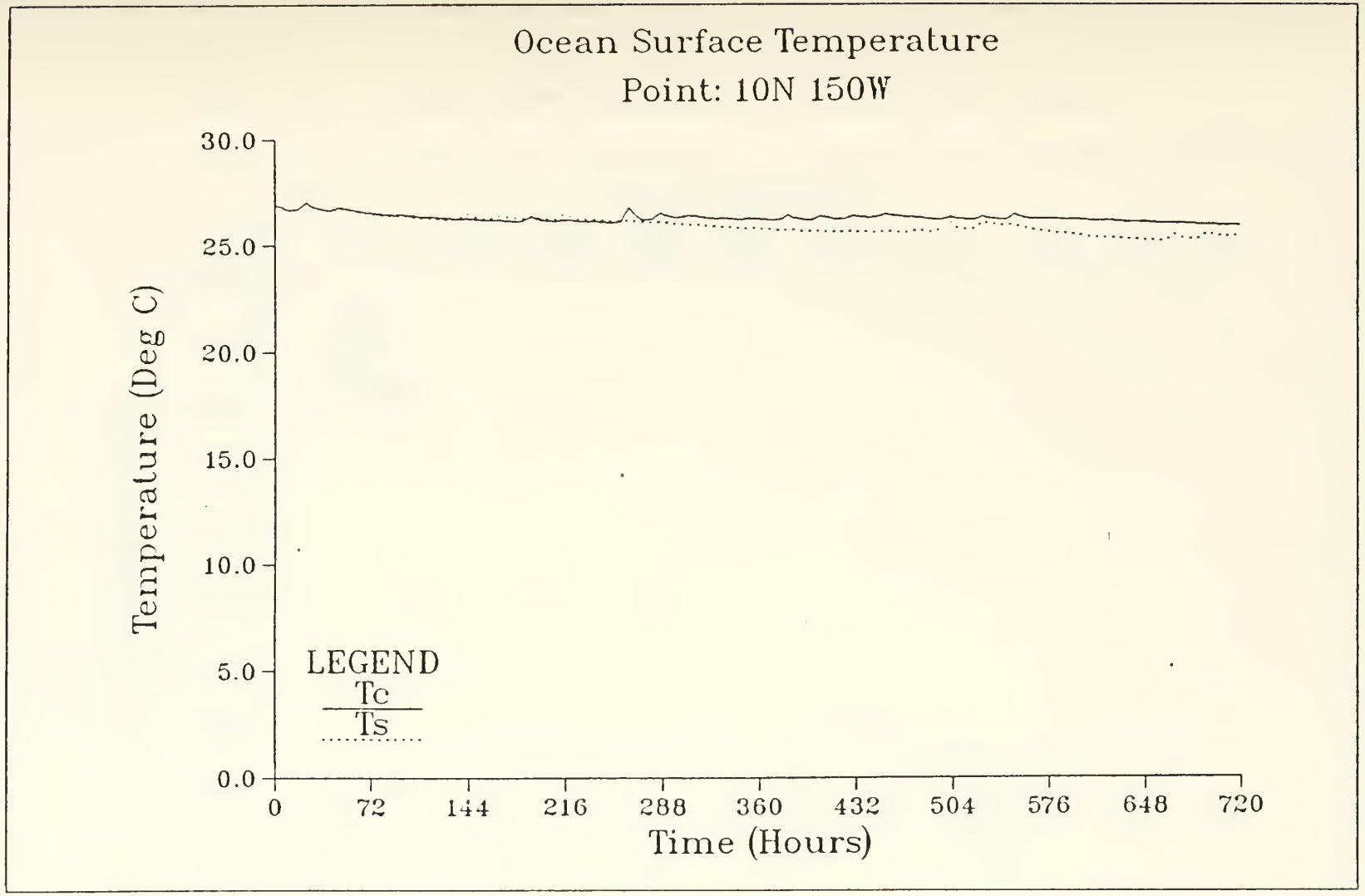

Fig. 5.9 Sea Surface Temperature at Point Five (10°N 150°W).

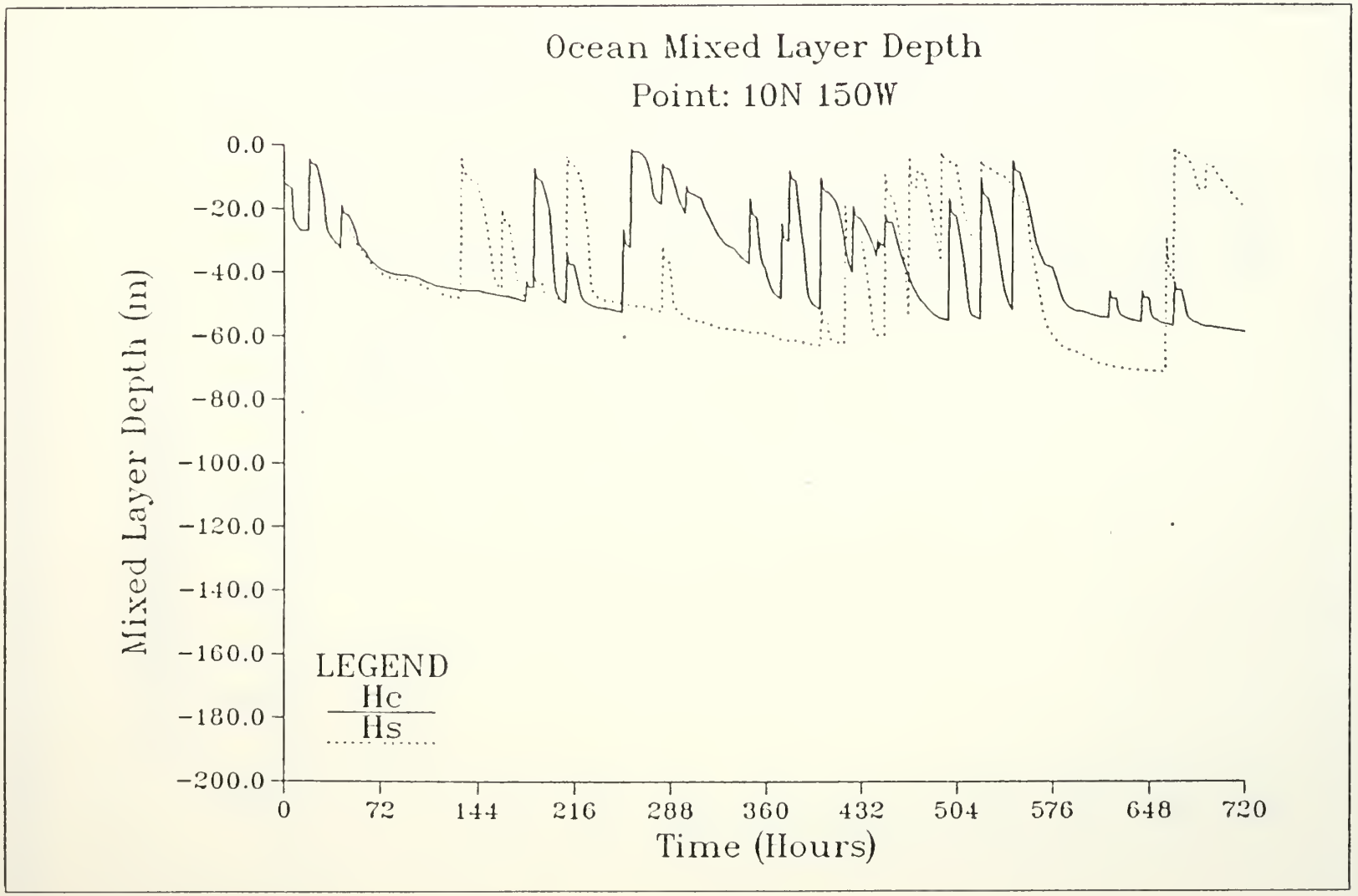

Fig. 5.10 Mixed Layer Depth at Point Five (10°N 150°W).

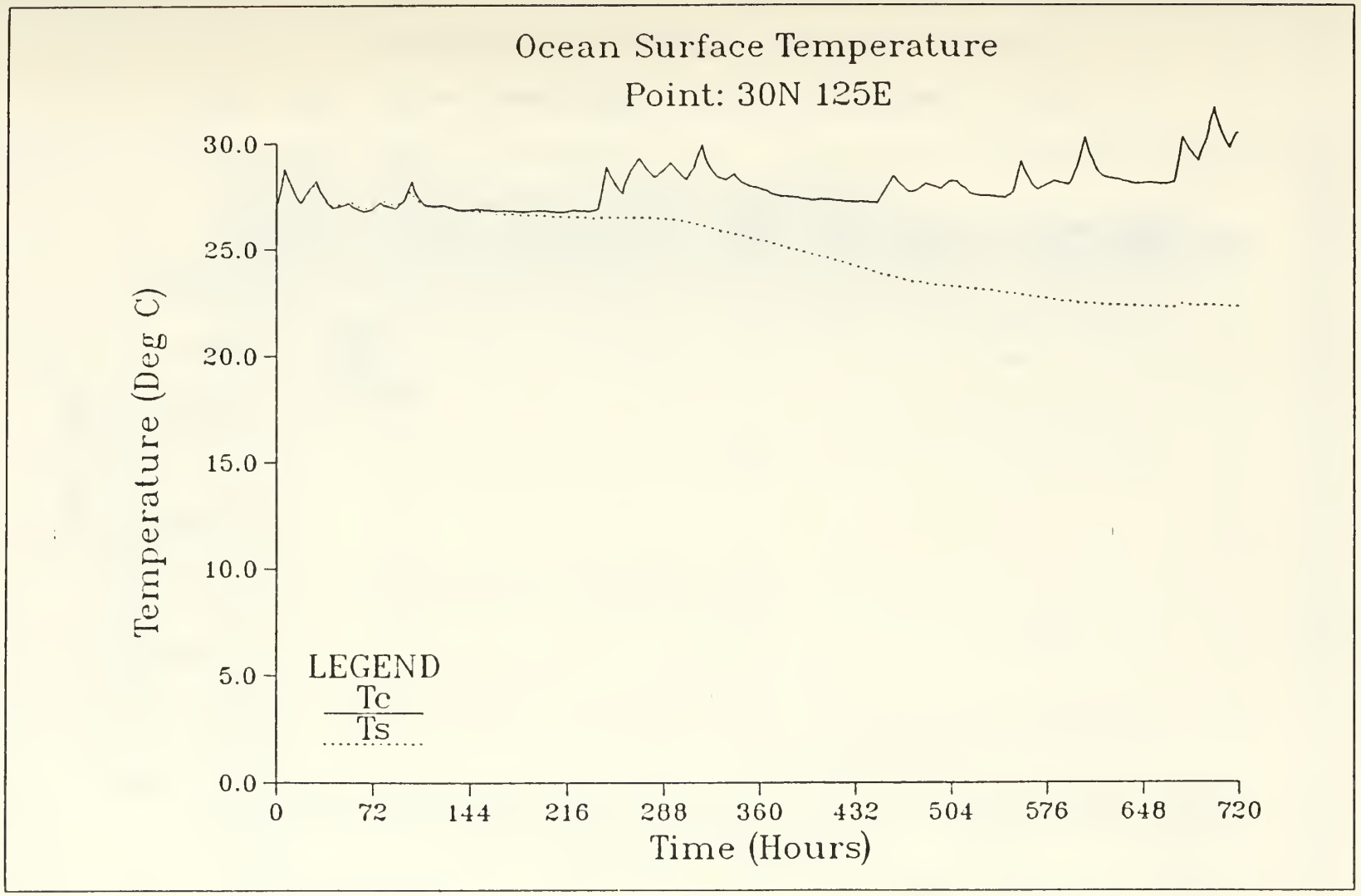

Fig. 5.11 Sea Surface Temperature at Point Six (30°N 125°E).

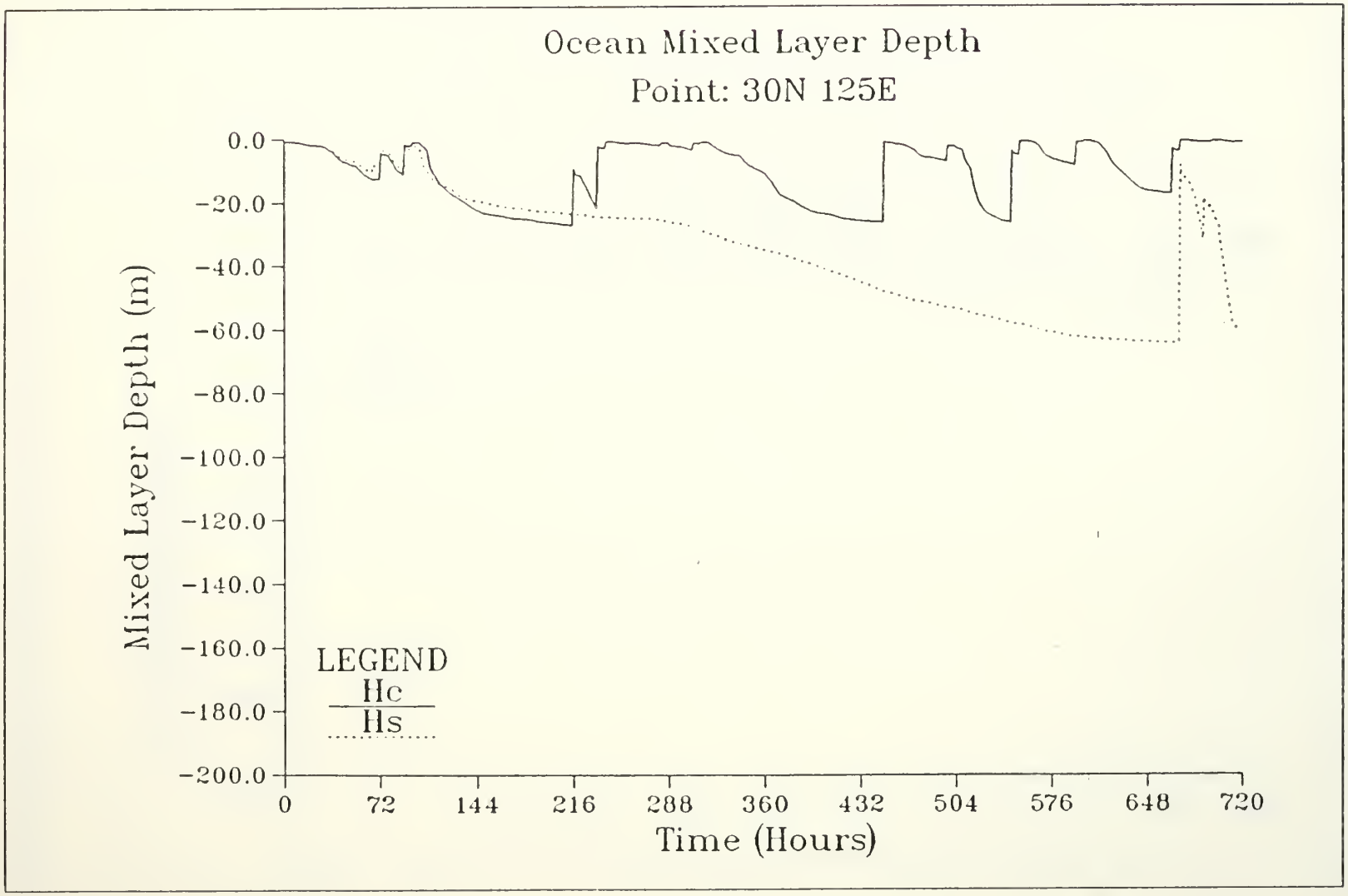

Fig. 5.12 Mixed Layer Depth at Point Six (30°N 125°E).

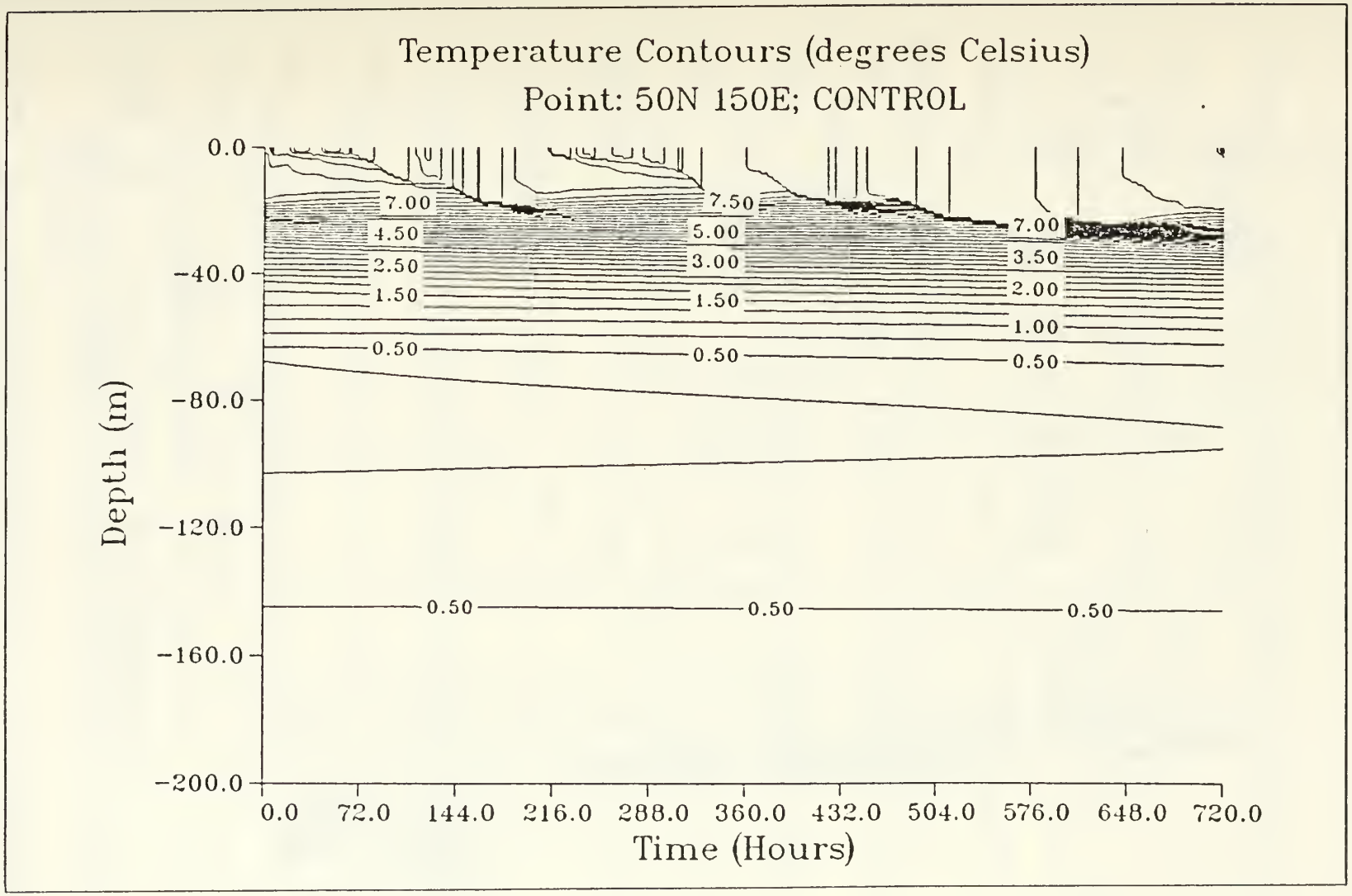

Fig. 5.13 Temperature Structure at Point Two (50°N 150°E) CONTROL.

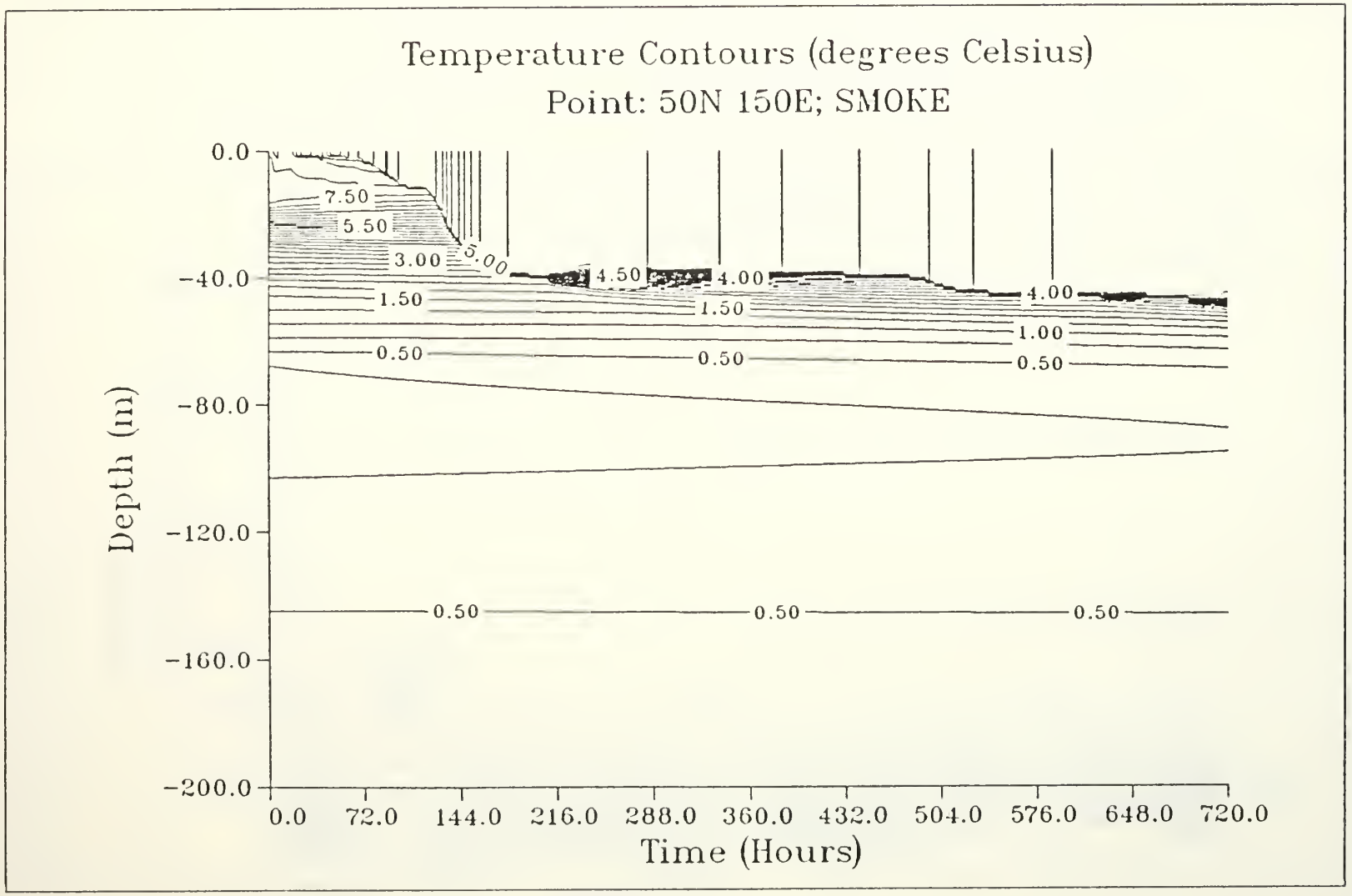

Fig. 5.14 Temperature Structure at Point Two (50°N 150°E) SMOKE.

LIST OF REFERENCES

Adamec, D. and R. L. Elsberry, 1984: Sensitivity of Mixed Layer Predictions at Ocean Weather Station Papa to Atmospheric Forcing Parameters. *J. Phys. Oceanogr. 14*, 769-781

Alvarez, L. W., W. Alvarez, F. Asaro, and H. V. Michel, 1980: Extraterrestrial causes for the cretaceous-tertiary extinction. *Science. 208*, 1095-1108.

Aleksandrov, V. V., and G. L. Stenchikov, 1984: numerical simulation of the climatic consequences of a nuclear war. *U.S.S.R. Computational Mathematics and Mathematical Physics, Vol. 24, No. 1*, 87-90.

Bathen, K. H., 1972: Distribution of The Mixed Layer in the North Pacific. *J. Geo. Res. 77(36)*, 7138-7150.

Broido, A., 1960: Mass Fires Following Nuclear Attack. *Bulletin of the Atomic Scientists, XVI, 10*, 409-413.

Cess, R. D., 1985: Nuclear War: Illustrative Effects of Atmospheric Smoke and Dust Upon Solar Radiation. *Climate Change, 7*, 237-251.

Covey, C., S. H. Schneider, and S. L. Thompson, 1984: Global atmospheric effects of massive smoke injections from a nuclear war: Results from general circulation model simulations. *Nature, 308*, 21-25.

Covey, C., S. L. Thompson, and S. H. Schneider,'Nuclear Winter': A diagnosis of atmospheric general circulation model simulations. *J. Geo. Res.(in press)*.

Crutzen, P. J., and J. W. Birks, 1982: The Atmosphere After a Nuclear War: Twilight at Noon. *Ambio, 11*, 115-125.

Crutzen, P. J., I. E. Galbally, and C. Bruhl, 1984: Atmospheric effects from post-nuclear fires. *Climate Change, 6*, 323-364.

Esbensen, S. K. and Y. Kushnir, 1981: The Heat Budget of the Global Ocean: An Atlas Based on Estimates from Surface Marine Observations. Climatic Research Institute Report No. 29, Oregon State University, Corvallis, 27 pp.

Garwood, R. W., Jr., 1977: An oceanic mixed layer model capable of simulating cyclic states. *J. Phys. Oceanogr., 7*, 455-468.

Garwood, R. W., Jr., 1979: air-sea interaction and dynamics of the surface mixed layer. *Review of Geophysics and Space Physics, 17, 7*, 1507-1524.

Gates, W. L. and M. E. Schlesinger, 1977: numerical simulation of the january and july global climate with a two-level atmospheric model. *J. Atmos. Sci., 34*, 36-76.

Ghan, S. J., J. W. Lingaas, M. E. Schlesinger, R. L. Mobley, and W. L. Gates, 1982: A Documentation of The OSU Two-Level Atmospheric General Circulation Model, Report No. 35, Climatic Research Institute, Oregon State University.

Ghan, S. J., M. C. MacCracken and J. J. Walton, Climatic Response to Large Summertime Injections of Smoke into

the Atmosphere: Changes in Precipitation and the Hadley Circulation, paper prepared for submittal to International Association for Meterology and Atmospheric Physics, Honolulu, Hawaii, Aug 5-16, 1985.

Glasstone, S., and P.J. Dolan (eds.), 1977: *The Effects of Nuclear Weapons*, Washington D.C., U.S Department of Defense. 653 pp.

Gouré, L., 1985: Nuclear Winter in Soviet "Mirrors", *Strategic Review*, Summer, 22-38.

Holton, J. R., 1979: *An Introduction Atmospheric Dynamics* (*Second Edition*). New York, Academic Press, 391 pp.

Kieffer, H. H., 1979: Mars Volatiles (and Meteorology and Dust). *J. Geo. Res*, *84*, *B6*, 2793.

Kraus, E. B. and J. S. Turner, 1967: A one-dimensional model of the seasonal thermocline II. The general theory and its consequences. *Tellus*, *XIX*, *1*, 98-105.

MacCracken, M. C., 1983: Nuclear war: Preliminary estimates of the climatic effects of a nuclear exchange, Paper presented at the Third International Conference on Nuclear War, Erice, Sicily, August 19-23, 1983.

MacCracken, M. C. and J. J. Walton, 1984: The Effects of Interactive Transport and Scavenging of Smoke on the Calculated Temperature Change Resulting from Large Amounts of Smoke. paper presented at the International Seminar on Nuclear War 4th Session: The Nuclear Winter and the New Defense Systems: Problems and Perspectives, Erice, Italy, August 19-24, 1984, Ettore Majorana Center for Scientific Culture. 20 pp.

Martin, T. Z., A. R. Peterfreund, E. D. Miner, H. H. Kieffer, and G. E. Hunt, 1979: Thermal Infrared Properties of the Martian Atmosphere 1. Global Behavior at 7, 9, 11, and 20-μm, *J. Geo. Res.*, *84*, *No. B6*, 2830-2842.

Martin, T. Z. and H. H. Kieffer, 1979: Thermal Infrared Properties of the Martian Atmosphere 1. The 15-μm Band Measurements *J. Geo. Res.*,*84*, *No. B6*, 2843-2852.

National Research Council Committee on Atmospheric Effects of Nuclear Explosions, 1985: *The Effects on the Atmosphere of a Major Nuclear Exchange*. National Academy Press, Washington,D.C., 193 pp.

Pickard, G. L. and W. J. Emery, 1982: *Descriptive Physical Oceanography*: *An Introduction*. Pergamon Press, 249 pp.

Robinson, M. K., 1976:, *Atlas of North Pacific Ocean Monthly Mean Temperatures and Mean Salinities of the Surface Layer*, U.S. Naval Oceanographic Office Reference Publication 2, Naval Oceanographic Office, Washington D.C., 19 pp.

Robock, A., 1984: Snow and ice feedbacks prolong effects of nuclear war. *Nature*, *310*, *No. 5979*, 667-670.

Secretary of Defense Caspar W. Weinberger, 1985: *The Potential Effects of Nuclear War On the Climate*: *A Report to the U.S. Congress*. Department of Defense, Washington, D.C. (March 1985) (reprinted in *Congressional Record*, March 6, 1985, at S2578-85.).

Thompson, S. L., V. V. Aleksandrov, G. L. Stenchikov, S. H. Schneider, C. Covey, and R. M. Chervin, 1984: Global

climatic consequences of nuclear war: Simulations with three dimensional models. *Ambio*, *13*, 236-243.

Tucker, G. B. and R. G. Barry, 1984: Climate of the North Atlantic Ocean, ed. H. Van Loon, *Climates of the Ocean (Vol. 15)*, editor-in-chief H.E. Landsberg, *World Survey of Climatology*, Elsevier, Amsterdam .pp 716.

Turco, R. P., O. B. Toon, T. Ackerman, J. B. Pollack, and C. Sagan, 1983: Nuclear winter: Global consequences of multiple nuclear explosions. *Science*, *222*, 1283-1292.

Turner, J. S. and E. B. Kraus, 1967: A one-dimensional model of the seasonal thermocline I. A laboratory experiment and interpretation. *Tellus*, *XIX*, *1*, 90-97.

U.S.S.R. Navy, Ministry of Defense, 1974: *World Ocean Atlas*.

Warrenfeltz, L. L., 1980: *Data Assimilation in a One-Dimensional Oceanic Mixed Layer Model*. M.S. Thesis, Naval Postgraduate School, Monterey, CA. 110 pp.

Wolbach, W. S., R. S. Lewis, and E. Anders, 1985: Cretaceous Extinctions: Evidence for Wildfires and Search for Meteoric Material. *Science*, *230*, 167-170

INITIAL DISTRIBUTION LIST

		No. Copies
1.	Defense Technical Information Center Cameron Station Alexandria, VA 22304-6145	2
2.	Library, Code 0142 Naval Postgraduate School Monterey, CA 93943	2
3.	Chairman (Code 68Mr) Department of Oceanography Naval Postgraduate School Monterey, CA 93943	1
4.	Chairman (Code 63Rd) Department of Oceanography Naval Postgraduate School Monterey, CA 93943	1
5.	Professor Robert L. Haney (Code 63Hy) Department of Meteorology Naval Postgraduate School Monterey, CA 93943	2
6.	Professor Roland Garwood (Code 63Gd) Department of Oceanography Naval Postgraduate School Monterey, CA 93943	2
7.	Director Naval Oceanography Division Naval Observatory 34th and Massachusetts Avenue NW Washington, DC 20390	1
8.	Commander Naval Oceanography Command NSTL Station Bay St. Louis, MS 39522	1
9.	Commanding Officer Naval Oceanographic Office NSTL Station Bay St. Louis, MS 39522	1
10.	Commanding Officer Fleet Numerical Oceanography Center Monterey, CA 93940	1
11.	Commanding Officer Naval Ocean Research and Development Activity NSTL Station Bay St. Louis, MS 39522	1
12.	Commanding Officer Naval Environmental Prediction Research Facility Monterey, CA 93940	1
13.	Chairman, Oceanography Department U.S. Naval Academy Annapolis, MD 21402	1

14. Chief of Naval Research
Naval Ocean Research and Development Activity
800 N. Quincy Street
Arlington, VA 22217 — 1

15. Office of Naval Research (Code 420)
Naval Ocean Research and Development Activity
800 N. Quincy Street
Arlington, VA 22217 — 1

16. Scientific Liason Office
Office of Naval Research
Scripps Institution of Oceanography
La Jolla, CA 92037 — 1

17. Library
Scripps Institution of Oceanography
P.O. Box 2367
La Jolla, CA 92037 — 1

18. Library
Department of Oceanography
University of Washington
Seattle, WA 98105 — 1

19. Library
CICESE
P.O. Box 4803
San Ysidro, CA 92073 — 1

20. Library
School of Oceanography
Oregon State University
Corvalis, OR 97331 — 1

21. Commander
Oceanographic Systems Pacific
Box 1390
Pearl Harbor, HI 96860 — 1

22. Library Aquisitions
National Center for Atmospheric Research
P.O. Box 3000
Boulder, CO 80307 — 1

23. Library Aquisitions
Lawrence Livermore National Laboratory
P.O. Box 808
Livermore, CA 94550 — 1

24. Professor K.E. Woehler (Code 61Wh)
Department of Physics
Naval Postgraduate School
Monterey, CA 93943 — 1

25. Dr. Steven Ghan (1-257)
Lawrence Livermore National Laboratory
P.O. Box 808
Livermore, CA 94550 — 1

26. Professor K. Kartchner (Code 56Kn)
Department of National Security Affairs
Naval Postgraduate School
Monterey, CA 93943 — 1

27. LT. T.R. Mettlach
20 Sunray Dr.
Highland, IL 62249 — 1

28. Officer-in-Charge — 1

Naval Oceanography Command Detachment-MET
Box 63, U.S. Naval Station
FPO San Francisco 96654-2909

29. LT. Philip Renaud (Section XS-51) 1
Air-Ocean Sciences Curriculum (Code 35)
Naval Postgraduate School
Monterey, CA 93943

30. Dr. Starley Thompson 1
National Center for Atmospheric Research
P.O. Box 3000
Boulder, Colorado 80307

216759

Thesis
M5623 Mettlach
c.1 Changes in the ocean mixed layer following extraordinary atmospheric forcing.